UNIVERSITY OF LIVERPOOL

Non-thermal air plasma discharges for food and water security applications

Thesis submitted in accordance with the requirements of the University of Liverpool for the degree of Doctor in Philosophy by

Yuan Ni

Feb 2017

Abstract

Non-thermal air plasma discharges for food and water security applications

Yuan Ni

The use of cold atmospheric pressure plasma for applications related to microbial decontamination has grown enormously over the last decade. Non-thermal plasmas generated in ambient air contain a wide variety of reactive oxygen and nitrogen species, or RONS. When such species interact with microorganisms they induce a number of biological changes, ultimately resulting in inactivation of the organism.

This thesis focuses on the design, development, optimisation and application of air plasma systems for microbial decontamination. The aim of the work is to gain a better understanding of how RONS are produced in air plasma and how they are transported through different phases of matter, including gases and liquids. It is shown that RONS generation is highly dependent on the discharge conditions and two distinct modes of operation are observed. Downstream of the discharge, the transport of RONS to the sample region is of paramount importance as many highly-reactive species are lost. To address this challenge, the structure of the plasma generating electrodes was systematically studied to optimise the plasma generated air flow and therefore the transport of species downstream. Optimised electrode structures were shown to generate flow velocities in excess of 1m/s which is an order of magnitude improvement over transport by diffusion alone.

Using the optimised plasma system, the impact of RONS in real decontamination scenarios linked to food and water security were considered. This included investigation of plasma decontamination of liquid samples, solid surfaces and tissues. It was shown that plasma decontamination can be extremely effective but many factors influence the efficacy of the approach. Microorganisms shielded within a liquid layer or by a complex surface morphology were shown to be particularly difficult to inactivate. Overall, this work has demonstrated that plasma can be a highly effective tool for microbial decontamination but careful consideration of both the discharge parameters and the sample properties is required to achieve the highest level of decontamination.

Acknowledgements

Firstly, I would like to express my sincere gratitude to my supervisor Dr. James L Walsh for the continuous support of my PhD study and related research, for his patience, motivation, enthusiasm and immense knowledge. His guidance helped me in all the time throughout the research, lab work and writing of this thesis. I could not have imagined having a better supervisor and mentor for my PhD study.

Also, I would like to thank Dr. Mohammad Hasan for his many helpful suggestions as a colleague and his kindness as a friend. Sincere thanks to Dr. TJ Petty and Dr. Frederic Bless for their unselfish and friendly support and help during my experiment and daily life in Liverpool. Many thanks to Dr. Xin Tu and his group for generously sharing their laboratory and research facilities with me. I also have to thank Modic and Natasa Hojnik for their microbiological knowledge and laboratory skills, this project could not be completed without their hard work.

During my PhD at University of Liverpool, I would like to thank all members of technological plasma research group of the EEE department, e.g. Dr. Mark Bowden, Dr. Kirsty McKay, Michael Barnes, Aaron Dickenson, Youssef Morabit, Patrick McCarthy, Peter Ryan, Francis Lockwood Estrin, etc. Thanks to them for creating a friendly and lively social vibe and I'm sure I was in the best research group of the University.

I would also like to thank Prof. Fran Smulders and his research group, for their kind support during my stay in Vienna, Austria. It was a privilege and pleasure to work with them, their insightful knowledge was helpful and inspiring.

Finally, a huge love and gratitude to my family. Thanks to my parents for their love, support and kind advice, and my girlfriend for her encouragement and good care during my PhD study. This work would have not been possible without their help and support.

Contributions

Journal Papers (In Print)

1. 'A solar powered handheld plasma source for microbial decontamination applications,' Y Ni, MJ Lynch, M Modic, RD Whalley, and JL Walsh (2016) J. Phys. D. Appl. Phys., vol. 49, no. 35, p. 355203.
2. 'The effects of atmospheric pressure cold plasma treatment on microbiological, physical-chemical and sensory characteristics of vacuum packaged beef loin,' A Bauer, Y Ni, S Bauer, P Paulsen, M Modic, JL Walsh, FJM Smulders (2017) Meat Science. Manuscript accepted on 5th Feb 2017.

Journal Papers (In Preparation)

1. 'Atmospheric pressure plasma technology and fungi decontamination,' H Natasa, Y Ni, M Modic, JL Walsh, U. Cvelbar (To submit to J. Phys. D)
2. 'Ozone generation mechanism in a Surface barrier Discharge' , Y Ni, A Dickenson, M. Hasan and JL Walsh

Conference Proceedings

1. M. Modic, N. Hojnik, Y. Ni, J.L. Walsh and U. Cvelbar. 'Plasma technology as a tool for the inactivation of food-related microorganisms.' International Workshop on Plasmas for Energy and Environmental Applications (IWPEEA-2016), 21 – 24 August, 2016, Liverpool, UK.
2. Y. Ni, M. J. Lynch, M. Modic, R. Whalley, D. L. Bayliss and J.L Walsh. 'Scale up of atmospheric pressure plasma systems for food treatment' CEI Workshop on Application of Advanced Plasma Technologies in Central Europe Agriculture. 17-21 April 2016, Ljubljana, Slovenia.
3. Y. Ni, M. J. Lynch, M. Modic, R. Whalley and J.L Walsh 'Flow effects in an atmospheric pressure plasma jet. 5th International Conference on Advanced Plasma Technologies - ICAPT-5, 28th February to 3rd March 2016, Rogla, Slovenia.

4. Y. Ni, M.J. Lynch, M. Modic, R. Whalley, D.L. Bayliss and J.L Walsh 'Development and optimisation of air plasma sources for microbiological decontamination' 22nd International Symposium on Plasma (ISPC 22), July 2015, Antwerp, Belgium.

5. Y. Ni, M.J. Lynch, M. Modic, R. Whalley, D.L. Bayliss and J.L Walsh 'Development and optimisation of air plasma sources for microbiological decontamination' COST Action MP1101: Biomedical Applications of Atmospheric Pressure Plasma Technology workshop, May 2015, Istanbul, Turkey.
6. Y. Ni, M.J. Lynch, M. Modic, R. Whalley, D.L. Bayliss and J.L Walsh 'Optimisation of air plasma discharges for microbiological decontamination' 75th Workshop on Plasma Science, International Union for Vacuum Science, Technique and Applications (IUVSTA), January 2015, Ljubljana, Slovenia.

Table of contents

List of figures

List of tables

Chapter 1 Introduction to food safety challenge and non-thermal air plasma

1.1 Plasma & non-thermal plasmas

Plasma, also referred to as the fourth state of matter, is an ionised gas, where its atoms or molecules are fully or partially ionised. By ionised, it means that at least one electron is not bound to the atom or molecule, thus changing neutral atoms or molecules into positively charged ions. As these ions and electrons are unbound plasma is electrically conductive and strongly responsive to electrical field [1].

Plasma comprises 99% matter of the universe, it presence ranges from stars, nebula, to aurora and lighting. The Sun itself is a giant plasma ball, where nuclear fusion in its core provides the energy to break down hydrogen atoms into free electron-ion pairs. The streams of charged particles project from the upper atmosphere of the Sun form the solar wind. When it is captured by Earth's magnetic field, the upper atmosphere of the earth near the poles is no longer in neutral state and an aurora is generated [1, 2].

In addition to naturally generated plasma, man-made plasma is widely used in laboratory and industry. A great number of applications benefit from plasma technology, including semiconductor fabrication, energy efficient lighting and materials synthesis.

Both natural and man-made plasma can occur over a large range of pressures, electron temperatures, and electron densities, as shown in Figure 1.1. The temperature of man-made plasma can be as low room temperature or as high as to the inner core of a star. The electron densities of different plasma ranges from 10^4 to 10^{18} cm^{-3}. In addition, both natural and man-made plasmas are quasi-neutral, which means the concentrations of positively charged particles is equal to negatively charged particles [1].

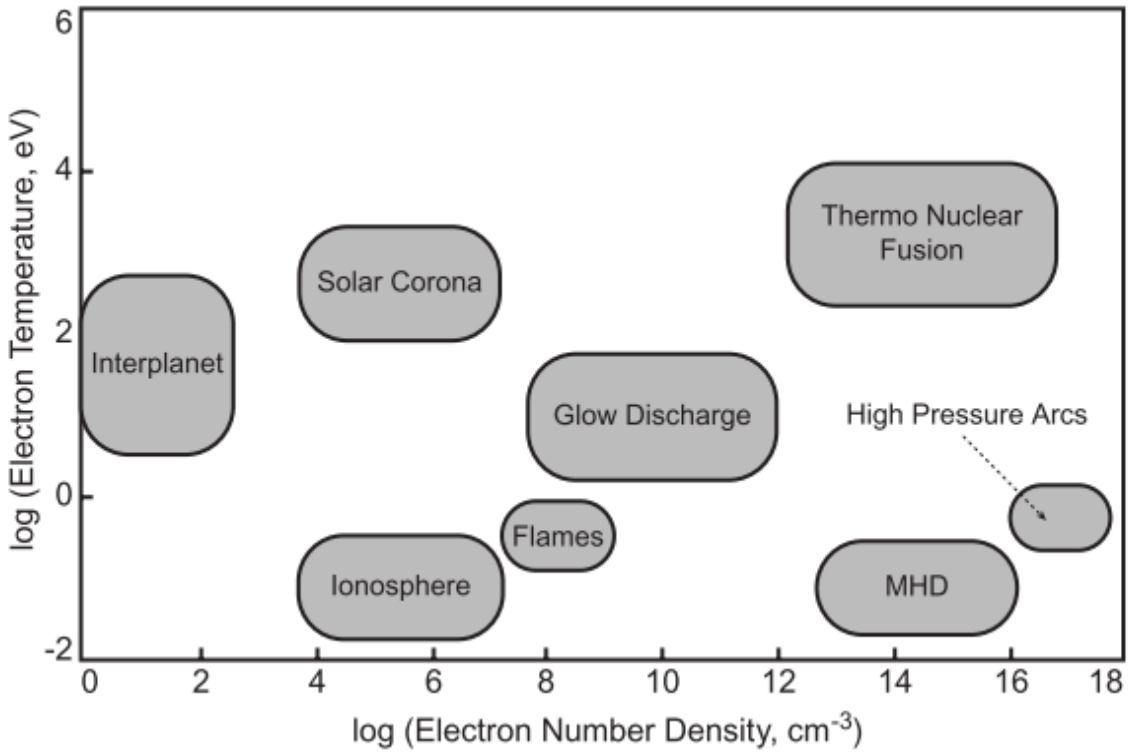

Figure 1.1 Electron temperature and electron densities for natural and manmade plasmas.

The degree of ionisation can vary enormously in a plasma, there are highly ionised plasmas and weakly ionised plasmas; the former has an ionisation degree close to unity, where almost all the particles are ionised; on the contrary, the latter has a relatively low degree of ionisation, where considerably less than 1% of the particles are ionised. Completely ionised plasma can be found in many thermonuclear plasma systems, such as tokomaks, stellarators, plasma pinches, etc. [1].

In partially ionised plasma, which forms the focus of this thesis, the ions, electrons and neutral particles can have very different temperatures depending on how they are generated. When the temperature of electrons is equal to the temperature of ions and neutral particles, the plasma is said to be in thermodynamic equilibrium and is thus called thermal plasma. Stars are examples of natural thermal plasmas. In the laboratory and industry, thermal plasma is usually generated at atmospheric and higher pressures, where the particles collide more frequently. The energy density of thermal plasmas ranges from 100 W cm^{-3} to above 10 kW cm^{-3} and, thus,

a great number of active species is created which leads to variety of industrial applications, such as plasma cutting, welding, deposition, etc. [1, 3]. On the contrary, when the electrons receive more energy and have a much higher temperature than ions and neutral particles, the plasma is called non-thermal plasma or cold plasma. Typically, in such plasmas, the electron temperature ranges from 10,000 K to 100,000 K while the gas temperature remains between 300 K and 1000 K.

Non-thermal plasmas produced in laboratory are usually in the form of an electric discharge between two electrodes inside a gas chamber. With the application of a strong electric field between the electrodes, a small group of "seed" electrons are generated and accelerated [3]. If the electric field is strong enough, these electrons gain sufficient energy that they can ionise other neutral particles through collision. As this process repeats, the density of electrons and ions grow exponentially and leads to a chain reaction. This is known as the electron avalanche process. Since most of the electrons lose their energy or are themselves lost during collisions, an insufficient electric field cannot sustain the avalanche process. At a point when the density of the electrons is high enough so that electric current can pass through the gas between the electrodes, it is said that the breakdown of the gas has occurred. After breakdown, the electrical properties of the gas are changed and thus it has become a weakly ionised plasma [1–3].

Depending on the applied voltage and current, gas composition and pressure and electrode arrangement, different types of discharge can be generated and sustained; typical examples include glow discharge, corona, discharge, dielectric barrier discharge (DBD), radiofrequency (RF) and microwave (MW) discharges.

1.1.1 Glow discharges

The glow discharge is one of the most widely used non-thermal discharges in industry. The name glow discharge indicates the discharge is luminous compared to the low-power dark discharge. The simplest glow discharge configuration can be defined as two electrodes placed in a low pressure (0.1 to 10 Torr) gas chamber

filled with neon or argon. A DC voltage of several hundred volts is usually applied between the two electrodes, with sufficient magnitude to initiate the process of gas breakdown. When the applied voltage is just above the breakdown point, a weak plasma is generated known as a Townsend discharge, with a current-voltage characteristic as shown in Figure 1.2. As the applied voltage increases, the discharge current increases and a subnormal glow discharge develops. This region has a lower discharge voltage and the plasma becomes more intense. When the electrodes are fully covered by the plasma, it is said that the discharge enters the normal discharge region. At the end of the normal glow region, the discharge enters the unstable anomalous glow region, or abnormal glow, where voltage and current rises to relatively high levels. With further increases in voltage and current, the anomalous glow discharge transits to an arc discharge with the current usually at 1 A or higher [2].

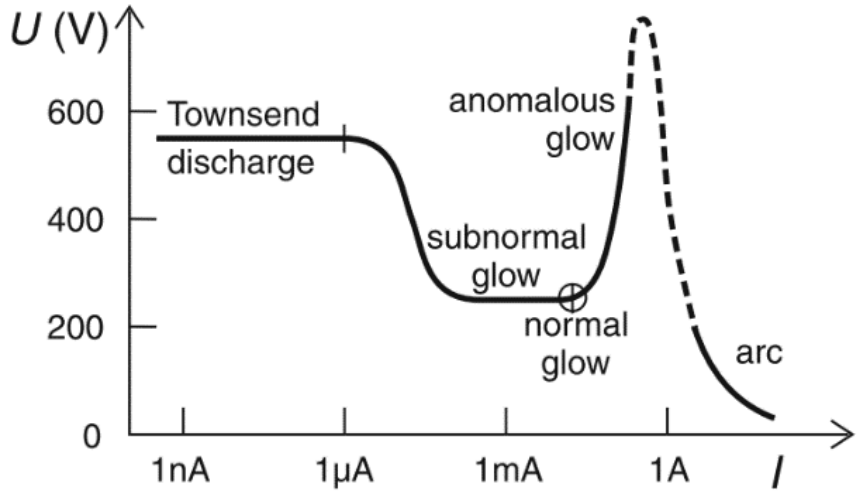

Figure 1.2 Voltage and current characteristics of a DC glow discharge.

1.1.2 Corona discharges

A corona discharge is a weak luminous discharge, which can usually be found near high electric field points such sharp points on electrodes, edges of ungrounded metallic objects, or thin wires. The electric field is sufficiently strong to form an ionised region, but not strong enough to cause electrical breakdown or arc

discharge to reach nearby objects. In comparison to the glow discharge, the intensity of a corona discharge falls somewhere between the Townsend discharge and subnormal glow discharge. Corona discharges can be observed around high-voltage transmission lines which have a strong electric field to create a region of plasma [1].

1.1.3 Dielectric Barrier Discharges and Surface Barrier Discharges

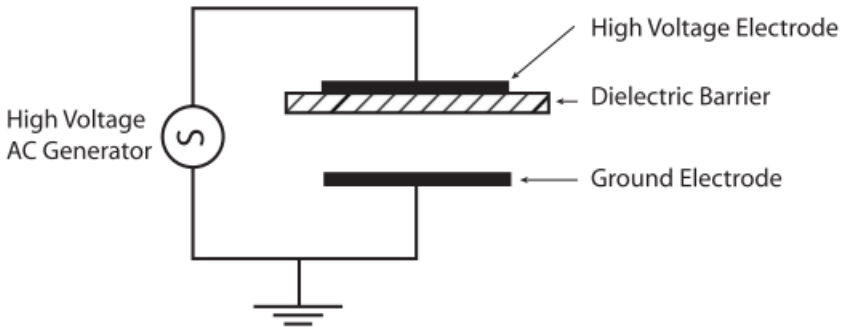

Figure 1.3 A general configuration of the dielectric-barrier discharge (DBD) which consists of a power supply, two electrodes and a dielectric.

As the current grows in a discharge, there is chance to form a spark or even an arc, as shows in Figure 1.2. To prevent this, a dielectric material, or an air gap, can be applied between the electrodes, hence a dielectric barrier discharge (DBD) device is formed. A DBD device generally consists of one or more layers of dielectric material that are sandwiched by two metal electrodes. The layer of dielectric can be made from a variety of materials, such as glass, quartz, ceramics, or other materials of low dielectric loss and high breakdown strength. A DC current cannot pass through a dielectric, so an AC, or pulsed DC, is usually required to operate a DBD. When a time-varying high voltage is applied (typically in the kV, kHz range), a strong electric field is formed between the two metal electrodes, which can break down the gas between the electrodes.

For a DBD operating at atmospheric pressure, the main source of 'seed' electrons is from photoionisation. In comparison to low pressure conditions, ions are more likely

to lose energy through collision with other particles, so they cannot be accelerated to the energy required for secondary electron emission. However, a portion of the neutral atoms are elevated to an excited state through collision with energised electrons. A portion of these excited atoms lose energy via a radiative decay and release a photon. If the photon has an energy high enough to ionise another atom, a new 'seed' electron is hence created and the electron avalanche process continues [3].

The growing electron avalanches create a net charge density where a self-propagating streamer is formed. A streamer is a narrow ionised channel that bridges the electrode and the head of the primary electron avalanche. As the density of electrons and ions increases, an internal electric field is generated inside the streamer, pulling the newly generated electrons towards the positively charged tail of the primary avalanche. As soon as the avalanche head reaches the other electrode, all the electrons flow into the electrode and leave an ionic trail in the gap, and the internal electric field of the streamer collapses at the same time. This process terminates the electron current in the conductive channel formed by the streamer and also leaves charges on the dielectric surface. As the charges accumulate on the dielectric surface, the local electric field is neutralised, resulting in the choking of the ionisation process and extinguishing of the discharge in a few nanoseconds [4, 5]. For this reason, an AC power input is usually required for the operation of a DBD. When the voltage polarity reverses, the charges deposited on the dielectric surface can help to create new avalanches and a large number of small streamers form [1].

A surface barrier discharge (SBD), or surface discharge, is a plasma device that is based on the principals of a DBD. The electrodes in a surface discharge are placed asymmetrically on both sides of a dielectric panel. This increases the non-uniformity of the electric field and thus decreases the breakdown voltage which is often considered an advantage. In addition, due to the distorted electric field, an Electrohydrodynamic (EHD) body force is created during the process of gas breakdown, making the surface discharge plasma a popular tool in aerodynamic researches [5].

1.2 Typical applications of laboratory plasmas

Plasma technologies have a wide spectrum of applications in industry. Depending on the characteristics of the plasma systems, the applications vary considerably. Due to the rich ions generated by the plasma in gaseous phase, surface treatment is widely applied to modify the property of different materials.

1.2.1 Low pressure plasma applications: Plasma surface modification

In the electronics industry, plasma etching plays a vital part in microelectronic circuit fabrication. The idea of plasma etching is to remove undesired materials from the surface and etch specific shape of trenches by applying a mask. Plasma can also be used in metal surface cleaning, with its rapid ion bombardment to react with the grease, oils, oxides, and fibres on the metal surface, providing a better condition for further processes such as bonding, soldering and gluing. Plasma treatment of polymer surface forms radicals that can increase the adhesion of the material. Further finishing such as painting and coating can be improved following plasma treatment. Plasma can also be used for polymerisation and deposit coatings on to a wide range of materials. Depending on the gas injection, different layers with different properties can be deposited on the material surface, such as hydrophobic layers, hydrophilic layers, and protective barrier layers. All these plasma surface treatment techniques have been widely applied in modern manufacturing, such as automotive, aerospace, home appliance, etc. [1].

1.2.2 Low pressure plasma applications: Energy efficient lighting

Lighting is one of the traditional field for plasma applications. 80% of the general lightings in our daily lives are plasma light sources, such as fluorescent lamp, high-intensity discharge lamps, low-pressure sodium lamps and light-emitting diodes [1] [2][6]. These light sources are widely used in offices, homes, factories, stores, and road ways. Among these light sources, mercury-containing fluorescent lamps have

an advantage of low power consumption and high efficiency compare to mercury-free ones, but have the cons in the toxicity of mercury [2]. Recently, a novel low-pressure metal halide discharge plasma lamp was reported with efficiency comparable to the mercury-containing fluorescent lamps but far less toxic [6].

1.2.3 Atmospheric pressure plasma applications: Plasma in environmental control

Each year, the industrial emission of SO_2 from power plants, steelworks, and oil refineries, that causes air pollutions, acid rain and other serious environmental pollutions. SO_2 released in air can be later oxidised in to SO_3 and then transfer into sulfuric acid (H_2SO_4) which leads to acid rains. Non-thermal atmospheric pressure plasma system can be installed and oxidise the SO_2 into SO_3 before it is released to the air. Non-thermal plasma can not only remove SO2, but also able to control the emission of NO_x and volatile organic compound (VOCs). VOCs are toxic pollutants and can lead to global warming. Conventional methods, such as carbon adsorption and catalytic/thermal oxidation, are cost too much annually and not efficient for large gas flow rate and low VOC concentrations. Non-thermal plasma is a popular alternative method in this situation for its low energy cost and high efficiency [1].

1.2.4 Atmospheric pressure plasma applications: Plasma in medicine

Plasma science and engineering is developing rapidly in the areas of biology and medicine. Plasma technologies are not only capable of basic surface decontamination but also more complicated applications like the treatment of living tissues, healing of wounds, blood coagulation, and treatment of skin diseases [7].

Non-thermal atmospheric plasma generates rich species of radicals, ions, excited atoms and molecules, and even UV radiation which make it a powerful microbial decontamination agent capable of inactivating viruses, fungal spore, and other microorganisms [7]. Consequently, non-thermal plasma has become a widely used

technique for surface decontamination, such as dry surface decontamination, liquid water decontamination, animal and human living tissue decontamination [7].

In addition to microbial decontamination, non-thermal plasma is able to assist blood coagulation in surgery. The traditional argon plasma coagulator was used in this application but could generate too much heat, causing localised tissue damage [7]. Recently, non-thermal plasma has been considered as a more effective means of blood coagulation without any thermal effects. Blood coagulation is important because the flowing blood can prevent wound closure and introduces a risk of microorganism invasion. Non-thermal plasma assisted blood coagulation can cause rapid coagulation of the flowing blood in a wound and at the same time, decontaminate the potential bacterial, fungal, or viral infection [1, 8].

1.2.5 Atmospheric pressure plasma applications: Plasma use in agriculture

According to the United Nations Food and Agriculture Organisation (FAO), in 2010, the total grain production of the world was approximately 2.216 billion tons, while the total consumption reached 2.254 billion tons, resulting a 38 million ton gap which led 9 million people in hunger [8]. As the progress of urbanisation and industrialisation, the demand of higher grain yield and grain quality has become the new challenge. Traditional methods to improve crop yield usually depends on the improvement of fertilisation and irrigation but limited by economic and environment. Novel methods merged recently including genetic engineering and plasma seed treatment.

Many reports stated that early germination of seeds could be achieved using cold plasma treatment [1, 9]. The penetration of plasma generated reactive species through the seed coat and directly affect the cells inside. The treatment can cause surface ablation and increase the transmission of oxygen and moisture to the embryo, resulting an increase in seed germination [9]. Experiments revealed that the cold plasma treatment of seed could increase the germination rate by up to 50 % [9]. Additionally, plasma treated seed resulted in better growth than

untreated ones. The plasma treated wheat was observed 21.8% higher in weight than the controls and the yield was found 5.89% more [8].

1.3 The challenge of water safety

People in many parts of the world still have no access to safe water and are blighted by water-borne and foodborne illness. The contamination agents, such as bacteria and fungus, are highly sensitive to the non-thermal plasma generated species. Given the low power and low cost nature of non-thermal plasma devices, such technology present a very promising solution for food and water decontamination [9].

Water is essential to sustain life and access to safe potable water is vital, despite this, ensuring potable supplies still remains a global challenge. Contaminated drinking water is a significant environmental contributor to the human disease burden. In 2011, approximately 768 million people still relied on inadequate water supplies, which are thought to have high levels of chemical and pathogen contamination [10]. Contaminated potable water is one of the most important risks to human health and contributed averagely 1.9 million deaths each year [11]. Bacterial contamination of potable water is the most common cause of disease compared to chemical contaminants. In 2012, over 500,000 people were killed due to Diarrhoea caused by inadequate potable water and estimate 3000 children were killed each day from diarrheal diseases [12].

1.3.1 Waterborne disease outbreaks

Although most of the threats are in low-income and developing countries, waterborne disease is still a burden for people living in developed countries. In the USA, it has been estimated that each year, inadequate drinking water contributes to 10 % of all hospitalisations. From 1991 - 2002, 207 cases of waterborne disease outbreak (WBDO) and 433,947 illness were reported in USA. While in UK, from

1991 - 2000, there were 38 WBDO and more than 4000 cases of illness reported [14, 15].

Most bacterial pathogens can infect the gastrointestinal tract via faecal-oral route, in which pathogens in faecal particles passing from one host to the oral cavity of another host. Etiologic analysis has shown that the most common bacterial pathogens implicated with WBDO include Salmonella, *Cryptosporidium*, *norovirus*, *E. coli*, *Campylobacter* and *Legionella*. *Legionella* was responsible for 55% of WBDO's in 2001 in USA; these are typically linked to contaminated distribution systems. In 2012, 92,438 confirmed cases caused by Salmonella were reported in the EU, meaning a rate of 21.9 cases per 100,000 populations [13–15].

1.4 The challenge of food safety

Besides water, food is also essential to sustain human lives as it provides nutrition to the body. Access to safer food is important to human health and is a global challenge area. However, food security and safety remains as a huge challenge to society. According to the World Health Organisation (WHO), there are an estimated 600 million people that suffer from foodborne illness (2010 data) and approximately 420,000 die due to the consumption of contaminated food [15]. Although children under 5 years of age take up only 9% of the global population, a disproportionate 43% of all foodborne diseases are among this group. In addition, pregnant women and elderly are at a greater risk from common foodborne diseases, as foodborne pathogens take advantage of their weaker immune systems [15].

Critically, it is in developing countries where challenges such as unsafe water is used for cleaning and processing of food products; inappropriate and poor food processing and handling; lack of adequate food storage infrastructure or poorly enforced food safety regulations have an enormous impact. All these factors contribute to making developing regions a high-risk situation. In addition, regions in tropical climate also suffers from pests and the natural emergence of toxins and parasitic diseases, including worm infestations [16].

Due to increased poverty and a challenging environment, it is difficult for people living in developing countries to prevent and deal with foodborne disease. According to research from the WHO, foodborne illness perpetuates the cycle of poverty for many living at or below the poverty line [15]. As the symptoms of foodborne illness can range from mild nausea, vomiting and diarrhoea to life-threatening cases, like kidney and liver failure, brain and neural disorder to even potential cancer, which may lead to long periods of absenteeism and premature death [15]. Foodborne diarrhoeal diseases are lethal particularly to malnourished infants and children. Infections from this disease in turn exacerbate the malnutrition and lead to a desperate circle of debilitation and mortality. Even those children who survive may still suffer from delayed physical or mental development which deprive them from fulfilling their full potential in society in the future.

Beyond the individual level, food safety issues negatively affect a region's economic development, especially in agriculture, food industries, food export and tourism. Agreement on the Application of Sanitary and Phytosanitary Measures (SPS) of the World Trade Organization (WTO) is the regulatory requirement for international food export and those that failed to meet the requirement may suffer significant economic losses from food export [15].

1.4.1 Foodborne disease outbreak

Foodborne illnesses are usually infectious or toxic in nature and caused by bacteria, viruses, parasites or chemical substances entering the body through contaminated food or water. Table 1.1, highlights the origin of foodborne illness worldwide, indicating that 91.3% of the foodborne illness were caused by diarrhoeal disease agents, such as norovirus and *E. coli*, and 5.8% were due to invasive infectious disease agents, like *Hepatitis A* virus and *Salmonella*, the rest, nearly 2.8%, were caused by parasites, like Helminths and Trematodes, and Chemicals and toxins [15].

Table 1.1 Global number of foodborne illness and deaths by WHO (2010).

Hazard	Foodborne Illness	Foodborne Death
Diarrhoeal disease agents	548,595,679	230,111
Viruses	123,803,946	34,929
Bacteria	349,405,380	187,285
Protozoa	67,182,645	5,558
Invasive Infectious disease agents	35,770,163	117,223
Viruses	13,709,836	27,731
Bacteria	10,342,042	85,269
Protozoa	10,280,089	684
Helminths	12,928,944	45,226
Cestodes	430,864	36,500
Nematodes	12,285,286	1,012
Trematodes	218,569	7,533
Chemicals and toxins	217,632	19,712
Total	600,652,361	418,608

In the case of diarrhoeal diseases, norovirus is a major concern, as are the bacteria including *Campylobacter spp.*, Enteropathogenic *E. coli* – EPEC, Enterotoxigenic *E. coli* – ETEC, Shiga toxin-producing *E. coli* – STEC, Non-typhoidal *S. enterica*, *Shigella spp.* and *Vibrio cholerae*; for Protozoa, the species including *Cryptosporidium spp.*, *Entamoeba histolytica* and *Giardia spp.*. In terms of invasive infectious disease agents, the most common virus is Haptitis A virus, and the most common bacteria include *Brucella* spp., *Literia monocytogenes*, *Mycobacterium bovis*, *Salmonella* Paratyphi A and *Salmonella Typhi*. Other invasive infectious disease agents include *Toxoplasma gondii* for Protozoa; *Echinococcus granulosus*, *Echinococcus multilocularis* and *Taenia solium* for Cestodes; *Ascris spp.* and *Trichinella spp.* for Nematodes; *Clonorchis sinensis*, *Fasciola spp.*, Intestinal flukes, *Optithochis spp.* and *Paragonimus spp.* for Trematodes; finally, there are chemicals and toxins, like aflatoxin from *Aspergillus flavus*, Cassava cyanide and Dioxin.

It is noticeable that bacteria accounted for 59.9% of the foodborne illness and 65% of the death; virus, on the other hand, caused 22.9% of the illness and 15% of the death.

A report from the Centers for Disease Control and Prevention of the U.S. Department of Health and Human Services shows that, during 1998 to 2008, there were 13,405 cases of foodborne disease outbreaks reported in the U.S., which resulted in 273,120 cases of illness reported, 9,109 cases of hospitalizations and 200 deaths. Of all the cases reported approximately 45% were caused by viruses, 45% were caused by bacteria, 5% were due to chemical and toxic agents and 1% were caused by parasites [17].

In the UK, the Food Standards Agency released a report in 2002 that showed in 2000, there were estimate 1,338,772 cases of foodborne illness, 20,759 hospital admissions, and 480 deaths in England and Wales [18].

1.4.2 Environmental factors

Different regions have different food safety challenges. The situations differ by income level, diets, local environment, civil infrastructures and development of economics.

In developing countries, typical food safety concerns include: the inappropriate use of agricultural chemicals; the use of untreated or partially treated water; the use of sewage or animal manure on crops; the absence of food inspection, including meat inspection; a lack of infrastructure, such as adequate refrigeration; and poor hygiene, including a lack of clean water supplies.

In these countries, the food trader and the consumer usually have a closer connection. Traditional markets provide most of the fresh food and there are fewer processed and packed foods compared to developed regions. Also, street vendors are popular and supply a large portion of food consumed outside the home. Moreover, due to the lack of preservation infrastructure and storage, perishable food is often processed and consumed immediately [16].

However, as the economy develops in these regions, there are some trends that can increase food safety challenges in both developed and developing countries, which include changes in animal husbandry, changes in agronomic process, increase in international trade and travel, increase in susceptible populations and changes in life style.

In order to maximise productivity, intensive animal husbandry practices have been applied in industry. One disadvantage of this is that it has increased the prevalence of human pathogens in flocks of production animals, for example, *Salmonella* can be found on poultry, cattle and pigs. In addition, the increased dose of antibiotics used in crowded animal farms has been linked to the emergence of new strains of antibiotic-resistant bacteria [15].

As to agricultural practices, the use of manure, chemical fertilizers, untreated sewage and irrigation system have increased the food safety risk associated with fresh fruits and vegetables. Outbreaks linked to fruits and vegetables have increased in some regions. For instance, the *E.coli* O157:H7 outbreak in Japan in 1996 resulted in 9,000 hospitalised and the *E.coli* O104:H4 outbreak in Germany 2011 that has killed 53 people [16, 20].

An increase of international trade and travel promotes the rapid transfer of microorganisms from one region to another. The longer the time between processing and consumption of the food can result in higher opportunities for contamination and thus increasing the risk of foodborne illness. Also, persons can be exposed to foodborne illness pathogens that originate from thousands of miles away.

Meanwhile, due to advances in medical treatment, people are living longer, yet the use of antibiotic can indifferently kill essential bacteria within the human body. Thus, new strains of antibiotic-resistant bacteria or foodborne illness pathogens may have a higher chance to colonise and cause disease.

Finally, the habits and attitudes of consumers are also a key factor in foodborne illness. In both developed and developing countries, the share of food budget has

been increasingly spent on food prepared outside the home. Street food, ready-to-eat meals and takeaways have become an important part of the daily diet.

1.4.3 Conventional food decontamination methods in Food industry

From section 1.3 to 1.4.2 it is obvious to see that, despite a small percentage of chemical contamination, the leading cause of foodborne illness is linked to microorganisms or their products. Moreover, microorganisms also cause food spoilage, which leads to food waste and economic losses. Therefore, in order to produce food efficiently and safely, whilst minimising spoilage and the risk of illness, it is necessary to control microorganisms on food by reducing their numbers or completely eliminating them. To achieve this goal, several methods have been used, which include: limiting the access of the microorganisms in food; physically removing the microorganisms in food; preventing or reducing the growth of microorganisms and germination of spores present in food; and killing microbial cells and spores present in food.

Food pathogens come from many sources, sometimes it is impossible to fully prevent their access to food, but it is possible to control their initial load and minimise the risk to food safety. In the modern food industry, a high level of sanitation has been introduced to help reduce the microbial load from various sources at all stages of food processing and handling. From the very basic food-processing plant design, quality control of water and air, training of personnel to cleaning of processing facilities, significant efforts have been implemented to minimise the opportunity for contamination of food products by pathogenic bacteria and thus reduce the incidence of foodborne diseases. Such efforts are both time consuming and costly, with new approaches being constantly sought to expedite the sanitation process without compromising the safety [20–22].

During food processing, microorganisms can also be physically removed from solid and liquid foods in order to control the microbial level. For liquid foods, like milk, fruit juice and syrups, centrifugation is used to remove some undesirable substances, such as dust and solid particles. Under high force, 90% of the microbial

population can be removed due to their heavier mass. For other liquid drinks, such as beer, soft drinks and wine, due to their sparkling nature, in which centrifugation is not appropriate, filtration can be used to remove undesirable solids and microorganisms. In addition, damaged fruits and vegetables which have a greater chance of microbial contamination and spoilage are usually trimmed, so that parts contaminated with microorganisms are removed. Trimming can also be used for food products with visible mould growth and spoilage, such as cheeses, bread, fermented meat products and sausages. However, just removing the visible tainted area by trimming is often not efficient enough to remove the pathogens nor the toxin produced by some strains of fungi from the surrounding areas.

Washing is another common physical decontamination method. Fruits and vegetables are washed regularly to remove soil and microorganisms from dirt; some meat products, like chicken and turkey, are also washed to remove gut materials and blood stains. Yet spray washing process can spread undesirable microorganisms and result in unexpected contaminations [20].

Heating, in the processing of food is not only a way of cooking but also a method to destroy vegetative cells and spores of microorganisms, including moulds, yeasts, bacteria and viruses. Heating of food can help destroy some enzymes that would affect the quality of food. Sufficient heating can degrade some heat sensitive toxins so that food will not cause health issues. Usually, holding food at a temperature above 50 ºC, often around 60 ºC for a certain amount of time is required to achieve the control of growth of many microorganisms, such as the pasteurization method for milk preservation. Unfortunately, while heating is extremely effective, it is unsuitable for many products such as fruit and vegetables and can have a negative impact on organoleptic properties [20].

In contrast to heating, lowing the temperature can also preserve food by preventing or reducing growth of microorganisms. Low temperature as well reduces metabolic activities of many microbial enzymes, especially for those heat-resistant proteinases and lipases. Freezing can also be lethal to microbial cells, 90% or more of the population can die during low temperature preservation. Although germination of spores is reduced, low temperature cannot kill spores [20].

Microorganisms need water for basic biological functions such as transport of nutrients, nutrient metabolism, and removal of cellular wastes. In food, the moisture is present in two ways, namely, free water and bound water, and only the former is important for microbial growth. When reducing the free water in food, microbial cells will suffer reversible damage and death. Thus, drying of food can effectively reduce the growth of microorganisms and germination of spores, and in such way the food can be preserved. Common drying method can be used on fruits, vegetables, fish, meat, and milk, however, depending on the situation, some strains of pathogenic bacteria, yeasts and moulds can still grow during drying [20].

As technology develops, there are many novel food preservation techniques that have started to emerge in order to meet the changes in consumer demand. The desire for fresh food and food with lesser preservatives has increased. In the early 20^{th} century, food preservation of packaged food using a modified gas atmosphere, typically nitrogen (N_2) or carbon dioxide (CO_2), was invented. In a high concentration of CO_2, the growth of moulds can be greatly reduced and ripening of fruits and vegetables can be delayed, as many of the metabolic activities are dependent on the level of oxygen (O_2). In raw meat, a composition of 75% CO_2, 15% N_2, and 10% O_2 is found to be most effective composition to limit the growth of *P. fragi* [20]. The advantage of this method is that the shelf life of fresh food is prolonged and no physical damage nor chemical substance is left on the food. However, even under these conditions, anaerobic and facultative anaerobic bacteria can still grow [20].

Chemical antimicrobial preservatives are also used in food to kill undesirable microorganisms or to retard their growth. But these chemical substances are either harmful to human body, such as Nitrites (NaNO2 and KNO2) that can cause potential cancers, or can affect the nutritional value of the food, such as sulphur dioxide and sulphites destroying vitamin B1 [20].

More recently, more advanced food processing technologies have been studied. Such as microwave and radio-frequency processing, pulsed electric fields, high-pressure processing, ultrasound, ultraviolet and non-thermal plasma processing methods [1].

Of these new methods, non-thermal plasma has shown enormous promise as an effective and low-cost means of food preservation. Non-thermal plasma is proven to be very effective in killing bacteria, yeasts, moulds and other hazardous microorganisms, including spores and biofilms that are generally very difficult to inactivate by conventional methods. In addition, the plasma method may be suitable for a large range of food types due to its non-thermal and gaseous nature. Although plasma food processing is regarded as a promising technique in future food industry, its elementary mechanism and potential hazardous effects are still under study and investigation. This thesis aims to address some of the gaps in our understanding relating to the application of plasma to food and water for the purpose of decontamination.

1.5 Outline of the thesis

Chapter 1 introduces the basic principles of plasmas and their typical applications. Followed by the background of the food safety challenges recently and potential of plasma techniques in food industry.

Chapter 2 comprises a comprehensive review of the plasma for food-borne pathogen decontamination in recent years. The review includes the plasma sources and configurations that has been used in food-borne pathogen decontamination studies, the exploration of the plasma microbiocidal mechanisms and a highlight of recent food sample decontamination experiments.

In Chapter 3, the plasma sources, experimental setups and the diagnostic method for plasma are elaborated. The details and principles of the experimental equipment used in this study is presented. Also, the designs of the plasma sources are discussed.

In Chapter 4, the characterisation results of the plasma system described in Chapter 3 is presented. Two scenarios are considered during the experiment, namely the afterglow species in gas phase and species interact with the liquid phase. This chapter not only talk about the test of the plasma systems but also determine the

optimal power conditions of systems for reactive species generation. In later experiments, the setups are optimised based on the results of the characterisation.

Chapter 5 explores the plasma species transport. Experiments are designed to determine the factors that can affect the mass-transport of the plasma generated species. Different geometric configurations of the plasma reactor are investigated. Optimisations inspired by the results are applied in the plasma system design for later experiments.

In Chapter 6, the plasma decontamination of bacteria in potable water and fungi on agar surface is discussed. In the first part of the chapter, the decontamination effect using plasma on potable water is described. Water samples inoculated with two strains of bacteria were subjected to treatment by the plasma system designed in Chapter 3 and used the power conditions set in Chapter 4. The second part involves the decontamination of fungi spores using plasma treatment. The results are presented and discussed.

Chapter 7 investigated the plasma decontamination of muscle meat and packaging materials. Differ to the situation in Chapter 6, which was a typical laboratory model system, Chapter 7 describes a study aimed at real world application. Muscle meat samples and packaging materials were prepared according to industrial standards. The capability of plasma decontamination on muscle meat and packaging materials was explored and the effects of plasma on muscle meat quality was studied.

Finally, the overall conclusions are set down and the suggestions for future studies are presented in Chapter 8.

Chapter 2 Literature review

2.1 Sources for the generation of non-thermal atmospheric pressure plasma

This chapter focuses on the applications and evolutions of non-thermal atmospheric plasma sources in food and water decontamination area. In recent years, a wide variety of non-thermal atmospheric pressure plasma sources have been explored for food safety applications. There are many advantages of using non-thermal atmospheric plasma sources, primarily there is no need for a vacuum chamber compared to low- or high-pressure plasma sources. Consequently, atmospheric pressure plasma sources are usually lower in cost, easier to build and more flexible in certain conditions. Atmospheric pressure plasma sources vary in configuration, electrical parameters and input gases. Different configurations include parallel plates, jets, surface discharges etc.; the operating frequency can be DC, pulsed DC and sinusoidal from a few Hz right up to microwave frequencies (GHz). Also, they can be operated in ambient air, noble gases (He or Ar) or other mixtures of gases.

One of the most common configurations for non-thermal atmospheric pressure plasma generation is the dielectric barrier discharge (DBD). The DBD was first investigated by Siemens in 1857 for ozone generation applications [4]. Later, at the beginning of the 20th century, the DBD gained more attention and the first laboratory for extensive investigation of the DBD was built by Emil Warburg [4]. The characteristics of a DBD plasma has been thoroughly studied and investigated since then. The DBD's major contribution is its use as an ozone generator in numerous industrial applications. In the 1970s, modern diagnostic technology and modelling tools were applied in DBD plasma research, this led to a better understanding of the plasma physics and plasma chemistry and also the invention of more applications using DBD, such as surface modification, chemical vapor deposition, pollution control, etc. Later in the 1990s, the application of DBD plasma in the biology and medicine area was considered. The first report of using DBD plasmas for inactivation of bacterial was made in 1996 by Laroussi [22]. Later, more

reports of DBD plasmas researches in decontamination of microorganism has been published.

2.2 DBD atmospheric pressure plasma system configurations

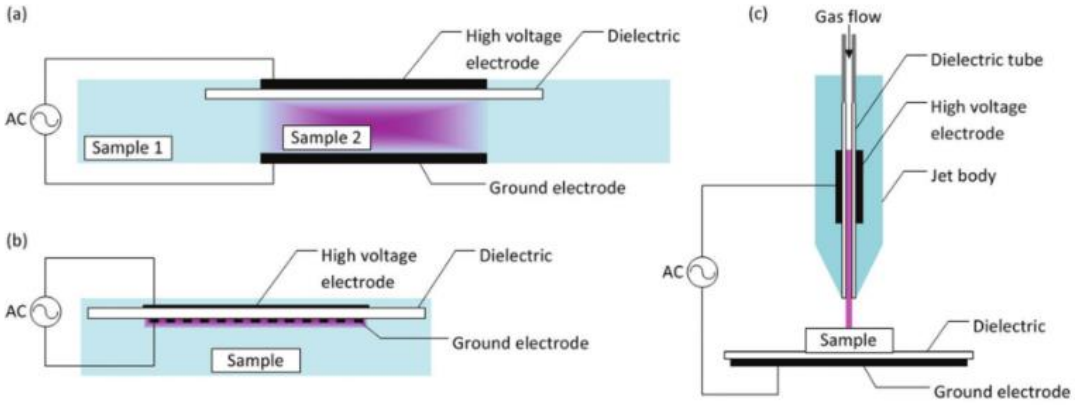

Figure 2.1 Examples of plasma actuator configurations, including (a) parallel plates, (b) surface discharge panel, and (c) plasma jets.

Some popular configurations of non-thermal atmospheric pressure DBD systems used in microorganism inactivation applications are shown in Figure 2.1 [24], namely, (a) parallel plates, (b) surface discharges and (c) plasma jets.

2.2.1 Parallel plate reactors

Parallel plates DBD systems consist of two parallel and separate electrodes which are usually fitted on the walls of a gas chamber, the plasma is formed in the space between the two electrodes. Samples are placed inside the gas chamber and are exposed directly to the plasma. Therefore, highly reactive and short-lived plasma generated species are impinging directly on the sample, which can lead to a better or more efficient decontamination effect, but, on the other hand, may well lead to a non-uniform treatment of the sample or excessive heating [23].

In 1996, research was done to show that bacteria can be inactivated by parallel plate DBD plasmas system. The feed gas used in the chamber was a mixture of helium and air, and the plasma system was operating at a frequency range of 300 Hz to 4 kHz and voltage up to 5 kV RMS. The sample consisted of *Pseudomonas fluorescens* inoculated in 10 ml suspension of YEPG (yeast extract polypeptone glucose) medium in a petri dish and a 6 log reduction after 10 minutes of treatment was observed [24].

Further exploration of the parallel plate DBD for microbial inactivation was conducted using other microorganism species, examples include *E. coli* inoculated on nitrocellulose filters and in liquid broth exposed to plasma generated at 17 kHz with 5 kV. On nitrocellulose filters, a 6 log reduction in 3 minutes was observed, while in liquid broth, only 2 log reduction was achieved in 10 minutes. *P. aeruginosa* was also test and it was shown to be more resilient than *E. coli*, taking 15 minutes for a 5 log reduction on nitrocellulose and only 1 log reduction in liquid broth in 15 minutes [22].

An enhanced version of the parallel plate DBD system was developed in 2002 by Laroussi [25], in which the basic configuration remained the same but the dielectric material was substituted for a high resistivity material. The advantage of using high resistivity layer is the limitation of discharge current and hence the prevention of arcing. This also allows the device to be operated using low-frequency power even DC power. A 4 log reduction of vegetative *B. subtilis* after a 10 minute plasma treatment using this resistive barrier device at 60 Hz with a 97/3% mixture of He/O_2 gas was reported [22].

In 2000, similar DBD devices were also tested and reported by the UTK (University of Tennessee at Knoxville) Plasma Science Laboratory, USA [26]. A variety of microorganisms were tested with discharges in ambient air with a maximum humidity of 14%. Under an applied voltage of 10 kV RMS and a frequency of 7 kHz, an initial loading of 6×10^6 cells of *E. coli* was completely inactivated after 25 seconds exposure time [27, 28]. The same device was used to test for inactivation of other microorganism species as well, including gram negative bacteria (*P. aeruginosa, S. marcescens*), gram positive bacteria (*S. aureus*), bacterial endospore (*B. stearothermophilus, B. subtilis var. niger, B. pumilus*), yeast (*C. albicans, S.*

cerevisiae), Virus (*Bacteriophage Phi X174*). The results showed that non-thermal atmospheric plasma is very effective against all these species on different surfaces, such as agar, glass, paper and polypropylene. For all the plasma treatments, at least 5 log reduction was achieved, depending on the treatment surface, the treatment time varies from 30 seconds to 15 min [28]. Another experiment using the UTK device was the inactivation of bacteria inoculated on to real food surfaces and showed that it was much harder to inactivate than those on fresh agar. The bacteria used was *L. monocytogenes*, a 1 minute exposure gave a 6 log reduction when treated on an agar surface, whereas it took 5 minute to reach the same inactivation on fresh iceberg lettuce [29].

The same group at UTK built an air filter system using multiple parallel plates. The electrodes were embedded in a chamber, and the test subject is place in a second chamber. A strong air flow is fed into the first chamber and the plasma generated reactive species transported into the second chamber. A 6 log reduction was observed for treatment of *S. aureus* in 10 minutes and a 4 log reduction for *bacteriophage Phi* X174 with the same treatment time. This device allowed the remote treatment using parallel plates, which reduce the heat dissipation, but inactivation rate was not as effective as the direct method [30].

2.2.2 Surface barrier discharge reactors

Another common configuration is the surface discharge, in which the electrodes are mounted asymmetrically on either side of a single piece of dielectric material. In this configuration, the plasma is only generated on the dielectric surface, and as a result, the reactive species are transported to the afterglow region by diffusion and Electrohydrodynamic (EHD) forces. When used in food decontamination applications, the treated samples are not directly in contact with the plasma but are only exposed to the longer-lived reactive species. This indirect treatment has proven to be effective against microorganism without leaving any heat damage to the sample. However, the decontamination effect can be weakened by the large distance between the plasma and the sample, effectively filtering the short-lived reactive species in some experimental arrangements [23].

An investigation exploring foodborne pathogen decontamination using a surface DBD discharge system was reported by Hähnal *et al.* in 2010 [31]. The configuration of the system used was very similar to the one shown in Figure 1(b). The system was operated with an applied voltage of 10 kV peak-to-peak and a frequency of 2 kHz in a pulse modulated mode of operation with a 50% duty cycle in ambient air. The microorganism species used was *B. atrophaeus*. The test results showed a strong dependence on ambient air humidity. At 60% humidity, a 4 log reduction was achieved after 150 seconds treatment time. The investigation also considered the impact of pulse modulation duty cycle, a 5 log reduction was achieved with 30% duty cycle in 5 minutes and an exponential correlation between the pulse on-time and reduction rate was concluded [28, 32].

Oehmigen *et al.* designed a round-shape surface discharge panel with a diameter of 50 mm in order to fit onto a petri dish to analyse the decontamination effect of microorganisms in a liquid solution. *B. atrophaeus* was inoculated into a 0.85% NaCl solution and a buffered saline solution (PBS). The experiment was conducted in ambient air with a pulsed sinusoidal voltage of 10 kV peak-to-peak, 20 kHz and with 33.8% duty cycle. The results showed a 6.5 log reduction from a 5 minute plasma exposure for bacteria in the 0.85% NaCl solution, while the bacteria in the PBS was only reduced by 3 logs following a 15 minute exposure. In addition, the pH value for the solution dropped as an effect of plasma treatment. For 0.85% NaCl solution, the pH value dropped to around 2.5, whereas the PBS stayed at 7 after the bacterial inactivation tests [32].

An experiment designed to decontaminate samples stored inside Tyvek packaging using a surface discharge was conducted by Eto *et al*. (2008). The device used a 40 mm by 40 mm resin panel as the dielectric and stainless steel mesh electrodes, an AC voltage of 2.5 kV peak-to-peak with a frequency of 5 kHz was applied so that the plasma would be generated on the mesh. In the experiment, the mesh electrode was directly contacted with the permeable side of the Tyvek packaging so that the plasma generated species could diffuse into the package. *G. stearothermophilus* spores were placed inside the packaging and plasma was ignited with different mixtures of N_2 and O_2. The maximum inactivation rate was observed with a 50%/50% mixture of N2 and O2 after 15 minutes of treatment time, in which all the spores were inactivated. In addition, the effect of humidity

was also explored. When air with a 64.4% humidity was used, a complete inactivation was achieved within 5 minutes of plasma exposure [33].

Another device, named PlasmaLabel, was aimed at treatment of products sealed inside the package was designed by Schwabedissen *et al*. in 2007 [34]. The device used an enclosed package as the dielectric, and two pieces of high voltage electrodes were mounted on the outer side of the package, while the ground electrode was mounted on the inner side of package. The material of the package was polycarbonate (PC) and the electrodes were made of aluminium tape with plastic layers. The plasma was formed in the ambient air inside the package, with an applied voltage of 8 kV peak-to-peak and frequency up to several kHz. *B. subtilis* inoculated and spread on a paper strip was tested and a 4 log reduction within 10 minutes of exposure was shown. Later the device was tested with cherry tomatoes and strawberries. Both treated group and control group were sealed in rigid plastic containers at room temperature. Mildew started to grow on untreated samples after 14 days, whereas no effects showed on treated ones [34].

2.2.3 Plasma Jets

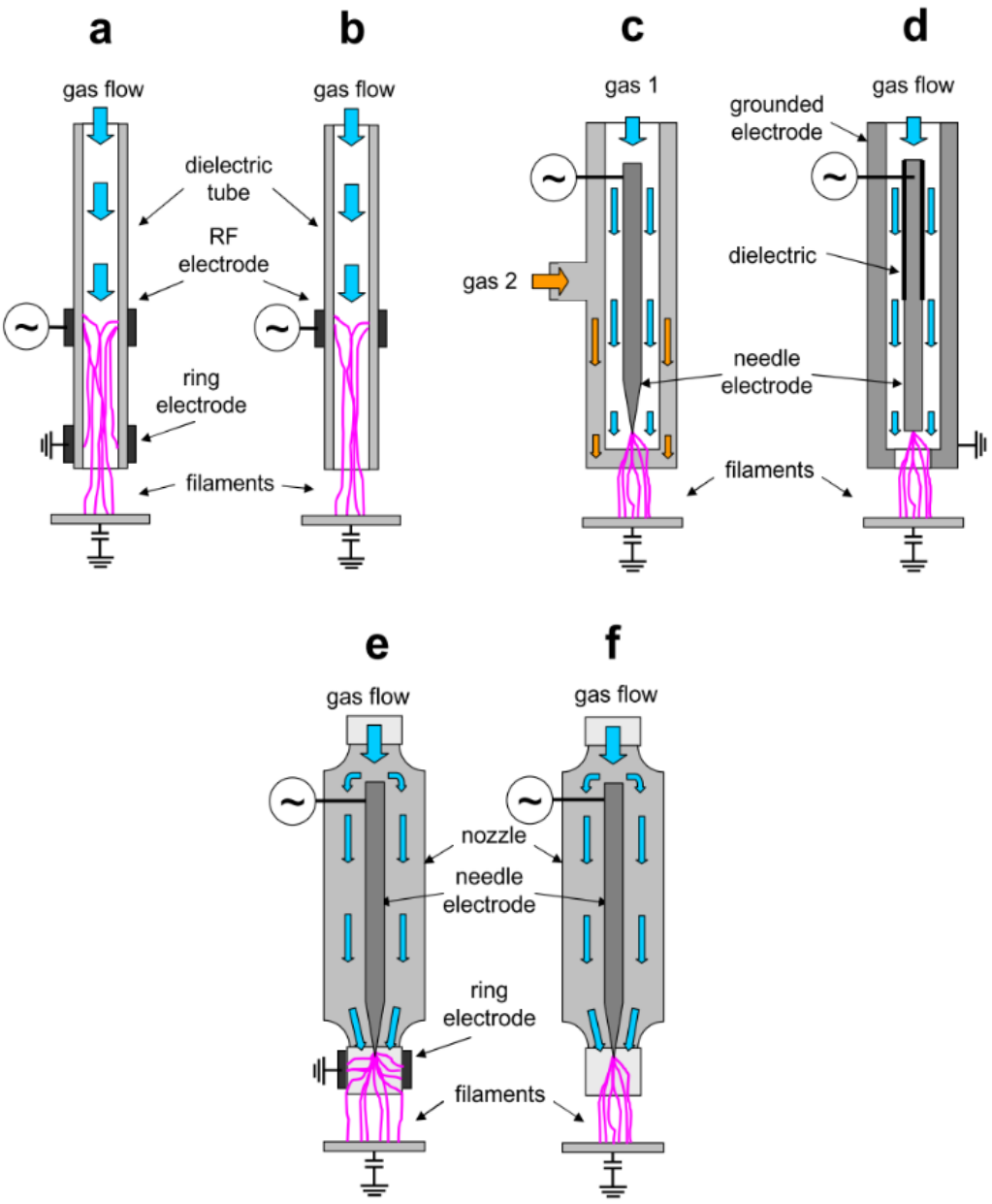

Figure 2.2 Configurations of plasma jets. Commonly consist of a wrapped tube and some have a ring electrode or a needle electrode.

Plasma jets, or atmospheric pressure plasma jets (APPJ), are another popular system widely used in food safety applications. Depending on the configuration of the electrode, a jet is suitable for both direct and indirect treatment of a sample. A

common configure of the plasma jet consists of a high voltage electrode inserted within or wrapped around a dielectric tube, with a noble gas flowing through, as in Figure 2.2. The tubing of the jet typically serves as the dielectric layer, but in some cases the tubing can also be made of metal so as to use as the ground electrode. In all jet applications, a plasma plume forms and projects through the nozzle, delivering all the reactive species onto the sample. Depending on the feeding gases, the reactive species can be customised for different applications. One limitation of the APPJ is that the diameter of the jet nozzle is typically of millimetre dimensions, which limits its application in large area treatments. Plasma jets are frequently used in applications involving narrow gaps and complex geometries, such as micro structured cavities or capillaries; and the small dimension has the advantage of dealing with precise treatment, which makes it very often used in biomedical applications, such as dentistry [24, 28, 36, 37].

APPJs have a variety of configurations and driven by different power sources, as shown in Figure 2.2, (a) and (b) are configurations of DBD jets, the rest are non-DBD jets that use RF or MW power supplies.

The first use of a plasma jet for biological decontamination was reported in 1999 by Herrmann *et al.* [37]. The jet employed a coaxial configuration and was powered using RF excitation, it was designed for the decontamination of biological and chemical warfare agents. The RF power was applied at 13.56 MHz with a maximum dissipated power up to 250 W, under such conditions the gas temperature reached a maximum of 150 °C. The feed gas was a mixture of O_2 and Helium at a ratio of 0.7% to 1 %. The microorganism used was *B. globigii* which is a variation of the deadly warfare agent *B. anthracis*. *B. globigii* spores were inoculated in 10 µl solution with an initial population of 10^7 Colony-forming Unit per millilitre (CFU/ml), and then spread and dried on glass surfaces for plasma treatment. After plasma treatment, the results showed that it only required 4.5 seconds to reach a 1 log reduction and a total inactivation was achieved in a 30 second treatment time. To match the thermal effect, a further examination using hot gas heat up to 175 °C blow through the APPJ without plasma ignition and a 2.5 log reduction was observed [37].

Another RF coaxial jet was reported in 2005 by Sladek and Stoffels. Using a 4 mm inner diameter Perspex tube as the nozzle and a 0.3 mm metal pin as the electrode plasma was generated in flowing helium gas at flow rate of 2 standard litre per minute (SLM). The electrode was driven at a frequency of 13.05 MHz and the dissipated power was up to 350 mW. *E. coli* inoculated on to agar plates with an initial concentration of 10^8 CFU/ml was used as the test subject and the distance between the pin electrode and agar surface was fixed at 1mm. The plasma treatment resulted in the formation of a bacteria-free circular area on the agar surface, the diameter of which was found to change as a function of treatment time and dissipated power. When using a power of 180 mW and treatment time of 10 s, a 6 mm diameter circle was formed; at 350 mW and with a treatment time of 60 s, the diameter of the circle increased to 12 mm [38].

A DBD plasma jet with a configuration similar to that shown in Figure 2(a) was designed and tested in 2006 by Laroussi *et al.* [39]. The dielectric tube of the jet was 12 cm long and had a diameter of 2.5 cm, two copper ring electrodes were mounted at 0.5 cm and 1 cm from the nozzle. The applied voltage was a 5 kV square pulse at a repetition rate of 1 - 10 kHz, the total power consumption was approximately 15 W. The plasma was ignited in a 1 – 10 SLM flow rate of Helium and 0.75% O_2 gas mixture. *E. coli* was inoculated on to agar plates, after 30 seconds of plasma treatment, a small area where the plasma had impinged on the agar surface showed complete inactivation. As the treatment time increased, the inactivation area also increased [39].

In 2007, a plasma jet device with a configuration similar to Figure 2(d) was reported by Uhm *et al*. [40]. The jet was made by using two dielectric coated coaxial cylinders: the inner one used as driven electrode and the outer one used as ground electrode. A radiofrequency power supply was applied to the driven electrode with a frequency of 13.56 MHz and a power up to 150 W. The microorganism used for the tests was *Bacillus atrophaeus* spread on to glass plates with a population of 2 x 10^9 spores/ml. In addition, the distance between the jet nozzle and the sample surface was fixed at 0.5 cm. The feed gas was argon with oxygen mixture, the volumetric percentage of oxygen was varied from 0 to 1 vol%. The optimum combination was using 0.15 vol% oxygen at 120 W power output.

The best decontamination efficiency was shown at 120, 130, and 150 W with oxygen volumetric percentage namely at 0.15, 0.25 and 0.35 vol% [40].

Another microorganism decontamination experiment carried out using a plasma jet with a configuration similar to that shown in Figure 2.2(e) by Daeschlein *et al*. [36]. The jet capillary was made from a quartz tube with an inner diameter of 1.6 mm, though which an 8 SLM argon gas flow was directed; the high voltage electrode was a metal pin with a diameter of 1 mm that was inserted in the tube. The system was driven by a 1.5 MHz, 1 – 5 kV voltage input. The plume of the plasma extended a length of 12 mm from the jet exit and heat up to 50 °C was measured depending on the dissipated power and gas flow rate. In the inactivation experiments, *S. aureus*, *P. aeruginosa*, *E. faecium*, and *C. albicans* were considered, these common wound pathogens were inoculated on to blood agar plates with an initial population of 7 x 10^2 CFU/plate. The treatment distance between jet nozzle and agar surface was fixed at 7 mm and for each species 20 agar plates received treatment. The results differed among different species, for *P. aeruginosa*, 19 out of 20 agar plates showed a complete inactivation; for *S. aureus* and *C. albicans*, 8 out of 20 agar plates showed total inactivation and for *E. faecium*, there was no inactivation observed [36].

Due to the simple configuration and low-cost components, plasma jets can be tailored for specific applications. A jet specialised for the decontamination of catheters was designed by Ehlbeck *et al*. with a configuration similar to that shown in Figure 2.2(e). A T-shaped quartz nozzle mounted at the end of the jet was used, so that the catheters could go through and be treated. The jet was operated with a total power dissipation up to 20 W at 27.12 MHz and the feed gas was pure argon or argon with 0.25% air admixture. In order to examine the decontamination efficiency, *S. aureus* was spread on to the catheter surface. The results indicated a 5 log reduction for pure argon treatment and a 6 log reduction for the mixture of argon and 0.25% air [41].

Another plasma jet device was designed specifically for the decontamination of fruit cutting surfaces by Kong *et al*. [42]. The electrode configuration was similar to that shown in Figure 2.2(b), the tubing was made of ceramic with an inner diameter of 1.5 mm. The powered ring electrode was warped around the tube and the ground

electrode was placed 1 cm below the nozzle. The plasma was ignited in a mixture of 5 SLM Helium and 0.025 SLM Oxygen, and an 8 kV peak-to-peak AC power supply with a frequency of 30 kHz. The maximum temperature measured on the ground electrode when operating was 30 °C. The samples selected for the study were two common foodborne pathogens, namely, *E. coli* and *L. monocytogenes*, and two common fruit spoilage organisms, namely *G. liquefaciens* and *S. cerevisiae*. The species were cultivated in melon (*Cucumis melo* var. reticulatus) and mango (*Magifera indica*) juices, which were spread on fruit cutting surfaces, with an initial concentration of $10^6 – 10^7$ CFU/ml. The result of the experiment showed that a 2 log reduction for *G. liquefaciens* in mango juice was achieved after a 10 seconds exposure. For *E. coli* and *L. monocytogenes*, a 2.5 log reduction was observed on mango juice spread following a 30 second plasma exposure. A similar reduction was observed on *S. cerevisiae* after 40 second exposure on mango juice spread. However, for samples on melon juice spread, no significant inactivation was observed [42].

2.2.4 Other configurations

A flexible DBD device was reported by Kim *et al*. [43]. The system consists of a biocompatible tubing as the dielectric layer and a metal wire inserted into the tubing serving as the powered electrode. The device was wrapped around the sample to be treated, and the plasma was generated on the outside surface of the tubing in the ambient air. In one investigation, the tested sample was a whole chicken and the plasma was operated at a voltage of 15 kV peak-to-peak and a frequency of 32 kHz. Scanning electron microscopy was used to show that the dielectric tubing was not damaged during the discharge, but no further biological analysis was reported [43].

A food decontamination device using an afterglow corona discharge in air was designed and reported by Mok *et al*. [44]. The system contained a treatment chamber, in which samples were placed, connected to an air pump that was used to introduce air into the chamber with a flow rate of 2.5 m/s. In between the pump and the treatment chamber, a corona discharge electrode was mounted. The

system operated using 20 kV voltage pulses at a repetition frequency of 58 kHz. A mixture of E. coli, S. aureus, B. cereus, L. monocytogenes, V. parahaemolyticus, and S. typhimurium was cultured in broth for the test. The temperature of the treatment chamber was also monitored and maintained at 40 °C. The inactivation rates were presented as D-values (time required to achieve 1 log reduction) that refer to the decimal reduction time. As a result, the D-value range from 3.6 to 12.8 s depending on different microorganisms [44].

2.3 Mechanisms of Plasma microorganism inactivation

Non-thermal atmospheric pressure plasma has shown great potential to inactivate a wide range of microorganisms, yet in order to optimise its efficacy and efficiency in practical applications, it is important to understand the mechanisms underpinning the microbial inactivation effect. Plasma discharges contain a complex mixture of charged particles, reactive species, UV photons, high temperature filament and intense electric fields. All of these agents play a role in microorganism inactivation and their simultaneous generation results in a synergistic interaction. In recent years, many experiments have been conducted in an attempt to determine the effects of each individual agent generated by the plasma. In this section, a review of the plasma inactivation mechanism will be presented.

2.3.1 Heat

Although non-thermal atmospheric pressure plasma has a much lower gas temperature than thermal plasma, the heat dissipated can still be effective for some heat sensitive microorganisms. From the previous section it is clear that most non-thermal plasma devices generate gas temperatures from 40 °C to 150 °C and many vegetative bacteria only have a heat tolerance up to 40 °C. A demonstration experiment conducted by Sladek and Stoffels has shown that *E .coli* could be inactivated by heat alone with a water bath of 42 °C for 5 min [38].

A comparison experiment was carried out to study the impact of gas temperature in plasma inactivation efficiency. A sample of *E. coli* was subjected to two treatments using the same plasma system with the same applied power for 60 s, but with different initial temperature: one at 37.8 °C and one at 43 °C. The results showed that the group exposed to higher temperature achieved 2 log more reduction than the one at 37.8 °C. For *E. coli*, the optimal cultivation temperature is at 37.8 °C, and they are very sensitive to higher temperatures, therefore for an application involving heat sensitive bacteria like *E. coli*, the heat dissipated by plasma can make a huge impact [30].

Sometimes, short-duration and localised high temperatures can contribute to the microbial decontamination effect. For instance, the non-thermal gliding arc discharge can be considered 'cold' on average, but instantaneous gas temperatures can exceed 1000 °C on short time scales potentially having a significant impact on the level of decontamination. Additionally, DBD's are considered strongly non-equilibrium and while the gas is close to room temperature in general, the streamers can reach localised temperatures of hundreds of degrees [1]. Even though heat is assumed not to play an important role in decontamination by itself, the temperature increase can additionally enhance the decontamination effect of other mechanisms that will be introduced in the following sections.

2.3.2 Ultraviolet (UV) radiation

Ultraviolet radiation has been demonstrated to be a significant role in microorganism decontaminations in low pressure plasma systems. DNA has an absorption peak around the 260 - 265 nm region, when UV radiation strikes a biological cell, most of the energy is absorbed by DNA. Depending on the condition and intensity of UV exposure, DNA damage could occur and be beyond repair resulting in the inactivation of the cell [45]. In atmospheric pressure air plasma systems, short wavelength UV radiation (< 300 nm) is mostly absorbed in the ambient air, consequently the dose to a sample is not particularly high and it is often assumed that plasma generated UV contributes very little to the inactivation of microorganisms [23, 28].

A reference experiment explored the impact of UV radiation in inactivation of *B. subtilis* spores using a helium plasma jet system. An optical filter that only allowed UV to pass was placed between the jet and the sample. Another group received normal plasma treatment (3 SLM helium flow rate and 6.5 kV driven voltage for 10 minutes). The normal plasma treatment resulted in a 4 log reduction of the *B. subtilis* spores, conversely, the UV treated sample showed only a 0.2 log reduction in 10 minutes [46]. In addition, many other researches showed similar results that UV radiation plays only a minor role in atmospheric pressure plasma microbiological decontaminations [23, 46, 48]. Nevertheless, the emission of UV radiation can be substantially increased with certain background gases. This makes UV radiation a potential important agent in atmospheric pressure microbiological inactivation applications under very specific experimental setups.

2.3.3 Charged particles

Charged particles in a low pressure plasma system are known to be highly effective for microorganism inactivation, in which high-energy ions bombard the microorganism resulting in the physical damage of cell membranes. However, in atmospheric pressure plasma, charged particles are considerably less energetic due to increased number of collisions with neutral particles in the background gas. In spite of this, several experiments considering charged particles effects in microorganism inactivation at atmospheric pressure have been reported in recent years.

A scanning electron microscope (SEM) was used to analyse bacteria following a parallel plate DBD treatment. The microscope images showed that the membranes of the *E. coli* were damaged, whereas the membranes of *B. subtilis* were intact, even though both of the bacteria were inactivated. The difference was attributed to the structure of the different bacteria. *E. coli* is Gram-negative bacteria that has a rougher membrane surface compared to the Gram-positive *B. subtilis*. It was suggested that the charged particles generated by the plasma could accumulate on the rough membrane surface and lead to the formation of a large electric field. As

the electric field increased, the electrostatic tension also increased until the bacteria cell wall could not hold and eventually broke down [22].

A similar experiment conducted by Gallagher *et al.* revealed the same finding as above using a glow discharge for the treatment of airborne microorganisms. After the treatment, the results showed that the culturability of *E. coli* was decreased whereas other bacteria showed no sign of membrane damage and were able to retain their viability [48]. Several researchers have presented the membrane damage caused by plasma treatment using SEM images, although it is not explicitly clear if such damage was caused by charged particles or through the etching effects of reactive neutrals [50–52].

An interesting investigation to compare the effects of charged particles and neutral species was reported Lu *et al.* [52]. The investigation employed a pulsed DC plasma jet system and considered a direct and indirect treatment. The direct treatment was conducted with the sample placed on a downstream ground electrode, whereas the indirect treatment was carried out with a ground electrode placed between the jet nozzle and the sample. The sample consisted of bacteria inoculated on an agar surface. The first group of tests were carried out using a He/N_2 gas mixture and the results showed similar levels of inactivation between direct and indirect methods. These results suggest charged particles played only a minor role in the microbial inactivation. A second group of tests used a He/O_2 gas mixture and showed the direct method to achieve a better level of inactivation compared the indirect one. In this group of tests, charged particles had an impact on inactivation. In a third group of test, pure helium was used as the feed gas, and the results indicated that the direct method was slightly better than indirect method for bacteria inactivation. The results of the experiments suggested that the neutral species played a large role in inactivation and the effect of charged particles was dependant on the feed gas composition. SEM and Transmission electron microscopy (TEM) were used to examine the impact of plasma treatment on the bacteria membrane. The images revealed that Gram-negative bacteria and yeast had membrane damage after the plasma treatment [54–56].

As well as electrical effects, charged particles may also exhibit a high degree of chemical reactivity introducing chemical effects in microbiological treatments. The

chemical effect of both charged and neutral species is considered in the next section.

2.3.4 Reactive species

Reactive species generated in a non-thermal atmospheric pressure plasma are believed to play the key role in microbiological inactivation. The reactive species include ground, metastable and excited states, many are short-lived and have high oxidation potentials. Many of the species produced can be grouped in the categories of Reactive Oxygen Species (ROS) or Reactive Nitrogen Species (RNS). The generation and composition of reactive Oxygen species and reactive Nitrogen species (RONS) in a plasma is highly dependent on the system configuration, such as background gas, temperature, humidity, driven power, etc. Nevertheless, typical RONS that can be detected from the air plasmas include O, O_3, OH radicals, hydrogen peroxide (H_2O_2), nitric oxide (NO), nitrogen dioxide (NO_2), nitrous oxide (N_2O), nitrite (NO_2^-), nitrate (NO_3^-) and peroxynitrite ($ONOO^-$). These species are known to have strong bactericidal effects and are considered to be the key species in bacterial decontamination applications. Table 2.1 presents a comprehensive of the reactive species generated in air plasma which is often used as a basis for computational simulations of air plasma [24, 46, 57–60].

Table 2.1 Species generated in air plasma.

Plasma region	Cations	N^+, N_2^+, N_3^+, N_4^+, NO^+, N_2O^+, NO_2^+, H^+, H_2^+, H_3^+, O^+, O_2^+, O_4^+, OH^+, H_2O^+, H_3O^+
	Anions	e, O^-, O_2^-, O_3^-, $O4^-$, NO^-, NO_3^-, H^-, OH^-, N_2O^-, NO_2^-
	Neutrals	N, N_2, H, H_2, H_2O, O, O_2, O_3, OH, HO_2, H_2O_2, NO, NO_2, NO_3, N_2O_3, N_2O_4, N_2O_5, HNO_2, HNO_3, N_2O, HNO
Afterglow region	NO, N_2O, NO_2, NO_3, N_2O_3, N_2O_4, N_2O_5, HNO, HNO_2, HNO_3, N, N_2, O, O_2, O_3, OH, H_2O_2, HO_2, H_2, H_2O	

Generally, both ROS and RNS have strong oxidative effects on the structure of microorganism cells. Cell membrane are made of lipid bilayers which consist of unsaturated fatty acids. This structure allows cell membrane to transport biochemical agents but unsaturated fatty acids are susceptible to OH radicals. The presence of OH radicals can compromise the function of the cell membranes [57, 61]. Also, many protein molecules are imbedded in the lipid bilayer, which control the transport of various biochemical compounds. These proteins are comprised of linear chains of aminoacids which are also susceptible to oxidative effects of RONS. For example, peroxynitrite ($OONO^-$) and NO_2 can oxidise proteins at different sites. In addition, similar damage caused by RONS can occur in nucleic acid (mainly DNA) as well. DNA can be damaged by oxides at both nucleic bases and at the sugars that link the bases. Excessive oxidative damage to the cell can results in the compromise of cellular respiration system, mutations or even cell death [5, 61, 62]. Moreover, NO can release iron from metalloenzymes and produce iron depletion. The presence of RNS can lead to nitrosylation of free thiol groups and cause the inactivation of metabolic enzymes in the cell [63, 64]. Also, the interaction of ROS and RNS can lead to the creation of a variety of antimicrobial species such as H_2O_2, O_2^-, $OONO^-$, NO_2, N_2O_3 and N_2O_4 [62]. Therefore, antimicrobial effect of plasma treatment is a result of synergistic action of both ROS and RNS.

2.4 Food related studies

A considerable amount of research in the use of cold plasma for food security applications have been carried out in recent years. Non-thermal atmospheric pressure plasma has shown promising antimicrobial effects, previous studied have not only focused on inactivation of food pathogens, but also on the direct treatment of actual food materials. In addition to the decontamination effect, the quality of food after treatment has also been investigated.

Experimental evidence has shown that plasma is capable of being applied to most kinds of food for the purpose of decontamination. In this section the recent investigation on different kinds of food are reviewed.

2.4.1 Vegetables & fruits

Table 2.2 shows the vegetative food decontamination applications using non-thermal atmospheric pressure plasma in recent years. A variety of vegetables, fruits and nuts were selected and used, typically these were inoculated with a range of different foodborne pathogens and a vast array of different cold plasma systems.

The recent literature indicates that cold plasma systems are quite effective for foodborne pathogen inactivation, generally a 1 – 6 log reduction can be achieved in timescales ranging from a few seconds to 15 minutes of plasma exposure.

In addition, post processed food quality was monitored as well. In many reports, food surface colour measurements were recorded in order to assess the impact of plasma to the food surface. In some reports, other nutritional properties, such as moisture level, vitamin C content, and even photosynthetic activity were measured and compared before and after the plasma treatment.

Wang *et al.* [64] conducted an investigation on plasma treated carrots, pears and cucumbers, L-ab colour spacing was used as colour measurement method. After 8 minutes of treatment using a plasma jet with compressed air at 15 W output power, the total colour difference ΔE* changed from 0.6 to 1.3, meaning a small change had occurred (total colour differences (ΔE*) are considered as very distinct (ΔE* > 3), distinct (1.5 <ΔE* < 3), and small differences (ΔE* < 1.5)). The plasma treatment also resulted in a < 5% moisture loss. Furthermore, vitamin C content was also measured. After the treatment, cucumbers, carrots and pears showed a vitamin C content loss of 3.6%, 3.2% and 2.8% respectively. Researchers suggested that vitamin C is light sensitive and the generation of UV from the plasma could have led to some degradation [64].

Baier *et al.* conducted a study on the plasma treatment of corn salad leaves, minor changes in total colour difference ΔE* after 90 seconds of cold plasma treatment was also reported. In this experiment, photosynthetic activity of corn salad leaves was measured. Results suggested that following treatment the leaves had severely lost their photochemical efficiency; however, the mechanism and reason was not revealed in the study and future investigations are required [65].

Table 2.2 Non-thermal plasma treatment of vegetables and nuts.

Food material	Pathogens	Results	Plasma set-up	Reference
Almonds	*E. coli*	5 log reduction in 30 seconds	DBD Air Direct	[66]
Almonds	*E. coli* O157:H7	1.3 log reduction in 20 seconds	Jet N_2 Direct	[67]
Apples	*Salmonella*	2.4-3.7 log reduction in 3 minutes	Gilding arc Air Indirect	[68]
	E. coli O157:H7	2.6–3 log reductions in 3 minutes		
Apples	*E. coli* O157:H7	2 log reductions in 2 minutes	DBD Indirect	[29]
	Salmonella	2 log reductions in 1 minutes		
	L. monocytogenes	1 log reductions in 1 minutes		
Apples	*E. coli*	4 log reduction in 20 seconds	Jet Argon, 1% O_2 Direct	[65]
Carrots	*Salmonella*	5 log reduction in 4 seconds	Jet Air	[64]

			Direct	
Corn salad leaves	*E. coli*	5 log reduction in 120 seconds	Jet Argon, 1% O_2 Direct	[65]
Cucumber	*E. coli*	4.5 log reduction in 60 seconds	Jet Argon, 1% O_2 Direct	[65]
Cucumber	*Salmonella*	1 log reduction in 4 seconds	Jet Air Direct	[64]
Lettuce	*E. coli* O157:H7	3 log reduction in 3 minutes	DBD O_2 Indirect	[69]
	Salmonella	5 log reductions in 5 minutes		
Lettuce	*Salmonella typhimurium*	2.7 log reductions in 15 minutes	Jet N_2 Indirect	[70]
Lettuce	*E. coli*	1.7 log reductions after 10 minutes	Needle Array Argon Indirect	[71]
Lettuce	*E. coli*	3.6 log reductions after 15 seconds	Jet Ar	[72]

			indirect	
Mango	*E. coli*	2.5 log reductions after 30 seconds	Jet He & O_2 Direct	[42]
	L. monocytogenes	2.5 log reductions after 30 seconds		
Cantaloupe	*E. coli*	1.5 log reductions after 40 seconds	Jet He & O_2 Direct	[42]
	L. monocytogenes	2 log reductions after 40 seconds		
	Saccharomyces cerevisiae	1 log reductions after 40 seconds		
	Gluconobacter liquefaciens	2 log reductions after 10 seconds		
Cantaloupe	*E. coli* O157:H7	3 log reductions after 3 minutes	DBD Air Indirect	[68]
	Salmonella	5 log reductions after 5 minutes		
Pear	*Salmonella*	1 log reduction in 4 seconds	Jet Air Direct	[64]
Potatoes	*Salmonella typhimurium*	0.9 log reduction in 15 minutes	Jet N_2 Indirect	[29]
Strawberries	*Salmonella typhimurium*	1.8 log reduction in 15 minutes	Jet N_2 Indirect	[29]
Tomatoes	*E. coli*	1.7 log reduction in 10 minutes	Needle Array	[71]

			Ar Indirect	
Tomatoes	*E. coli*	3.1 log reduction in 10 seconds	DBD Air Indirect	[73]
	Salmonella typhimurium	6.3 log reduction in 1 minutes		
Tomatoes	*E. coli*	3 log reduction in 20 seconds	Jet Argon, 1% O_2 Direct	[65]
	L. monocytogenes	4 log reduction in 20 seconds		

Attempts on inactivation of *A. flavus* using non-thermal plasma has been reported. S. Preechayan *et al*. has explored the capability of plasma decontamination on *A. flavus* by using glow discharge plasma [74]. The plasma electrode was set up in a glass tube with fans blowing the generated species into the sample chamber, in which were food samples, such as corn, bean, garlic, and shallot, incubated with *A. flavus*. The counted number of contaminated fungi was $7x10^4$ CFU/g before the treatment. The plasma was operated at a low frequency range of 400-800 Hz and the applied voltage at 30 kV. After a treatment of 30 minutes, the fungi on corn and bean was completely reduced, and in the case of garlic and shallot, there was $2x10^4$ CFU/g left.

Another attempt of eliminating *Aspergillus* using plasma was done by P. Basaran *et al*. using low pressure cold plasma using air and SF_6 as feeding gas [75]. The plasma operating condition was 1k Hz at 20 kV peak-to-peak voltage. The pressure of the plasma chamber was controlled at 500 mTorr and the temperature was maintained at 20-30 °C. For the treat sample, *Aspergillus parasiticus* (*A. parasiticus*) was inoculated on hazelnuts, peanuts and pistachio nuts. After a treatment of 5 minutes, 1-log reduction of CFU was achieved and a further 5 minute treatment resulted in addition 1-log reduction. The direct treatment of aflatoxins was also

conducted, with a 20-minute low pressure air plasma treatment, the total aflatoxins was reduced by 50%.

2.4.2 Meat & Dairy Products

Both fresh and processed animal products, such as pork, beef, chicken, eggs, bacon, and cheese were considered for plasma treatment to reduce foodborne pathogen inactivation. Table 2.3 summarises recent investigation using cold plasma to treat meat and dairy products.

Plasma decontamination of animal products, especially meat, has received an increasing amount of attention in recent years. The experiments listed in table 2.3 show a wide variation in decontamination efficacy from 1 – 6 log reduction with a treatment time up to 10 minutes for meat products. On the contrary, it usually took significantly longer to achieve a significant level of inactivation on eggs shells.

Due to the different chemical composition between vegetable and meat foods, the analytical methods employed to assess the impact of plasma exposure are also different. In meat treatment, typical properties under consideration include pH, surface colour and lipid oxidation. In an investigation reported by Kim *et al*. [76], pork cutlets were treated using a plasma jet with an O_2 and He mixture. The jet was driven by a 3 kV, 30 kHz bipolar square wave, the treatment times from 30 seconds to 10 minutes. After the plasma treatment, the pH value of the meat was examined. The pH value drop was observed to drop slightly from 5.4 to 5.3 after treatment, which was a minor change and this was probably due to the feed gas consisting of only He and O_2. In other reports using air plasma where large amount of RNS was generated, the pH value drop was more significant [77]. Surface colour is another property used to determine meat quality, this especially important to the consumer and off-coloured meat often goes unsold. The experimental results of Kim *et al.* revealed that the lightness of pork cutlet surfaces was decreased, as well as increased yellowness following plasma treatment. In addition, the redness was slightly decreased, however, the greenness increased slightly. This could be caused by the reaction of plasma generated hydrogen peroxide and the myoglobin in the

meat. Moreover, lipid oxidation was also investigated using the TBARS values, which is Thiobarbituric acid, a byproduct of lipid peroxidation. ROS were assumed to be the main species that contributed to the lipid oxidation. The TBARS value in a He and O_2 plasma treatment was found to be higher than those recorded using a pure He plasma alone, 0.51 and 0.35 respectively, compare to the untreated sample with a value of 0.31. These results indicate that oxygen species played the key role in lipid oxidation [76].

Choi *et al*. (2015) also reported the measurement of L-ab colour spacing on plasma treated pork. The plasma system he used was a corona jet using ambient air, with a frequency of 58 kHz and 20 kV output. The results were varied considerably depending on treatment time, a 30 second treatment results in ΔE* 1.54 total colour difference, whereas for 60 seconds, ΔE* was 4.42, for 90 seconds, ΔE* was 4.28, and for 120 seconds, ΔE* was 5.27. Additionally, the redness dropped significantly, while the yellowness increased slightly, and there was not much difference in lightness after treatment. In this investigation, no significant changes of the plasma treated pork TBARS value was observed [78].

Table 2.3 Non-thermal plasma treatment of meat and dairy products.

Food material	Pathogens	Results	Plasma set-up	Reference
Bacon	*L. monocytogenes,* *Salmonella typhimurium,* *E. coli* (Mixture)	4.6 log reduction in 90 seconds	DBD He & O_2 Direct	[79]
Beef (raw)	*Listeria monocytogenes*	1.9 log reduction in 10 minutes	DBD	[80]

	E. coli	2.57 log reduction in 10 minutes	Air Indirect	
	Salmonella typhimurium	2.58 log reduction in 10 minutes		
Beef (dry and cured)	*L. monocytogenes*	1.6 log reduction in 10 minutes	DBD Air Direct	[81]
Cheese (sliced)	*L. monocytogenes*	8 log reductions after 2 minutes	DBD He & O_2 Direct	[82]
Chicken (raw)	*Listeria innocua*	3 log reductions after 4 minutes	Jet He & O_2 Direct	[83]
Chicken (cooked)	*L. monocytogenes*	1.37 log reduction in 2 minutes (He) 4.73 log reduction in 2 minutes (N_2+O_2)	Jet He, O_2, N_2 Direct	[84]
Shell Eggs	*Salmonella enteritidis*	2.2–2.5 log reductions after 90 minutes at 35% Relative Humidity (RH)	DBD Air Indirect	[85]
	Salmonella typhimurium	3.8–4.5 log reductions after 90 minutes at 65% RH		

Ham	*L. monocytogenes*	1.9 log reductions after 2 minutes (He) 6.5 log reductions after 2 minutes (N_2+O_2)	Jet He, O_2, N_2 Direct	[84]
Ham	*L. monocytogenes*	0.25–1.73 log reductions	DBD He & O_2 Direct	[72]
Pork (raw)	*E. coli*	6 log reductions after 30 seconds	DBD Air Direct	[86]
Pork (raw)	*E. coli*	2.54 log reduction in 10 minutes	DBD Air Indirect	[80]
	L. monocytogenes	2 log reduction in 10 minutes		
	Salmonella typhimurium	2.68 log reduction in 10 minutes		
Pork (raw)	*E. coli*	1.5 log reduction in 120 seconds	Corona discharge Air Indirect	[78]
	L. monocytogenes	1 log reduction in 120 seconds		
Pork (raw, frozen)	*E. coli*	1 log reduction in 60 seconds		
	L. monocytogenes	1 log reduction in 120 seconds		

2.4.3 Food processing materials

Beside food itself, plasma has also been considered for the decontamination of food packaging materials and food processing equipment. As the protection for food materials during handling, transport and distribution, food packaging is required with high hygiene levels. It has been demonstrated that non-thermal plasma is effective in decontaminating many typical packaging materials, including polymer foils, aluminium foils, plastic trays, paper cups, and polyethylene terephthalate (PET) bottles [23].

An investigation exploring the decontamination of PET foils using two types of DBD plasma systems was reported by Heise *et al.* [87]. A parallel plate DBD device and a cascade DBD device were used in the experiment. *B. subtilis* and *A. niger* were inoculated and spread on to pieces of PET foil to mimic typical foodborne pathogen contamination. Different feed gases were considered including argon, nitrogen, and synthetic air (80% nitrogen + 20% oxygen). When using the parallel plate DBD system, a >4 log reduction of *B. subtilis* was observed in 10 seconds' treatment with argon and nitrogen as the feed gas, whereas less than 1 log reduction was observed using synthetic air. A 6 log reduction was achieved for *A. niger* using argon within 10 seconds of treatment, while for synthetic air the log reduction was halved. With nitrogen alone, only 1 log reduction was achieved with the same treatment time. On the other hand, when using cascade DBD device, a 6 log reduction was observed for decontamination of *B. subtilis* using Oxygen combined with a 282 nm flat lamp in a treatment time of 10 seconds. When the feed gas was changed to Argon no colony forming unite was observed after 10 seconds of treatment [87].

Decontamination of other packaging materials such disposable plastic trays (polystyrene), aluminium foil, and paper cups, were considered by Yun *et al.* [88]. The plasma system used was a cylindrical DBD with a floating ground, powered by a radio frequency source operating at a frequency of 13.56 MHz with a maximum output power of 150 W. *L. monocytogenes* was inoculated uniformly on to the various packaging materials. The decontamination results showed that, at 150 W output power and exposure time of 120 seconds, a 6.79 log reduction was achieved

on plastic trays, a 3.09 log reduction on aluminium foil, and a 2.85 log reduction on paper cups [88].

In another experiment, the DBD decontamination effect of a rotating cutting blade was investigated by Leipold *et al*. [89]. A 100 mm x 100 mm aluminium plate was used as the powered electrode and placed 2 mm above the rotating cutting blade which served as the grounded electrode. *Listeria innocua* (*L. innocua*) was inoculated on the surface of the blade and was later treated by air plasma with a discharge power of 0.36 kW. Results showed that a 5 log reduction was observed after a 340 second treatment and the temperature of the blade was found lower than 30 °C after the exposure.

2.5 Summary

In this chapter, a comprehensive review of the recent developments of DBD plasma devices and their food related studies was presented. Non-thermal plasma has shown great promise for the decontamination of both biotic and abiotic samples; however, there is still an enormous potential for improvement as there is a wide variation in the reported efficiency of the plasma technique and the treatment times are still far too long to be industrially relevant (ideally an exposure < 1 seconds to fit in with line processing speeds). Although the mechanism of plasma decontamination effect was briefly explained in the chapter, many antimicrobial pathways are still not fully understood. Most of the studies focused mainly on the decontamination efficiency, the changes in the organoleptic and nutritional properties of the plasma treated food by specific plasma conditions are yet to be investigated.

Chapter 3 Plasma source & diagnostics techniques

This chapter details the design and development of the plasma systems used for experiments throughout the thesis and the diagnostics techniques employed to understand it.

3.1 Plasma source

Chapter 1 and 2 shows that DBD systems can be highly effective for microbial decontamination, are low-cost to operate and can be developed to treat a large area. Based on this, it was decided to explore a DBD based device. Out of all the possible DBD configurations, the SBD was chosen because it is suitable for the large area generation of air plasma without requiring extremely high voltages. Additionally, the in-direct nature of the treatment prevents direct contact between hot filaments in the plasma and the food surfaces. It is also suitable for the treatment of both liquids and solids. However, a drawback of the configuration is the lack of mass transport of short-lived reactive species, such as OH and O.

3.1.1 Surface Barrier Discharge design

A Surface Barrier Discharge (SBD) is typically constructed on a flat dielectric sheet made from polymeric or ceramic materials. Electrodes are adhered to either side of the dielectric material. With one electrode held at ground potential and the other electrode raised to a high voltage using a time-varying voltage plasma forms around both electrodes. In this configuration, the visible plasma is confined to the edges of the electrodes, typically in a thin layer that extend 1 – 5 mm from the electrode edge. Highly reactive species are confined to the visible plasma region whereas longer-lived species are able to propagate beyond the visible region. It is generally assumed that longer-lived species diffuse in to the afterglow region (away from the plasma region) but this is not the only mechanism capable of mass transport. Electrohydrodynamic (EHD) forces produced by charged particles drifting in the electric field result in a flow of the neutral fluid surrounding electrode. The

details of the EHD force will be presented in Chapter 5. The flow generated by EHD forces can reach several m/s and manipulation of the electrode configuration on the dielectric surface can be used to steer the direction of the fluid flow to enhance mass-transport [90].

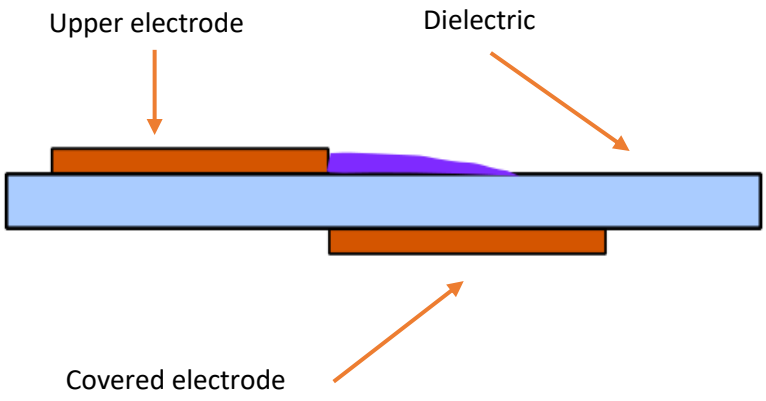

Figure 3.1 The cross section of a surface barrier discharge reactor design.

Figure 3.1 shows the cross section of a basic SBD plasma reactor design, with a quartz dielectric in the sandwiched between two copper electrodes. When a high voltage input is applied to the upper electrode and the lower covered electrode held at ground potential, the plasma discharge forms on the dielectric surface around the edge of the powered electrode. The direction of the electric field causes charged particles produced in the plasma to move toward the electrodes. Given that positive ions have a significantly larger mass than electrons, they are capable of imparting momentum on the background neutral gas through collisions, resulting in a gas flow in a given direction. In Figure 3.1, the induced flow occurs from the left to right of the Figure. The addition of a second powered electrode, at the opposite side of the covered electrode would induce a flow in the opposite direction (right to left). When the two induced flows meet, they coalesce resulting in a flow that moves away from the dielectric surface in a perpendicular fashion.

In Figure 3.2 shows the different designs of SBD reactors used in the project, (a) is a single strip shaped design; (b) is a multi-strip shaped pattern design; (c) is a mesh electrode design; (d) is a ceramic dielectric panel with stainless steel strips design.

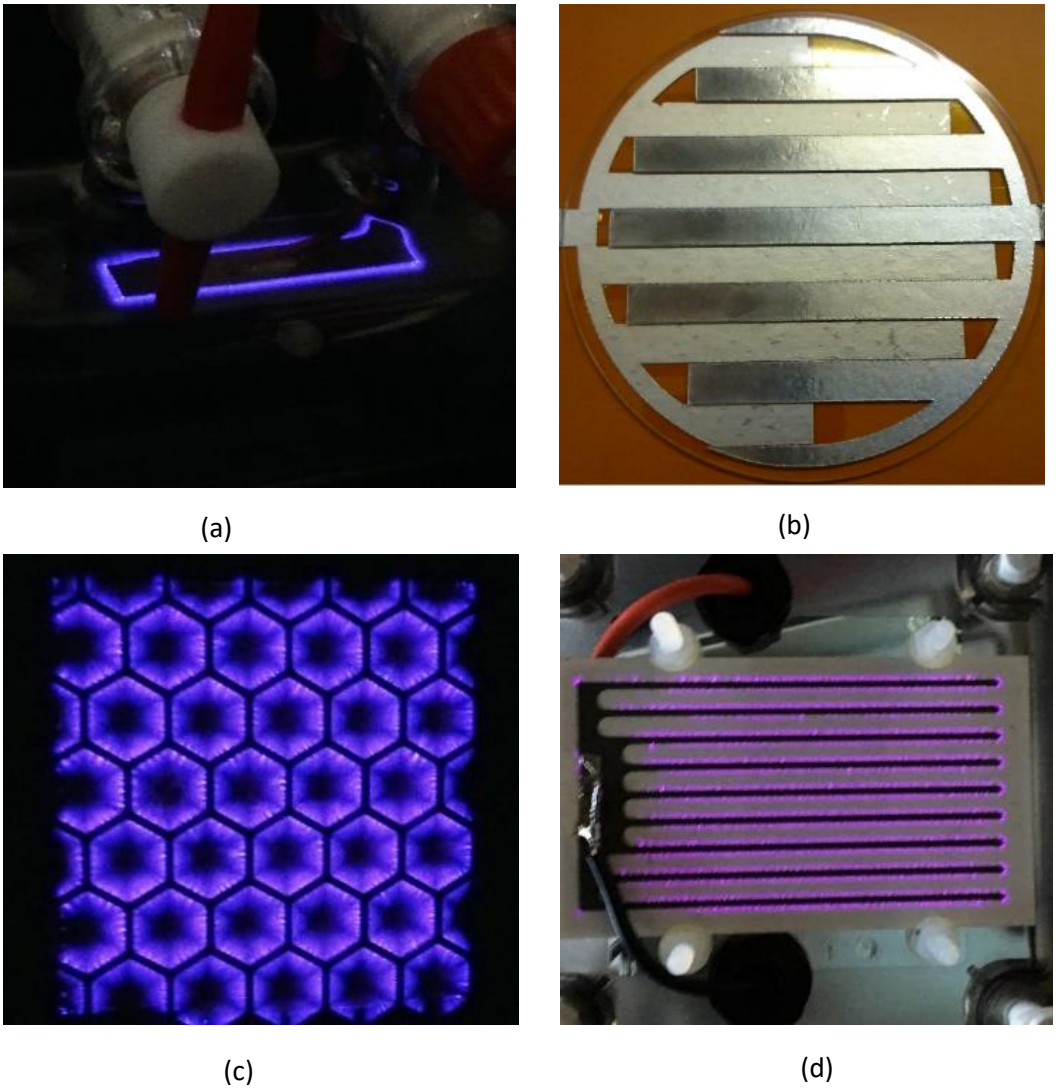

Figure 3.2 Different designs of SBD electrode. (a) is the single strip shaped design; (b) is the multi-strip shaped pattern design; (c) is the mesh electrode design; (d) is the ceramic panel.

In this investigation, multiple SBD configurations have been developed and explored. Specific details of each electrode design are listed table 3.1.

Table 3.1 SBD Reactor specifications.

Name	Dielectric material	Electrode material	Discharge length
Single strip shaped design (5 cm x 0.5 cm)	Quartz plate	Copper tape	11 cm
Multi-strip shaped pattern design (handheld device panel)	Quartz disc	Aluminium tape	65.4 cm
Mesh electrode design (5 cm x 5 cm)	Quartz plate	Copper tape & Stainless steel mesh	63 cm
Ceramic panel	Ceramic plate	Stainless steel strips	92.8 cm

The single strip shaped design used a 6 cm x 2 cm quartz plate as a dielectric material, 50 µm copper tape was adhered to each side of the dielectric to form the electrodes, and the grounded electrode side was covered with Kapton tape to prevent plasma discharge forming on that side.

The multi-strip pattern, shown in Figure 3.2 (b), used a 1 mm-thick and 10 cm-diameter quartz disc as the dielectric material with electrodes adhered to both sides made from 50 µm aluminium tape. The width of each strip electrode is 1 cm and the gaps between them is 1 cm, this was determined as the optimum value based on comprehensive testing detailing in Chapter 5. On the ground side of the electrode, the strip edges were sealed with Kapton tape to prevent discharge formation. The total length of the strip edges that produced plasma was approximately 65.4 cm.

The mesh electrode design shown in Figure 3.2 (c), is widely reported in literature. In this investigation a 5 cm x 5 cm quartz plate was used as the dielectric material. A hexagonal stainless steel mesh was used as a ground electrode. Each side of the hexagons was 3 mm in length, providing a plasma generation length of 18 mm per

hexagon. The driven electrode was made from 50 µm copper tape and covered with Kapton tape to prevent plasma formation.

The ceramic electrode, in Figure 3.2 (d), consisted of an alumina dielectric printed with metallic grids as electrodes. The dielectric was 1 mm thick, 4.1 cm wide and 11.7 cm long. The total length of the metallic grid was 92.8 cm.

The designs mentioned above were mainly used in characterisation experiments, which will be discussed in the next chapter. It is worth noting that many designs were used to investigate and optimise plasma species transport, which will be introduced in Chapter 5. Additionally, a new design is introduced in Chapter 7 for use in the treatment of meat products.

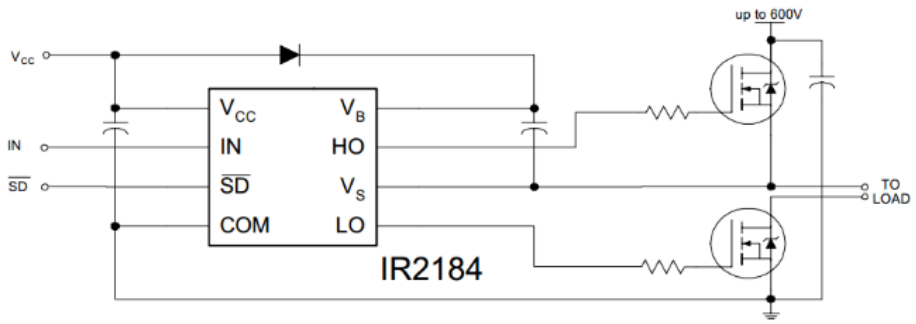

Figure 3.3 Typical connection diagram using an IR2184 half-bridge driver.

3.1.2 Power supply design and development

The plasma source used in all experiments consisted of a home-made half-bridge switched mode power supply, shown in Figure 3.3. The half bridge configuration was chosen as it offers a good compromise between efficiency, cost and complexity; it is well suited to the generation of kHz waveforms up to 500 W. As shown in Figure 3.4 the input to the half bridge was fed from a 60 V DC power supply (GW Instek programmable DC power supply, model PSP-603) and TTI

instruments function generator as a trigger source (TTi TG2000 20 MHz DDS function generator). The output of the half bridge was connected to a high-voltage transformer, during experiments several different transformers were tested, all had similar properties in that they operated resonantly with the electrode unit forming part of a series LC network. Given this configuration, the optimum frequency of operation differed between the differed SBD reactors employed.

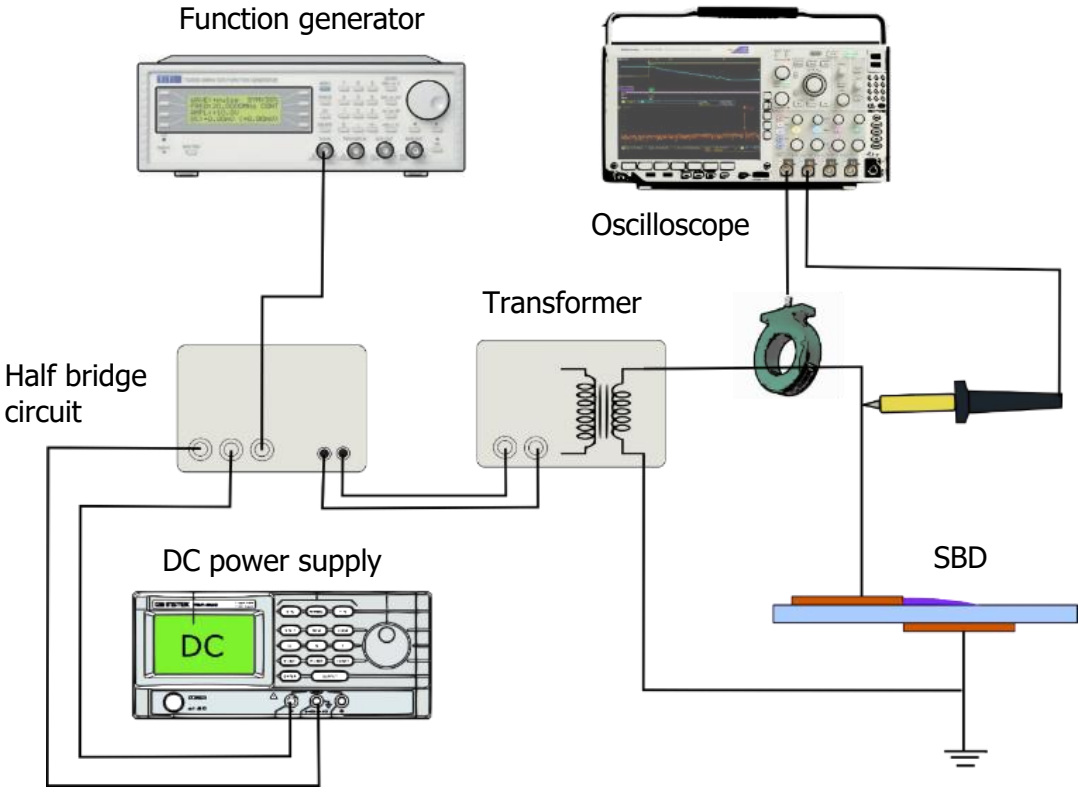

Figure 3.4 Typical experimental setup for a SBD device.

In order to monitor the electrical properties of the plasma and calculate the dissipated power within the discharge, a mixed signal oscilloscope (Tektronix DPO5054 digital phosphor oscilloscope 500 MHz 5 GS/s) combined with high voltage probe (Tektronix P6015A 1000:1 75 MHz) and current monitor (Pearson 4100 1V/1A) were used in all experiments. In all experiments, the high voltage output was sinusoidal wave and was typically in the 7 kV – 12 kV peak-to-peak voltage range, with an operating frequency in the 30 kHz – 40 kHz range. Figure 3.5 shows typical applied voltage and current waveforms obtained from a discharge

operating at 10 W dissipated power. The current waveform clearly shows multiple spikes indicate that the discharge is filamentary in nature. The total dissipated power is calculated and monitored by the oscilloscope.

In certain experiments the discharge temperature needed to be carefully controlled, in these tests a pulse modulated mode of operation was used. A pulse generator (TTi TGP110 – 10 MHz pulse generator) was used to modulate the trigger waveform to the plasma source resulting in a pulse modulated sinusoidal waveform (figure not shown).

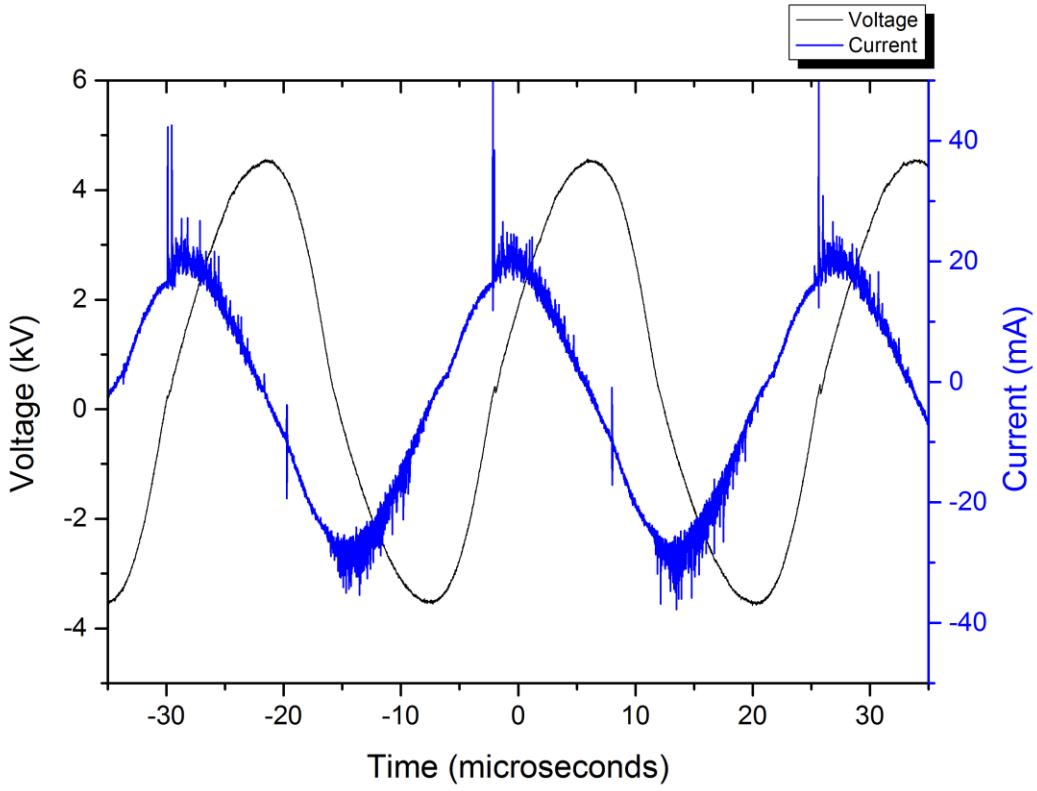

Figure 3.5 Voltage-current waveform of plasma discharge at 40 kHz.

3.2 Fourier Transform Infrared spectroscopy

Fourier transform infrared (FTIR) spectroscopy is a well-known technique for the analysis of solid, liquid and gaseous samples. It is an ideal technique to identify and quantify the long-lived chemical species in the afterglow of the plasma system.

The infrared spectrum is a result of transitions between quantised vibrational energy states of molecules. Depending on the number of atoms, the vibrations vary from the coupled motion of the two atoms in a diatomic molecule to the much more complex motion in a large polyfunctional molecule. For molecules consisting of N atoms, there are 3N modes of motion. These include three modes of translational motion, three modes of rotational motion, and the remaining 3N-6 modes are

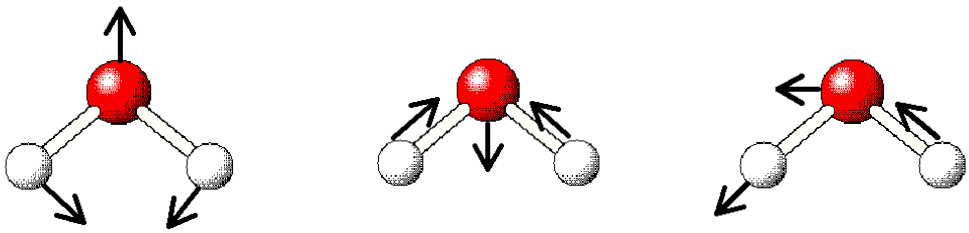

(1) (2) (3)

Figure 3.6 Water, H_2O, molecules consist of three atoms, according to the theory above, they have three modes of vibrational motions, namely: (1) Bending, (2) Symmetric stretch, (3) Asymmetric stretch.

vibrational modes. Linear molecules only have two modes of rotational motion; thus, linear molecules have 3N-5 modes of vibrational motion. Due to this, diatomic molecules (N=2) only have one vibrational mode [1, 2].

Every motion mode is formed by harmonic displacements of the atoms in their equilibrium positions and all the atoms vibrate at a certain characteristic frequency. These vibrational frequencies are usually given in units of wavenumber, defined as the number of waves per unit length, usually having the unit of cm^{-1} [91].

Molecules have distinctive vibrational modes and frequencies, which results in a unique infrared spectrum for each species. The energy difference for transitions between the ground state and the first excited state of most molecule vibrational modes corresponds to the energy of radiation in the mid-infrared spectrum (400 to 4000 cm^{-1}), which is typical of the range of operation of a laboratory FTIR instrument.

3.2.1 Beer's law

The Beer Lambert law, or simply Beer's law, is the fundamental law of quantitative spectroscopy analysis [91]. The transmittance T of any spectral sample at a certain wavenumber is given by the ratio of the radiant power emerging from the rear face of the sample at that wavenumber, I, to the power of the radiation at the front face of the sample, I_0. In this case, the radiant power source is an infrared beam passing through the gas sample, some of which will be absorbed by the molecules at a certain wavenumber. The transmittance of the gaseous sample can be affected by the path length of the infrared beam, l, which is passing through the sample and the concentration of the sample, c. Beer's law presents the relationship of these factors as follow [92, 94, 95]:

$$I = I_0 e^{-\varepsilon c l} \tag{3.1}$$

Where ε is the molar absorption coefficient. The absorption, A, of a sample at a given wavenumber can be described as:

$$A = -\ln\left(\frac{I}{I_0}\right) = \varepsilon c l \tag{3.2}$$

3.2.2 FTIR spectrometer components and setup

The key components in any Fourier Transform infrared spectrometer include an infrared source, interferometer, optics and detectors. Figure 3.7 presents a basic setup of the components for a FTIR spectrometer. A broad range of infrared radiation, usually 500 cm^{-1} to 8000 cm^{-1}, is produced by the infrared source. The source is usually a rod made of a rare earth oxide or a resistively heated silicon carbide rod known as Globar.

The interferometer of FTIR spectroscopy is based on the two-beam interferometer designed by Michelson in 1881 [91]. The interferogram is created by the interference of two beams with different path lengths, as shown in Figure 3.8. The infrared beam projected from the source is directed to a beam splitter which partially reflects the beam to a fixed mirror and partially transmits the beam to a movable mirror. The two partially split beams reflect back to the beam splitter where they will interfere with each other due to different path length caused by the moveable mirror. Thus, the interferogram is created by the interference and the FTIR spectrum can be calculated from it by using Fourier Transform [92, 95, 96].

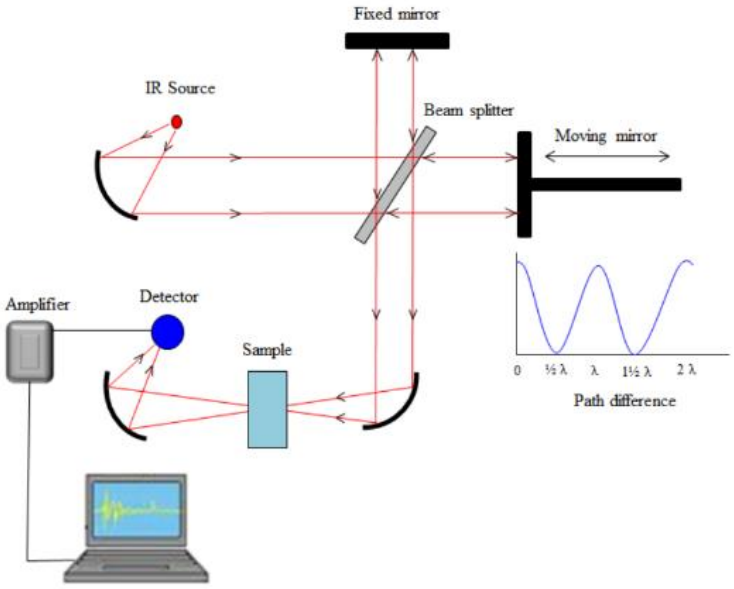

Figure 3.7 Basic elements of a FTIR system.

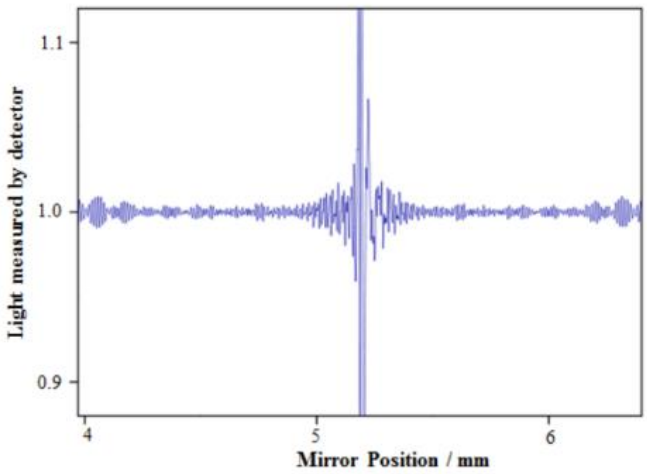

Figure 3.8 An example of FTIR interferogram.

3.2.3 FTIR spectral analysis and quantification of measurements

For all FTIR measurements reported, a Jasco FT/IR-4000 series (Jasco analytical instruments) with a mid-IR optical bench from 7800 cm^{-1} to 500 cm^{-1} was used. The resolution for data acquisition was varied between 0.5 cm^{-1} and 8 cm^{-1} depend on the specific requirments of the test and all data was recorded between 10 and 25 times to provide an average measurement.

Two different gas cells were used for the gaseous species characterisation. A short path length gas cell (model Specac GS05000), which had a fixed path length of 10 cm, and a multiple light passes gas cell (model Piketech 163-1600) with variable path length from 1 m to 16 m. Both gas cell used KBr windows for infrared transmission.

The corresponding vibrational bands of key air plasma generated species are shown in table 3.2 [1, 7].

Table 3.2 Corresponding infrared spectra wavenumbers of key species.

Species	Absorption Peak Wavenumber (cm^{-1})		
O_3	1054, 1034	2123, 2107, 2097	
NO	1900, 1853		
N_2O	2236, 2212	1299, 1272	
NO_2	1628, 1602		
N_2O_5	1718	1245	742
HNO_3	1722, 1711, 1699	1339, 1325, 1317	895, 878

The concentration of the gaseous species was estimated by fitting the measured FTIR absorption profile with the standard reference spectrum profiles which were taken by Pacific Northwest National Laboratory (PNNL) (http://www.pnl.gov/). These standard reference spectrums were collected as 1 part-per-million-meter (ppm-meter) at 296 K (room temperature) with a path length of 1 m. To calculate the concentration, *C*, from the experimental spectrum the following equation is used:

$$C = \frac{A}{B \times l} \tag{3.3}$$

Where A is the experimental peak area of the spectrum, B is the standard peak area, l is the difference of experimental gas cell path length and standard path length (usually 1 m) [94].

The HITRAN database (http://hitran.iao.ru/) was also used to simulate the absorption profile from certain species to be used as an alternative method for gas phase chemical quantification. By fitting the simulated spectrum to the experimental spectrum, the best fit can be found to estimate the concentration of species of interest. The advantage of this method is that the HITRAN database can simulate a single chemical species or several gases mixtures with adjustable apparatus settings, such as optical path length and FWHM.

3.3 Ozone measurement

The ozone concentration was measured using an ozone monitor from 2B technologies (model 106-M). The ozone monitor used had a measurement range up to 1000 ppm and a resolution of 0.01 ppm. The measurement interval of the instrument was 10 seconds.

The measurement principle of the ozone monitor is quite similar to that of FTIR, both use optical absorption and beer's law as foundation. In contrast to FTIR, the Ozone monitor uses ultraviolet light and focuses on one specific wavelength. Figure 3.9 highlights that the ozone molecule has the highest absorption cross-section at approximately 254 nm. The monitor has a pump that pulls gas in to the absorption cell in which a mercury lamp projects a beam; at the receiving end, a photodiode is placed to sense the difference of radiation intensity at 254 nm, and hence the concentration of ozone.

The concentration of ozone measured by the ozone monitor was recorded and used as a comparison with the measurement from FTIR and the simulation based on HITRAN database.

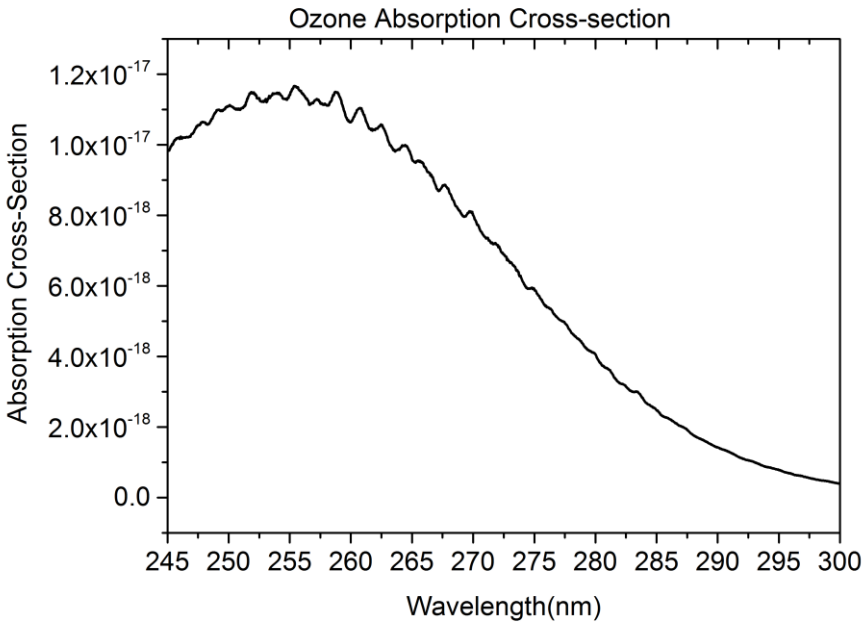

Figure 3.9 Ozone absorption cross-section at 300K.

3.4 Particle Image Velocimetry (PIV)

Particle Image Velocimetry (PIV) is an optical method of flow visualisation and quantification that has been widely used to obtain instantaneous velocity measurements of fluids. Many researchers have used the technique to explore the use of SBD configurations in aerodynamics applications.

3.4.1 PIV principle

A typical PIV system consists of a high-speed camera, a strobe or pulsed laser with an optical arrangement to illuminate a certain region, a synchronizer to use as an external trigger for controlling the camera and laser and a seeding particle

generator, as shown in Figure 3.10. Furthermore, PIV software is used for post processing the optical images [96].

The seeding particles are a vital component in any PIV experiment. The choice of particles is decisive for the accuracy of the PIV analysis result. The nature of the particles must be able to match the fluid properties in order to yield the best results. Ideally, the density of the particles should be the same as the fluid being invested, and the size of the particles, usually range from 10 to 100 μm, should be small enough to be responsive to the motion of the fluid. In addition, the shape of the particles should be spherical or similar, so that the light beam can be scattered and reflected towards the camera. For investigations involving gases, such as those considered in this thesis, oil droplets are usually used as the seeding particles [8, 9]. The Stokes numbers of the seeding particles used throughout this study was <0.1. This ensured that the seeding particles followed the fluid flow closely with tracing errors being <1% [98].

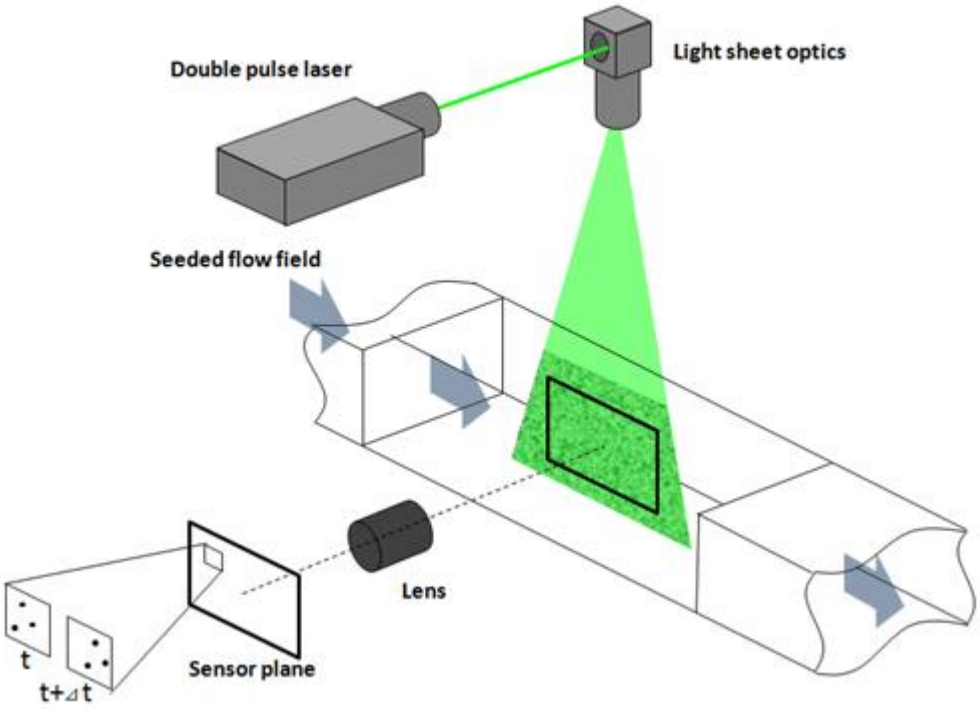

Figure 3.10 A typical setup of a PIV system.

To determine the flow velocity two laser pulses are used to illuminate the seeding particles in a given area with a short off-time between the pulses. The high-speed camera captures these two laser pulses in image pairs. By comparing the small displacement of the seeding particles between the image pairs, the flow speed and direction can be determined. The interval time between the two lasers pulses determines the maximum and minimum velocity that can be measured and is a critical parameter to obtain accurate measurements of the flow under investigation [8, 10, 11].

The laser lens consists of a spherical lens and a cylindrical lens, the former lens expands the laser into a plane while the later lens compresses the plane into a thin laser sheet. The thickness of the laser sheet is critical, as in a one-camera PIV system only a 2D-dimension region can be investigated. Thus, the motion that is perpendicular to the laser sheet cannot be measured. A thicker laser sheet can illuminate particles that move normal to the laser sheet and thus disturb the post processing analysis. It should be mentioned that the laser sheet could not be compressed into an ideal 2D-dimension plane. The thickness is on the order of hundreds of micrometres, depending on the wavelength of the laser light and it is divergence from the focal point of the spherical lens. Therefore, the ideal focus of view by the camera should be near the focal point [93, 94, 96].

The laser and the camera are triggered by using the synchronizer. Controlled by a computer, the synchronizer controls the timing of the high-speed camera such that it is synchronized with the firing of the laser within few nanoseconds [96].

After the image capture process, images are split into a large number of small subsections called interrogation areas, among which cross-correlations are established pixel by pixel, then a signal peak can be produced to indicate the particle displacement. Particles can be matched with a number of candidates, the correlation process is repeated many times to find all the matches. Wrong combinations will create a noise correlation and good matches will produce a strong correlation peak, identifying the common particle displacement and thus the velocity. To avoid in-pair loss or too much spatial averaging, each interrogation area is set to overlap with the previous one to maximise the dynamic range. By repeating

the cross-correlation process for each interrogation area over the image pairs, a velocity vector map over the whole target area can be obtained [96].

3.4.2 PIV instrument setup

A standard TSI High-Speed High Resolution Particle Image Velocimetry System was used in the experiment.

To create the space for plasma and airflow visualisation, a large enclosed black chamber (dimension 1 m x 1 m x 1.5 m) was built and featured windows for the laser light sheet to enter and camera, the windows were orientated in a perpendicular fashion. The enclosure is essential to ensure the airflow detected by the PIV is that induced by the SBD plasma without external interference, it is also important to prevent the seeding particles from escaping.

A New Wave Research Pegasus PIV laser was used with a wavelength of 450 nm, and the laser sheet was aligned to the SBD reactor perpendicularly. A high frame rate camera (Photron APX RS) with 1024-by-1024-pixel resolution was used to capture image data. A synchronizer was used to control the capture rate, which was set to 750 frames per second, which collects 1500 image pairs, and used for triggering the laser and plasma system. The delay between laser pulses was varied from 100 - 750 microseconds depending on the plasma power input.

Data collected was processed using INSIGHT 4G software from TSI. Vectors of plasma flow generated the software with a 32 x 32 pixel interrogation area with a 50% overlap and a peak-to-noise rate at 1:1.2, which provided velocity data with a 1 mm spatial resolution to an accuracy of 3-5 %. TecPlot 10 was used for vector display and analysis [12, 13].

3.5 Temperature measurements

Temperature measurements of solid surfaces were conducted using a K-type thermocouple probe (Apuhua TM-902C) with a measurement range of -50 ˚C to 750 ˚C.

In situations where a thermocouple was not viable, such as discharge area, a handheld infrared camera (model FLIR E40bx) was used. The infrared camera is capable of capturing an IR image with a resolution of 160 x 120 pixels, temperature ranges from -20 ˚C to 120 ˚C and has a thermal sensitivity smaller than 0.045 ˚C and an accuracy of ±2 ℃.

Chapter 4 Characterisation of Air Plasma

In this chapter, details of the characterisation of afterglow chemical species generated by an air SBD air presented. The number of species produced and the reactions they take part in is extremely complex. As highlighted in the review chapter, the species generated from an air plasma vary dramatically depending on the operating conditions and equipment configuration. While this complexity presents a number of challenges, it also indicated that air plasma systems may be tailored to generate desired species for specific applications. In order to achieve this, an understanding of the plasma chemistry arising is fundamental.

This chapter will not only discuss the gas phase plasma chemistry but also the chemistry arising when such species interact with liquids; this is vital as many emerging applications involve the interaction of plasma with a liquid.

4.1 Afterglow chemistry of SBD

From Chapter 2, previous reports have revealed that atmospheric pressure air plasmas generate a wide variety of RONS, including O, OH, O_3, N_2O_5, N_2O, HNO_3, HO_2, NO_3, H_2O_2, HNO_2 and NO_2. These RONS have been proven effective against food- and water-borne pathogens.

It has also been reported that a typical SBD air plasma system exhibits different modes of operation when driven at different power conditions [4, 58]. Under low power excitation ROS is primarily produced, under high power conditions RNS are produced. Therefore, each particular plasma system must be carefully characterised before it can be used in a given application.

4.1.1 Experimental setup

The experimental setup for the SBD air plasma system afterglow chemistry characterisation, shown in figure 4.1, consisted of the plasma source, FTIR system

and an ozone monitor. The plasma source contained an SBD electrode panel placed within a polycarbonate enclosure and connected to a high voltage power source. The enclosure was not air-tight (a 1 mm diameter hole was made to allow gas to flow) and was connected to the FTIR via a short length of Tygon tubing. The outlet of the FTIR was connected to the ozone monitor which also acted as a pump to cause a gas flow through the entire system at a rate of 1 L/min. Depending on the size of the SBD reactor under consideration, the size of the enclosure varied. Different power settings for each SBD were used. The power density was calculated as dissipated power per unit length of the electrode that generates plasma. This was deemed as the most appropriate measure of power, albeit somewhat unconventional, as the discharge area and volume are both difficult to measure and vary widely according to discharge conditions and the power conditions for each SBD reactor are listed table 4.1.

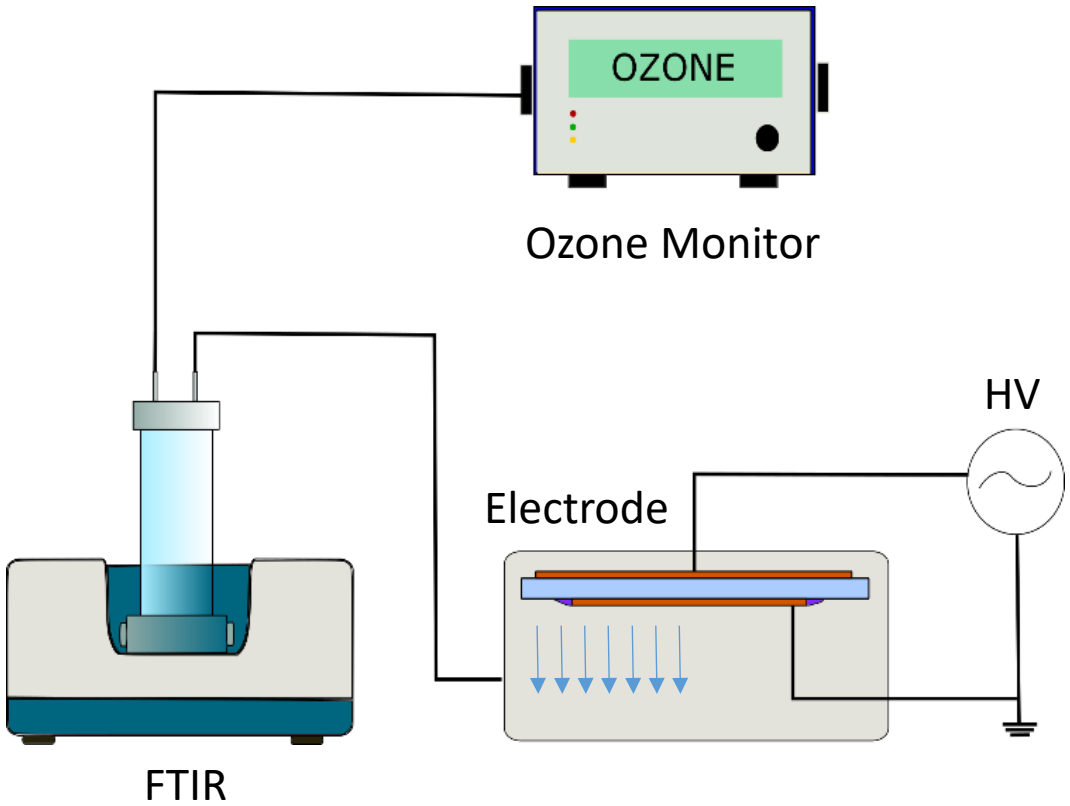

Figure 4.1 Experimental setup for SBD air plasma system afterglow chemistry characterisation.

The absolute dissipated power ranged from 2 W to 30 W depending on the sizes of the electrode, but the power densities were usually set between 0.13 W/cm to 0.4

W/cm. These values are typical of those reported in the before literature and enable access to both the ROS and RNS mode of action [57]. The driving frequencies were set to the natural resonant frequency of the transformer secondary and dielectric capacitance.

Table 4.1 Power conditions used for different plasma sources.

Name	Single strip reactor (5 cm x 0.5 cm)				
Details	Discharge Edge length (cm):		11	Frequency (kHz):	35
Power Density	Dissipated (W):	2	2.5	3	3.5
	Density (W/cm):	0.18	0.23	0.27	0.32
Name	Multi-strip reactor (handheld system)				
Details	Discharge Edge length (cm):		65.4	Frequency (kHz):	40
Power Density	Dissipated (W):	10	15	20	25
	Density (W/cm):	0.15	0.23	0.31	0.38
Name	Mesh electrode reactor (5 cm x 5 cm)				
Details	Discharge length (cm):		63	Frequency (kHz):	35
Power Density	Dissipated (W):	10	12	15	18
	Density (W/cm):	0.16	0.19	0.24	0.29
Name	Ceramic reactor				
Details	Discharge Edge length (cm):		92.8	Frequency (kHz):	15
Power Density	Dissipated (W):	12	20	28	
	Density (W/cm):	0.13	0.22	0.3	

4.1.2 Gas Phase Species Characterisation

The identification and quantification methods for gaseous plasma chemistry was introduced in Chapter 3. Infrared spectra were acquired using FTIR at 60 second intervals from the point of ignition of plasma. Figure 4.2 shows the spectra acquired from different power settings after 15 minutes of plasma operation. Figures 4.3 &

4.4 show the time evolution of reactive species generated by the plasma. Most of the absorption peaks of reactive species are found in the mid-infrared range, 2500 cm^{-1} to 500 cm^{-1}. From the recent literature, the peaks of nitrous oxide (N_2O), nitric oxide (NO), nitrogen dioxide (NO_2), ozone (O_3) and nitric acid (HNO_3) have been identified. Certain species are only found at certain power densities; for example, NO_2 and NO are only seen in Figure 4.2(d), where the power density is high at 0.32 W/cm. Under these high power conditions, O_3 or HNO_3 may be produced but quenched at stable state, appearing only in lower power cases. The production and loss pathways will be discussed later.

It is interesting to note that HNO_3 could only be observed in experiments using ambient air which contains water vapour. In later experiments, detailed in section 4.3, synthetic air was used which contains far less water vapour than ambient air; under these conditions no trace of HNO_3 was found but N_2O_5 instead.

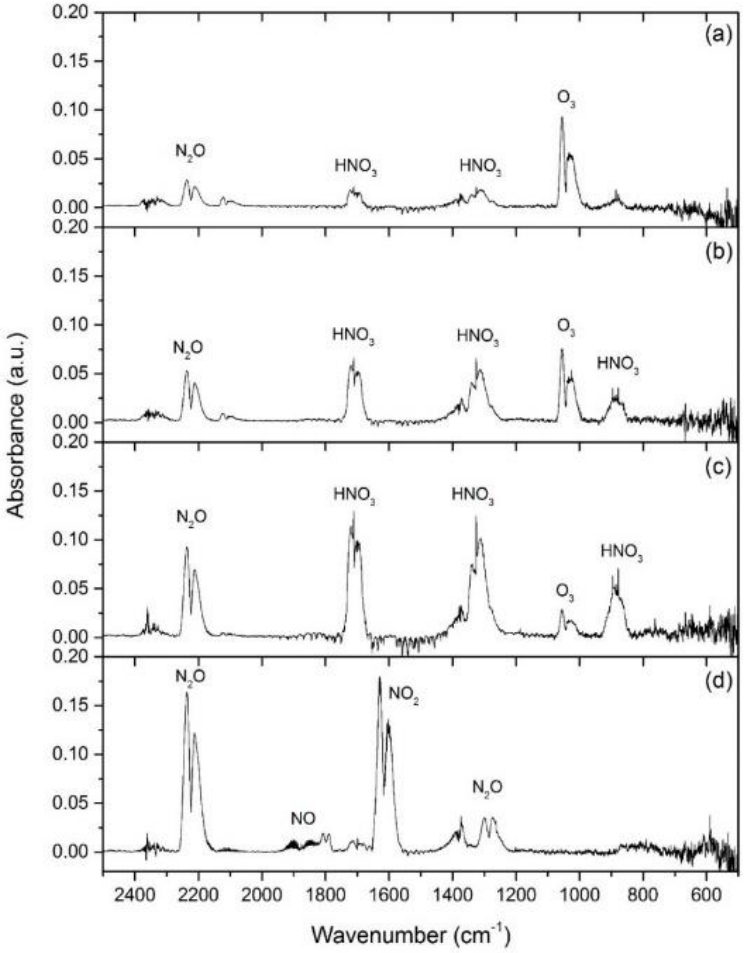

Figure 4.2 FTIR spectrum of reactive species at different power settings: (a) 0.18 W/cm, (b) 0.23 W/cm, (c) 0.27 W/cm and (d) 0.32 W/cm. Spectra were acquired at 15 min after the ignition of plasma.

In Figure 4.3, four quantified reactive species are presented as function of concentration versus time. It can be seen that the N_2O concentration increased in a linear fashion with respect to time and the gradient of the line increased when power was increased. NO_2 could only be detected at the highest power condition case (0.32 W/cm) and was seen to increase over 1000 ppm in 90 seconds. A concentration of approximately 800 ppm of ozone was measured at each power condition; however, the curves decay after reaching the peak, with the decay rate being strongly dependant on power. The higher the power the earlier the O_3 peak and the faster the decay, with ozone being fully quenched within 10 minutes in the

0.32 W/cm case. HNO_3 showed a similar linear trend to N_2O in the low power cases, yet after 10 minutes it was fully quenched from above 1000 ppm to 0 ppm within 2 minutes. The transition between HNO_3 increase and decay matches the point where NO_2 is seen to increase. Although NO was observed at 0.32 W/cm, its absorption profile was too small to quantify accurately; this is expected as NO has a relatively short lifetime and the distance between discharge and gas cell is likely to be a limiting factor.

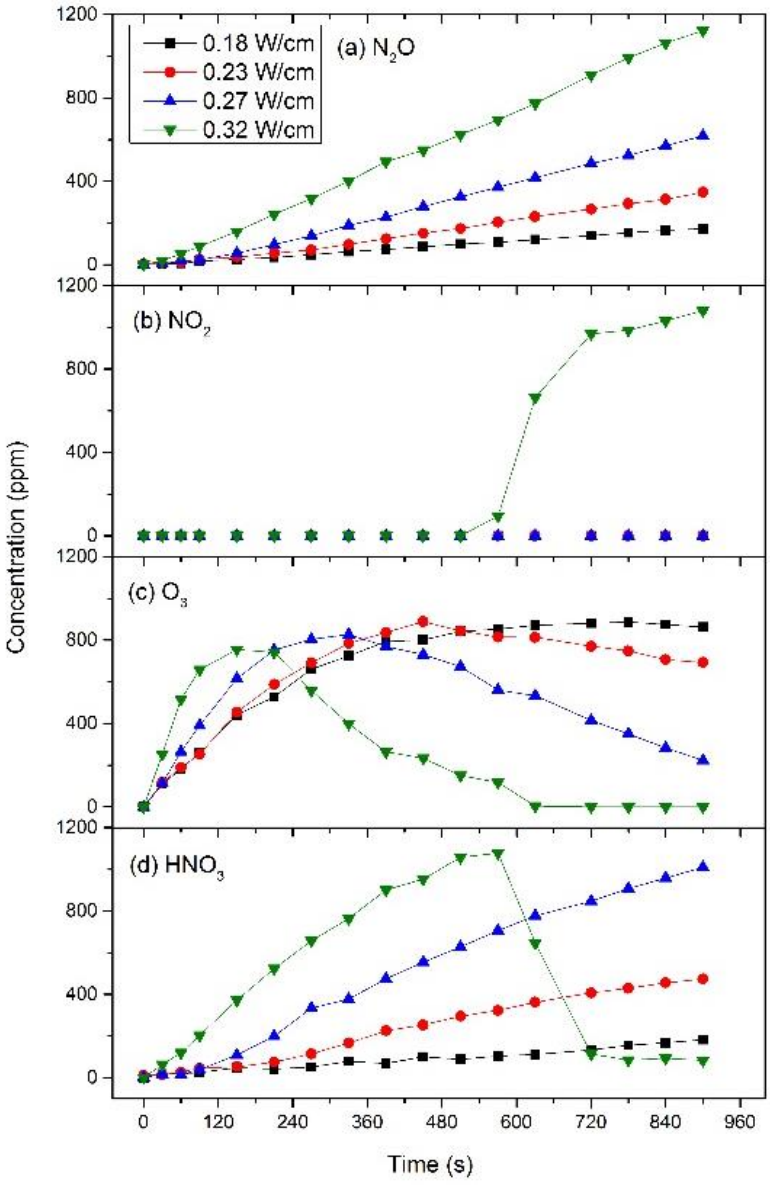

Figure 4.3 Evolution of reactive species under different power conditions as a function of time.

The dramatic change in chemistry under high power conditions is of particular interest as it can have significant consequences in any application. A comparison of the evolution of reactive species at 0.27 W/cm and 0.32 W/cm is presented in Figure 4.4. In the 0.27 W/cm case, shown in Figure 4.4 (a), the concentration of HNO_3 and N_2O increase with time, ozone decreases but is still above 0 ppm and no trace of NO_2 is observed. In the 0.32 W/cm case, shown in Figure 4.4 (b), the evolution of the reactive species is similar to the 0.27 W/cm case up to 540 seconds. After 540 seconds, the concentration of NO_2 increases and HNO_3 decreases sharply, ozone is fully quenched within 90 seconds after the increase of NO_2.

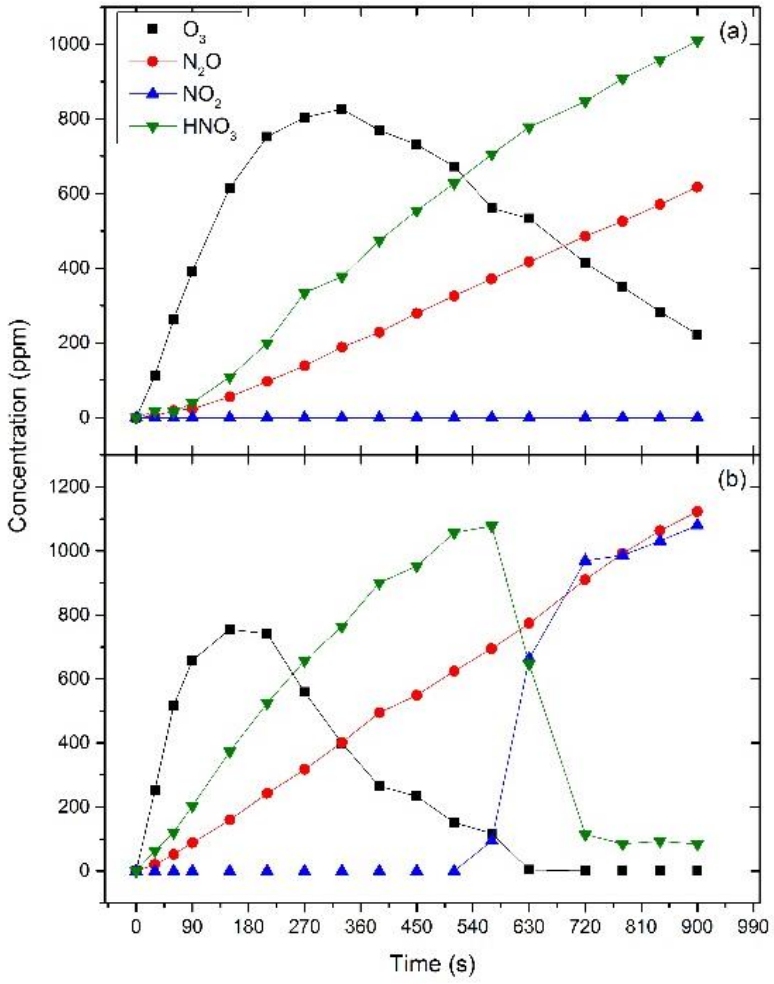

Figure 4.4 Evolution of reactive species over time at (a) 0.27 W/cm and (b) 0.32 W/cm.

4.1.3 Discussion

The evolution of plasma generated species under different power conditions are in agreement with those reported in the literature; the exact mechanisms leading to these trends are still under intense debate [102]. It is, however, clear that two different modes of operation occur. Under low power conditions, ozone is dominant, conversely high power conditions result in a NO_x dominant mode. For all the reactors detailed in table 4.1, the two modes were observed. It is worth nothing that the experimental setup (enclosure volume, frequency, temperature and humidity) had a significant impact on the transition point between the two modes.

By repeating the discharge characterisation with different SBD configurations and power levels, it was observed that the ozone quenching transition occurs only above a certain power density threshold. Below the threshold power density, ozone generation never ceases and its concentration slowly increases, finally reaching an equilibrium density. Above the power density threshold, ozone concentration decreases after reaching a peak concentration, eventually dropping to zero. Further increases above the threshold power density resulted in accelerated ozone quenching.

Understanding the ozone quenching process requires a comprehensive understanding of the reactions in both the plasma region and afterglow, which are known to be extremely complicated. Sakiyama *et al.*'s developed an air plasma model for an SBD reactor including over 600 reactions and 53 species. Based on the reactions uncovered by Sakiyama, the ozone quenching mechanism are discussed below [57].

In ambient air, the main species include O_2, N_2 and H_2O; CO_2 and minor noble gas impurities are not considered to play a role. Following application of a voltage sufficiently high to cause breakdown, the plasma region is populated by a wide variety of highly reactive species such as N, N_2^+, $N_2(A)$, $N_2(B)$, O, O_2^+, H^+, OH, etc. Beyond the discharge region, these highly reactive species are transported in to the afterglow region and take part in a wide variety of reactions, leading to the formation of RONS that eventually reach a downstream sample surface.

In all of the FTIR measurements conducted in the afterglow of an ambient air SBD, O_3, N_2O and HNO_3 appear initially.

The predominant ozone is shown in reaction 1 [57, 103, 104, 105].

$$O + O_2 + M \rightarrow O_3 + M \quad (1)$$

Where M is a third-body collision partner, such as O_2, N_2 in the background gas.

The main generation pathways for NO and N_2O are given in reactions 2 and 3 [1, 104, 105].

$$N + O_2 \rightarrow NO + O \quad (2)$$

$$N_2(A) + O_2 \rightarrow N_2O + O \quad (3)$$

HNO_3 is only formed in humid air, while in dry air, N_2O_5 production is favoured. N_2O_5 is oxidised from NO via NO_2 and NO_3 [104]. The formation of N_2O_5 and subsequent formation of HNO_3 is highlighted in reactions 4 – 9 [57, 104].

$$O + NO + M \rightarrow NO_2 + M \quad (4)$$

$$NO + O_3 \rightarrow NO_2 + O_2 \quad (5)$$

$$O + NO_2 + M \rightarrow NO_3 + M \quad (6)$$

$$NO_2 + O_3 \rightarrow NO_3 + O_2 \quad (7)$$

$$NO_2 + NO_3 + M \leftrightarrow N_2O_5 + M \quad (8)$$

$$N_2O_5 + H_2O \leftrightarrow 2HNO_3 \quad (9)$$

Notably, reactions (5) and (7) consume ozone to form NO_2 and NO_3, which become the reactants in (8), leading to N_2O_5 production. These reactions tie in well with the results presented in Figure 4.2 (a) - (c), where HNO_3 is seen to increase as ozone decreases. In addition to reactions (5) and (7), several other pathways for ozone destruction are shown in reactions 10 – 13.

$$N + O_3 \rightarrow NO + O_2 \quad (10)$$

$$N_2 + O_3 \rightarrow N_2 + O_2 + O \quad (11)$$

$$O + O_3 \rightarrow 2O_2 \quad (12)$$

$$OH + O_3 \rightarrow HO_2 + O_2 \quad (13)$$

According to Sakiyama *et al.*[57], reaction (7) and (13) are the main pathway for ozone destruction. Under the highest power conditions, no HNO_3 or ozone are detected; the concentration of N_2O and NO_2 are high under such conditions and a small amount of NO is also present. Reaction 9, 14 and 15 highlight a potential reaction pathway to explain these observations.

$$2HNO_3 \leftrightarrow N_2O_5 + H_2O \quad (9)$$

$$N_2O_5 + M \rightarrow NO_2 + NO_3 + M \quad (14)$$

$$NO_3 + NO_3 \rightarrow NO_2 + NO_2 + O_2 \quad (15)$$

The quenching of N_2O_5 is mainly because of thermal decomposition as surface temperature would increase by 10 to 20 °C when reaching the ozone to NO_x transition [105, 106]. However, this does not explain the rapid decrease of N_2O_5/HNO_3 and the significant concentration increase of NO_2.

Moreover, the mechanism of ozone quenching is not well understood. Many researchers believed that the generation of NO and NO_2 are the key to ozone quenching. Reactions involving NO and NO_2 have larger rate coefficients, so the O needed for ozone formation are consumed rapidly. Moreover, as shown above in reactions (5) and (7), NO reacts with ozone to generate NO_2 which further reacts with ozone to generate NO_3. Shimizu *et al.* proposed an alternate explanation suggesting that $N_2(A)$ reacts with O to produce NO, under higher power operation more vibrationally excited N_2 is produced, accelerating NO production quenching ozone [105].

From the experimental results, it can be seen that ozone and NO_x can be found in both low and high power modes of operation. In the low power mode, the generation of NO_x is not fast enough to consume all the ozone produced; while in high power mode, ozone dominates initially but is then quenched by NO_x. N_2O is stable in both modes.

In the FTIR measurements not all of the species predicted by computer modelling are observed. Only four species appear in the FTIR measurements in significant concentrations, N_2O, HNO_3, O_3 and N_2O_5. From the species predicted but not observed it is assumed that NO_3 is too reactive at room temperature to be observed HNO_2 is difficult to observe because its absorption spectrum overlaps with HNO_3, and finally NO is observed but in very low concentrations.

An understanding of the different modes of operation and what initiates their transition is extremely important for practical applications as the mode of operation could be used to tailor the composition of species produced. Indeed, the results from the FTIR measurements were used to optimise the chemistry of an SBD device for use in an antimicrobial application, discussed later.

4.2 Liquid phase species characterisation

This section considers the interaction between the SBD afterglow species and a liquid phase. As discussed previously, many emerging applications of atmospheric pressure plasma involve the interaction between plasma and liquid. Examples include the use of plasma as an Advanced Oxidation Process for wastewater treatment, or the use of plasma for wound healing where the liquid could be biological in nature (e.g. blood).

Differ to gas phase species characterisation, liquid phase species characterisation would be focus on reactive species dissolved in water, such as nitrite (NO_2^-) and hydrogen peroxide (H_2O_2). Also, pH value of water after treatment would be monitored.

In previous reports [32, 58, 107], plasma treatment of water led to a significant drop of pH value. Plasma treated water itself is a strong oxidant and could be used an effective disinfectant in many situations. However, in certain cases such as decontamination of potable water, the pH drop is not acceptable. Control of the plasma chemistry to minimise the production of NO_x is one possibility to overcome this limitation. This section explores how plasma generation parameters can be manipulated to influence the plasma species transported to the liquid phase.

4.2.1 Experimental setup

The experimental setup used for liquid phase characterisation and treatment is shown in Figure 4.5. The SBD device used was the multi-strip design detailed in table 3.1 [108]. The dielectric disc had a diameter of 10 cm and could perfectly fit on the top of a petri dish, forming a reasonably tight seal. For the measurements, one set of samples consisted of 25 ml of autoclaved tap water, and a second set consisted of 3 ml of peptone broth. During all treatments, a magnetic stirrer was applied to ensure that the liquid sample was continuously mixed. In all cases, the SBD panel was placed on the petri dish with the grounded side facing the liquid surface. The distance between the surface of the panel and the surface of the liquid sample was roughly 0.5 cm.

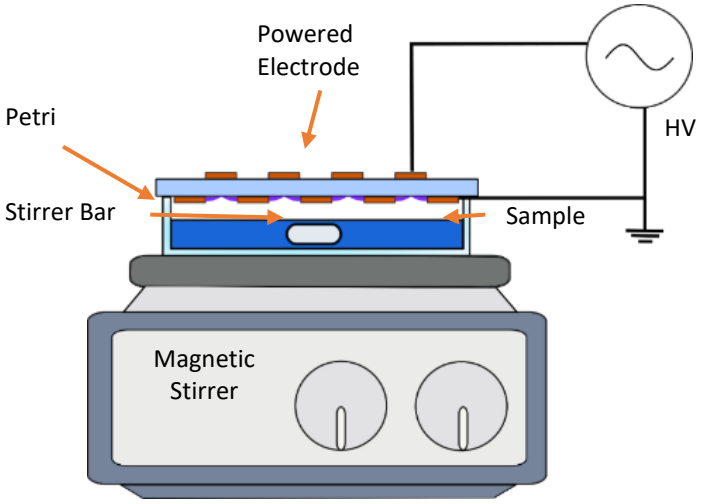

Figure 4.5 Liquid phase air plasma treatment experimental setup.

Table 4.2 Continuous mode & pulse modulated mode power conditions for water treatment.

Details	Discharge Edge length (cm):		65.4	Frequency (kHz):	40
Continuous mode power Density	Output (W):	10	15	20	
	Density (W/cm):	0.15	0.23	0.31	
PWM mode Power density	Output (W):	2.5	3.75	5	
	Density (W/cm):	0.038	0.057	0.076	

All liquid samples were treated at three different power conditions as shown in table 4.2. The output power and frequency settings was the same as those used in section 4.1. In addition, a pulsed modulated mode of operation was also used, in which the duty-cycle was set to 25%, with a 2.5 ms pulse width and a 10 ms period. The treatment time of each sample was between 15 seconds to 16 minutes.

Following plasma treatment, the pH of the treated solution was obtained using a pH meter (Pocket Checker pH tester Hanna Instrument HI98103). A Hydrogen peroxide

(H_2O_2) assay with the ferric-xylenol orange complex (xylenole orange, sorbitol and ammonium iron sulfate; all obtained from Sigma-Aldrich) was used to determine the concentration of H_2O_2 produced after each treatment. The Nitrite (NO_2^-) concentrations were also measured with standard Griess reagent assay (Promega: Griess reagent system).

4.2.2 Results

The results will be discussed in two parts; initially, plasma exposure of tap water will be considered. Secondly, the plasma treatment of broth solution is considered.

The results for tap water treatment is focused on the comparison between continuous mode and pulsed modulated mode. As shown in Figure 4.6, the pH value of plasma treated water varies considerably under different plasma generation conditions. When treating water using a power setting of 0.15 W/cm in a continuous mode, which is the lowest possible power setting, the pH value of the water dropped to 3.5 in 3 minutes. In contrast, in PWM mode the pH value of treated water was maintained around 6 for the duration of the test.

In order to have a better understanding of the two operating modes, the gas phase ozone and HNO_3 were measured, as shown in Figure 4.7. It can be seen that ozone concentration in continuous mode reaches a peak of 2200 ppm within 180 seconds, after which there is a sharp decrease. Conversely, in the PWM mode ozone increases at a slower rate, reaching a plateau of 2100 ppm at 840 seconds of exposure and showing no appreciable decrease after a 960 second test duration. On the other hand, HNO_3 concentration in the continuous mode increases in an almost linear fashion and reaches over 800 ppm by the end of the test. In the PWM mode, HNO_3 gradually reaches 200 ppm by 360 seconds and plateaus for the reminder of the test.

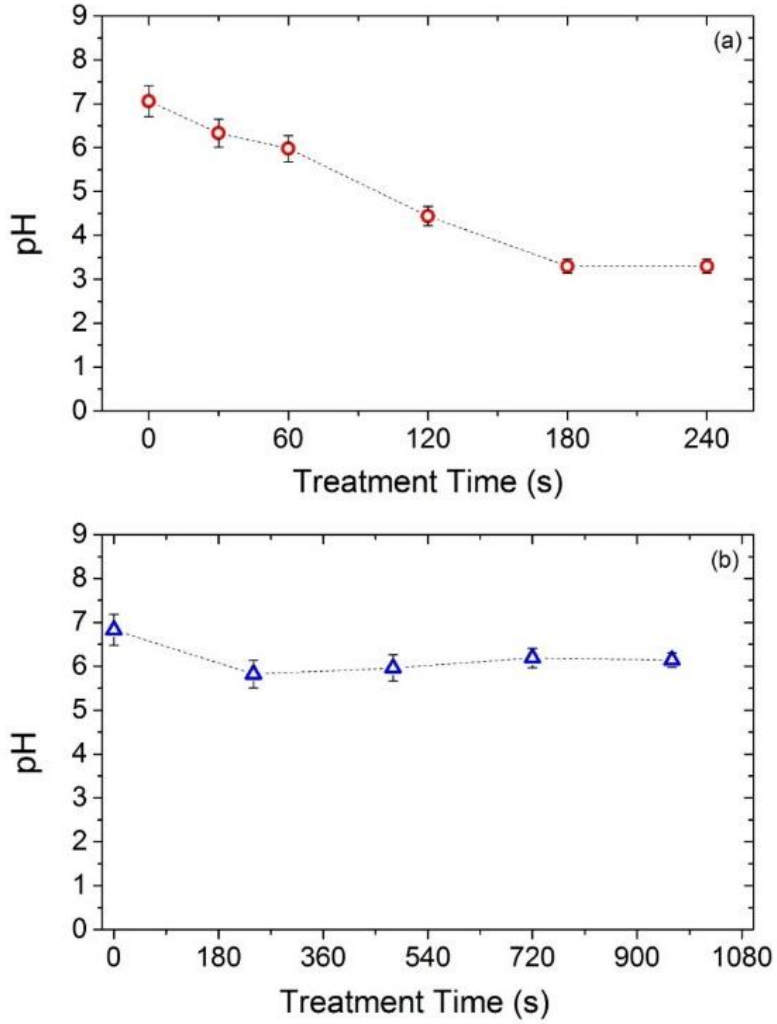

Figure 4.6 Treated water pH value as a function of time at different operation mode. (a) the continuous mode and (b) the 25% duty cycle pulsed width modulated mode. Both mode operates at 0.15 W/cm.

The observed trends in water have been reported previously [109]. For the treatment of broth solution, the situation is more complex and few studies are yet to consider the impact of plasma treatment on the chemistry of the solution. Measurements of pH, H_2O_2 and NO_2^- concentration from plasma treated broth solution are shown in Figure 4.7 - 4.9. These results focus on the comparison between different output power conditions. A drop in pH is desirable for many decontamination applications (with the exception of potable water), hence the pulsed modulated mode of operation is not required.

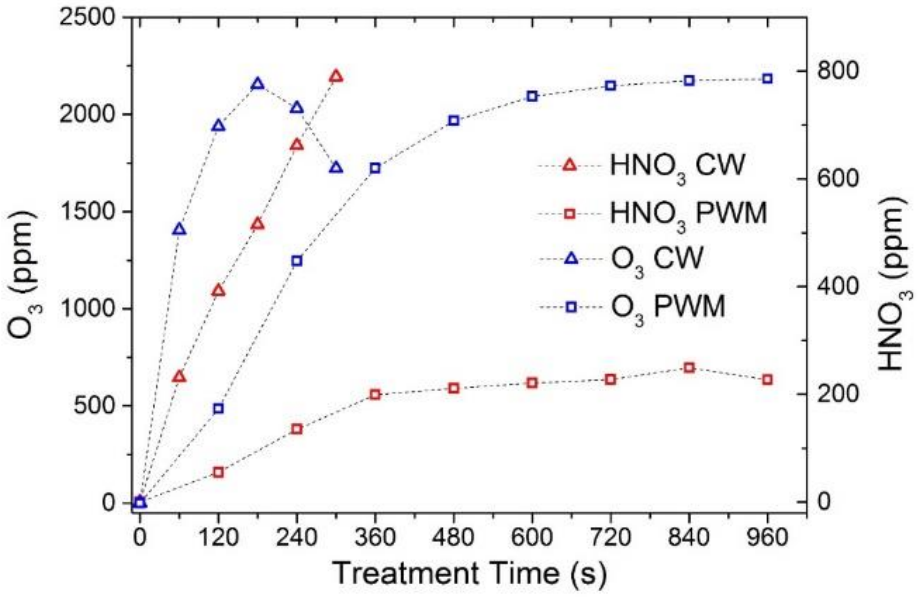

Figure 4.7 Gas phase evolution of ozone and HNO_3 during continuous mode (CW) and PWM mode operation.

From Figure 4.8 it can be seen that at the lowest power output of 0.15 W/cm, the pH drops to 4.5 after 8 minutes of treatment. The pH curves at 0.23 W/cm and 0.31 W/cm are similar, they drop quickly after 60 seconds of treatment, probably when the natural buffering capacity of the broth is overcome. After 4 minutes of treatment the pH has fallen to 3.5 and is below 3 at the end of the test.

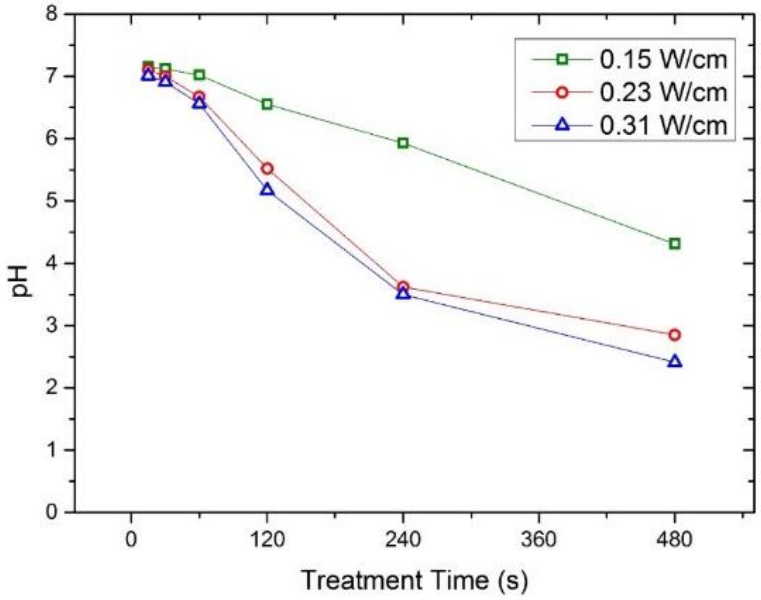

Figure 4.8 Treated broth pH value as a function of time at different power conditions.

Figure 4.9 shows the H_2O_2 concentration of the treated broth under different power conditions. At the lowest power, the concentration of H_2O_2 raises to a plateau of 800 μM (10^{-3} mol/m^3) within 120 seconds. Under the highest power conditions, the concentration reaches a plateau of 1720 μM in 120 seconds and remained at this level to the end of the test. At medium power 0.23 W/cm, the concentrations raise gradually, reach a peak of 1800 μM by the end of the test.

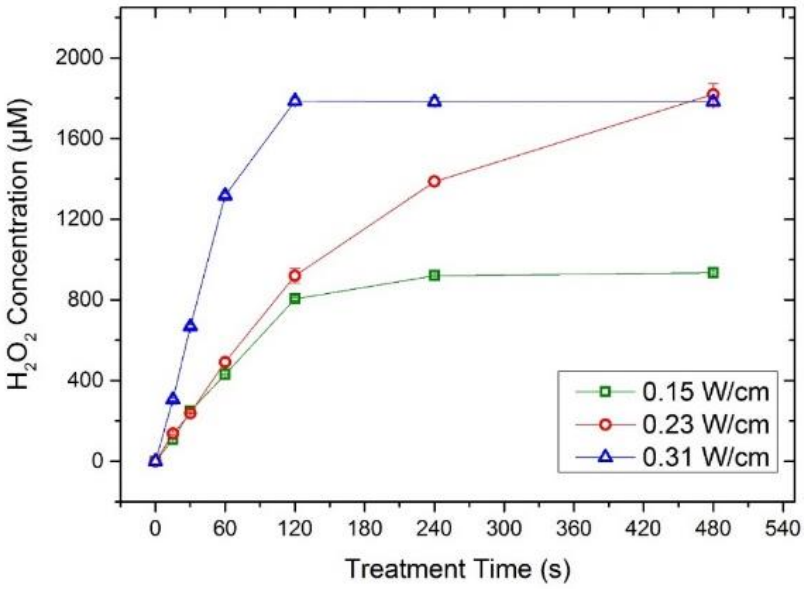

Figure 4.9 Hydrogen peroxide concentration of treated broth as a function of time at different power conditions.

Nitrite concentrations at different operating powers are shown in Figure 4.10 as a function of plasma exposure time. At the lowest power condition, nitrite concentration reaches a peak of 400 μM in 240 seconds then drops below 200 μM at 480 seconds after treatment. At the 0.23 W/cm medium power condition, the nitrite increases sharply and reaches the peak of 900 μM in 120 seconds followed by a rapid decay to 100 μM, finally dropping to 0 by the end of the test. For the highest power considered, the concentration raises sharply and reaches over 600 μM at 120 seconds. After reaching the peak, the concentration drops slowly, finally reaching 0 at 480 seconds.

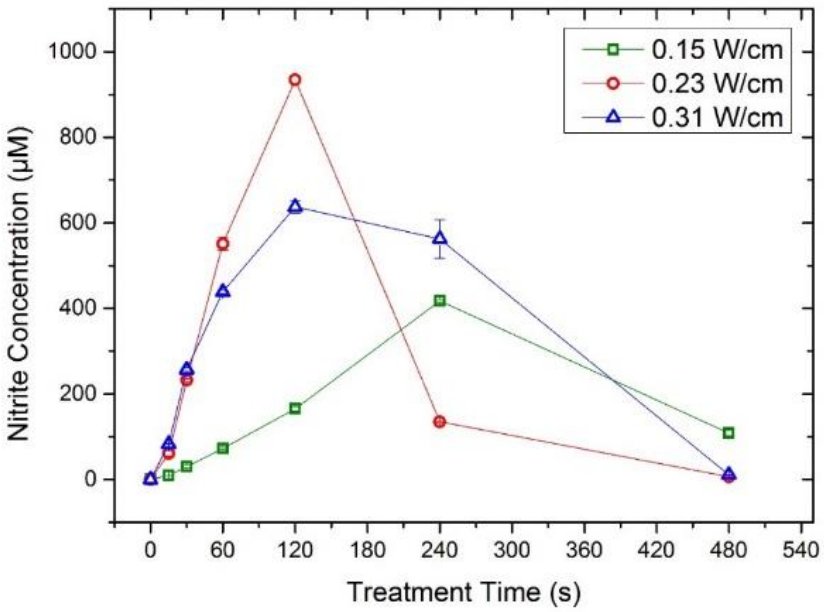

Figure 4.10 The nitrite concentration of treated broth using different power conditions.

4.2.3 Discussion

As discussed previously, many computer simulations have indicated that the major long-lived RONS in the gas phase are H_2O_2, N_2O, NO_2, HNO_2, HNO_3, O_3 and N_2O_5. Among which, RNS are known to lead to an acidification of water. The distance between the SBD and water surface is only 0.5 cm, meaning all long-lived species, and even some short lived species, are transported to the liquid surface.

The acidification of the solution is a consequence of the formation of nitrous acid (HNO_2) and nitric acid (HNO_3) [32]. NO_2 and NO_3 are abundantly formed in the gas phase, this can lead to the generation of NO_2^- and NO_3^- through reactions (16) and (17):

$$e + NO_2 + M \rightarrow NO_2^- + M \quad (16)$$

$$e + NO_3 + M \rightarrow NO_3^- + M \quad (17)$$

In humid air, or through the interaction with a liquid surface, NO_2 can react directly with water molecules to form nitrite and nitrate through reaction (18):

$$NO_2 + NO_2 + H_2O \rightarrow NO_2^- + NO_3^- + 2H^+ \quad (18)$$

N_2O_5 can also contribute to the formation of HNO_2 and HNO_3 as detailed in the previous section, reactions (8) and (9). N_2O_5 can be decomposed in to NO_2 and NO_3 which is then able to further react to form nitrites and nitrates through reactions (16) and (17), or it can directly react with water to form HNO_3.

In Figure 4.9, the concentration of NO_2^- is observed to decrease after 120 seconds at high and medium powers, under low power conditions the decrease occurs after 240 seconds. While in Figure 4.7, the pH continuously drops despite the decreasing NO_2^- concentration.

The decrease in nitrite (NO_2^-) concentration could be a result of further oxidation, yielding nitrates (NO_3^-). This explains why decreases in NO_2^- did not lead to a rise in pH. O_3 is both long-lived and a strong oxidising agent that could be responsible for the formation of NO_3^- from NO_2^-, as in reaction (19). In addition, NO_3 can also react with nitrite to form nitrate, as shown in reaction (20):

$$O_3 + NO_2^- \rightarrow O_2 + NO_3^- \quad (19)$$

$$NO_3 + NO_2^- \rightarrow NO_2 + NO_3^- \quad (20)$$

According to the work of D. X. Liu *et al.* [59], reactions (19) and (20) contribute 90 % of the nitrite loss in plasma treated liquid. Noticeably, the drop of nitrite

accelerates under acidic conditions, as seen in Figure 4.9; according to Machala *et al* [110], reaction (21) is a significant contributor to this:

$$3NO_2^- + 3H^+ + H_2O \rightarrow 2NO + NO_3^- + H_3O^+ \quad (21)$$

Furthermore, H_2O_2 can react with nitrite to form peroxynitrite ($ONOO^-$), as shown in reaction (22):

$$H_2O_2 + NO_2^- \rightarrow H_2O + ONOO^- \quad (22)$$

Peroxynitrite is an unstable structural isomer of the nitrate ion. It is also considered a key oxidative species in plasma treated water for biological applications, as it leads to the damage of microbial DNA and protein. Peroxynitrite also reacts with dissolved NO_3 to form nitrate as shown in reaction (23):

$$H_2O_2 + NO_3 \rightarrow HO_2 + H^+ + NO_3^- \quad (23)$$

Considering other RNS produced in the gas phase, N_2O is very stable in both air and water, but plays a key role in antimicrobial applications. NO is consumed quickly in gas phase, but it still can be traced at high power conditions in Figure 4.2. Despite this, most of the NO in the liquid phase are likely to come from the decomposition of peroxynitrite and nitrous acid as shown in reaction (24) and (25):

$$ONOO^- + OH \rightarrow OH^- + NO + O_2 \quad (24)$$

$$2HNO_2 \leftrightarrow NO + NO_2 \quad (25)$$

For the ROS, most (88%-100%) of the H_2O_2 is generated in the humid gas phase rather than formed directly in the liquid [59]. Although H_2O_2 cannot be detected by FTIR, it can be easily characterised in liquid phase. Another long-lived ROS in the liquid phase is ozone, which is entirely produced in the gas phase and transported in to the liquid. The concentration of dissolved ozone was not measured in the experiment, but from computer simulations it is known that small amount of ozone is consumed through the oxidation of RNS, such as reaction (19); the rest is relatively stable and reaches the liquid surface where it can be dissolved.

The pulse modulated mode of operation was introduced to overcome the significant drop in pH observed under all power conditions in the continuous mode, which is unacceptable for water decontamination applications. As demonstrated, pulse modulation allows plasma to be produced using very low mean dissipated power, favouring ROS production, but does not compromise the discharge uniformity. Both in this study and in the previous experimental work of Ni *et al*. [108], an SBD operating in a pulsed mode of operation was shown to produce high levels of ozone with significantly lower levels of nitrous oxide. Such conditions cannot be achieved in a continuous mode of operation as further reductions in the applied power have the undesirable side-effect of reducing the spatial uniformity of the plasma on the SBD panel.

4.3 Conclusion

The chapter reports on a systematic characterisation of the chemical species produced by the SBD reactor designed in Chapter 3 for both the gas phase and liquid phase. Using FTIR analysis and a commercial ozone monitor the key species generated by the plasma were identified and quantified at different power conditions. Also the time-evolution of the key species was presented. Based on the measurements of key species, different operation modes were distinguished, which include a low power ROS dominated mode and a high power RNS dominated mode. To understand how these two modes of operation arise, the production and loss

pathways of key species was discussed. A key phenomena was the ozone poisoning effect and NO production was identified as the key that led to the rapid drop in ozone concentration, yet the exact mechanism is still not well understood.

In addition to the gas phase species characterisation, the interaction between the afterglow region and a liquid phase was investigated. The concentration of key chemical species, such as H_2O_2 and HNO_2, under different power conditions was measured. Pathways of other reactive species such as NO_3^- and $OONO^-$ were explored based on the available experimental data. It was shown that a pH drop always occurred in the treated liquid sample, yet the amount of drop in pH and the concentration of other plasma generated species in the liquid phase depended strongly on the mode of plasma operation. Given that the applications considered later in this thesis are intended for decontamination of items that may be released in to the environment or consumed by humans and animals, such contaminates are undesirable. A pulsed width modulation technique was introduced to minimise the pH drop in the liquid by reducing the production rate of RNS.

Chapter 5 Plasma species transport

A defining characteristic of the SBD reactor is the gas gap between the plasma and the sample. While this configuration offers some advantages, it has the disadvantage of limiting the mass transport of highly reactive species created in the plasma region to a downstream sample. In order to improve mass-transport for plasma generated species, the electrode geometry of the SBD can be optimised to generate a high gas flow perpendicular to the electrode unit, thus enhancing the transport of reactive species from the plasma region to the sample.

5.1 Introduction

It is well known that dielectric barrier discharges are capable of generating an air flow with a velocity of several m/s, the highest reported being 20 m/s [90]. Charged species produced in the plasma and drifting in the electric field transfer momentum to neutral species in the ambient air through collisions. This phenomena is known as the Electrohydrodynamic (EHD) effect and results in a net body force transmitted to the background gas [111]. While this effect has been explored widely for aerodynamic application, few (if anybody) has considered it as a means to improve the mass transport of species in an SBD reactor.

Typically, the electrode geometry used in the area of plasma assisted aerodynamics comprises of a single strip electrode attached to a dielectric surface with a counter electrode attached to the opposite side, as shown in Figure 3.1. Operating this arrangement in quiescent air typically results in a filamentary plasma, Boeuf *et al* provided an approximate expression to calculate the EHD force generated under such conditions as equation:

$$f(EHD) \approx \varepsilon_0 V^2 s^{-3}$$

Where V is the potential drop in the cathode sheath, s is the sheath length, and ε_0 is the permittivity of air, although difficult to measure such parameters, numerical studies have shown that the range of forces expected to be on the order of 5×10^2 to 5×10^4 N/m^3, with resulting velocities in the m/s range [97]. In addition,

Kriegseis *et al.* demonstrated that the EHD force increases with an increase in operating frequencies and output voltage [112]. In such an arrangement, initiation of the discharge in quiescent air creates a starting vortex which moves along and away from the electrode in a direction parallel to the dielectric surface. However, for the applications considered in this thesis, it is desirable for the reactive plasma species to be transported perpendicular to the dielectric surface and towards the sample. In order to achieve this, two electrodes are placed side-by-side on the dielectric surface, such that a discharge forms in the gap between the two electrodes.

In this chapter a combined analysis of SBD configuration, plasma operating condition and plasma generated airflows is provided, in order to optimise the electrode geometry to achieve the highest flow rate, promoting the transport of species to a downstream sample.

5.2 Experimental setup

Particle image velocimetry (PIV) was used for global measurements of the velocity field generated by SBD reactor. The Setup of the PIV system is detailed in Chapter 3.4. For the capture of images, the frame rate of the camera was set at 750 Hz and the time gap between the laser pulses was 500 µs. For each test run, a sequence of 500 captures were recorded for processing. Following processing, the instantaneous velocity vector field of the airflow around the SBD is obtained. In order to capture the starting vortex generated by the SBD, a pulse generator was used to trigger the laser of the PIV system and the power supply of the SBD simultaneously.

For much of the optimisation activity a simple SBD reactor was considered, employing two parallel copper tape strips separated by a gap variable from 5 mm to 35 mm in 5 mm steps. The dielectric comprised of a Kapton film was used as the dielectric, on which a third piece of copper tape was placed as driven electrode, as shown in Chapter 3.1.

In order to scale the configuration, multiple electrodes are placed side-by-side, thus creating multiple airflow directed perpendicularly from the dielectric surface and

towards the sample. It should be noted that the airflows generated in such a configuration are always created perpendicular to the dielectric surface irrespective of the device orientation.

The plasma power supply used was the same as that described in Chapter 3.1 and the SBD was setup in the chamber as shown in Figure 3.10. The power conditions are listed in table 5.1. For all the configuration tested, the frequency was fixed at 26 kHz.

Table 5.1 Power conditions of tested strip pairs.

Name	Strip Pairs			
Details	Frequency = 26 kHz. Discharge length (mm): 5, 10, 15, 20, 25, 30, 35.			
Output Power (W):	10	15	20	25
Output Voltage (kV_{pp}):	8.5	9.7	10.6	11.4

5.3 Results

PIV results are presented as velocity vector maps, where each vector denotes the magnitude and direction of the flow in that given region; the background colour indicates the mean velocity magnitude at a given point: $\sqrt{(u^2 + v^2)}$.

Figure 5.1 shows the ensemble-averaged vector field of the plasma generated airflow at an applied voltage of 9.7 kV_{pp} with an electrode separation distance of 10 mm. Figure 5.2 shows the initial staring vortex generated by the plasma in a sequence of 6 graphs which capture at 20 t to 120 t, where 1 t equals 1/750 seconds, approximately 1.33 ms.

On initiation of the discharge two starting vortices are created, which move toward one another, collide, and lift vertically away from the dielectric surface by vortex induction, as shown in Figure 5.2. Under continual plasma forcing, the two counter-rotating vortices are followed by a jet flow, which also moves vertically away from the dielectric surface, as seen in Figure 5.3, which shows the ensemble averaged

velocity field around one set of electrodes. Here, data close to the wall is omitted due to the glare caused by the laser reflection on the dielectric surface. As to compare the airflow velocity generated by the discharge with different electrode configurations and voltage conditions, the peak velocity at y = 40 mm from the dielectric surface were recorded from each condition, shown in Figure 5.2. To avoid the un-steady starting vortex, only the final 100 velocity maps from the PIV were used to determine the ensemble-average, after this point the steady-state jet flow conditions had been reached.

At y = 40 mm, it can be seen that higher applied voltages result in a higher flow velocity except in the 0.5 cm gap case, where the 10.6 kV_{pp} condition generates a slightly higher flow compared to the 11.4 kV_{pp} case. For the lowest applied voltage of 8.5 kV_{pp}, the highest flow rate was achieved with a 1 cm electrode separation, whereas for 9.7 kV_{pp} the optimal flow rate was achieved at 1.5 cm separation with a peak flow rate of ~0.5 m/s. Flow rates at 10.6 kV_{pp} show a similar trend as the 9.7 kV_{pp} case, but with a slightly 0.1 m/s higher flow. For the highest voltage, the flow rate increases linearly until the electrode separation of 2 cm is reached, at this point the velocity plateaus between and then drops sharply at 3.5 cm.

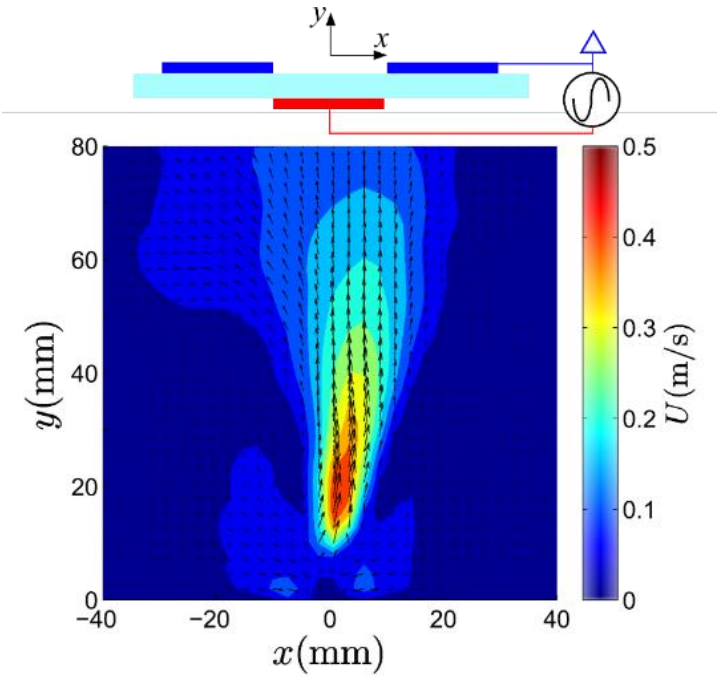

Figure 5.1 Ensemble-averaged velocity vectors generated by SBD using an output voltage of 9.7 kV_{pp} with a gap distance of 10 mm. This image is ensemble-averaged from t=400 to t=500, t=1.33 ms.

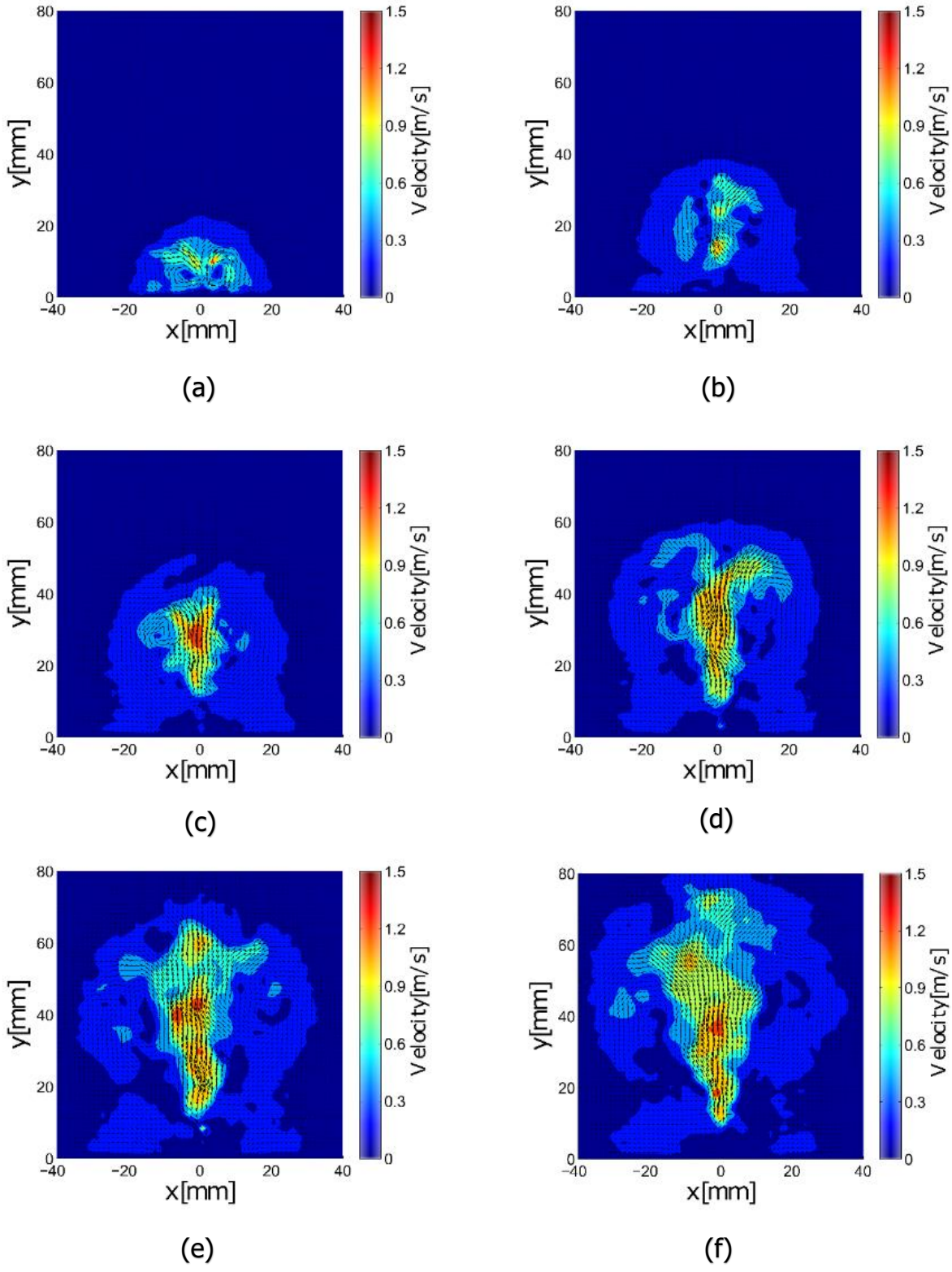

Figure 5.2 Starting vortex generated by SBD actuator at 11.4 kV_{pp} with a gap distance of 30 mm. Images are captured namely at (a) t=20, (b) t=40, (c) t=60, (d) t=80, (e) t=100 and (f) t=120, t=1.33 ms.

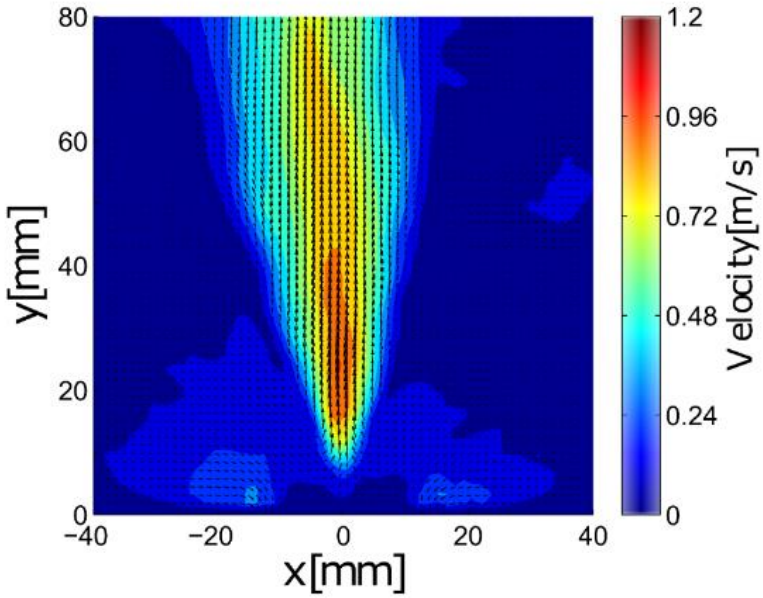

Figure 5.3 Ensemble-averaged velocity vectors generated by SBD actuator at 11.4 kV_{pp} with a gap distance of 30 mm. Original data captured at between 400 t to 500 t, t=1.33 ms.

5.4 Discussion

Kriegseis *et al.* stated that the body force generated by plasma reactor is dependent on the operating voltage and frequency [112]. As to isolate the impact of operating voltage and gap distance on the body force magnitude, the operating frequency in this study was fixed. The velocity field measure at y = 40 mm shows agreement with previous reports that indicate that the airflow velocity increases as output voltage increases [90].

When using parallel strip electrodes, the gap distance between the two facing electrode edges is a key factor in determining the velocity of the flow generated from the dielectric surface. This provides a convenient way to enhance the mass transport of species from the discharge region without having to change the electrical parameters of the plasma, which could negatively impact the discharge chemistry (*e.g.* higher power gives higher flow, but also higher RNS production). If the gap between the two opposing electrodes is small (*e.g.* 5 mm or less, as shown in Figure 5.1), the two discharges interact, resulting in a lower induced velocity. In

addition, as the wall jets travel over the dielectric surface the jet half-width increases, and energy is dissipated through skin-friction drag, which results in a lower induced velocity downstream of the discharge explaining why a large separation distant can lead to a lower flow velocity. Figure 5.4 show the impact of the gap distance between two strip electrodes at various applied voltages. Taking the 10.7 kV_{pp} case as an example, it is clear that the peak velocity is achieved at an electrode separation of 1.5 cm; away from this optimum separation the velocity rapidly drops. Enhancing the electrode geometry to improve the mass transport of plasma generated species to a location is clearly advantageous for any application which relies on their subsequent reaction at the gas-surface interface. On the other hand, separating the electrodes by a significant distance ultimately means fewer strips can be placed within a given area, resulting in a lower density of plasma species produced. Clearly it is necessary to strike a compromise between the spacing of the electrodes (with large gaps resulting in higher velocities) and the amount of plasma coverage in a given area (with smaller gaps favour more plasma volume in a given area).

These results were used to optimise the design of the SBD for the treatment of water (discussed in the previous chapter). In this application, the distance between the SBD surface and sample liquid was around 1 cm and ROS mode of operation highly desirable. Based on the PIV measurements, an electrode spacing of 1 cm was chosen to give a compromise between efficient mass transfer (with flow velocities in the 0.3–0.6 m/s range) whilst still generating a significant amount of plasma (1950 mm^2 of plasma coverage on the 100-mm diameter dielectric disc at a 8.5 kV_{pp} operating voltage). Under such conditions, species in the plasma region are transported to the liquid surface in 20 ms. The velocities required for the strip arrangement are typically five times greater in magnitude than those measured from the widely used hexagonal mesh electrodes typically found in many SBD system (data not shown).

By opting for an electrode separation of 1 cm, rather than the optimum 1.5 cm observed in Figure 5.4, enabled six electrode pairs of varying length to be attached to the dielectric surface. Using the optimum of 1.5 cm reduced the number of electrode pairs to five, resulting in significantly less plasma generation.

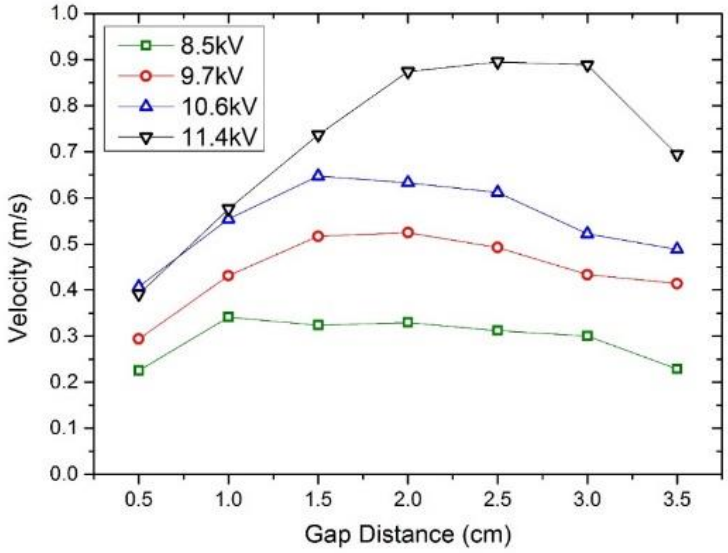

Figure 5.4 Velocity measured at y=40mm of a single electrode pair as a function of electrode gap distance at different power conditions.

5.5 Conclusion

The results presented in the chapter showed that the EHD force induced by the SBD reactor increases as the input power increases, resulting in an increased flow velocity. However, as discussed in chapter 4, a higher power input also leads to the generation of undesirable RNS and ultimately a quenching of the ozone.

To enhance the transport of species, the effect of the electrode configuration on the flow velocity was explored. By changing the gap distance between the electrodes, the induced flow rate could be manipulated. The results showed a non-linear relationship between the gap distance and the flow rate: the highest velocities at different power conditions were observed mainly with 1 cm or 1.5 cm electrode separations. However, from an application perspective, a trade-off is required between plasma generation volume and induced velocity. A 1.5 cm electrode

separation gives a higher flow velocity but reduces the volume of plasma produced in a given area (so less species are produced). As a compromise, a 1 cm gap separation was chosen for the electrode configuration to enable a reasonable amount of plasma to be generated whilst benefiting from the enhanced flow velocity.

Chapter 6 Plasma decontamination of model systems

This chapter explores the antimicrobial potential of air plasma for the decontamination of abiotic samples. In particular, the decontamination of typical waterborne organisms *Escherichia coli* (*E. coli*) and *Pseudomonas fluorescens* (*P. fluorescens*) in drinking-water are considered to highlight the potential for plasma to play a role in water security applications. Secondly, the inactivation of *Aspergillus flavus* (*A. flavus*) spores in both a peptone broth and on an agar surface are considered to highlight the potential for plasma to play a role in food-security applications. In all experiments, the optimised multi-strip SBD reactor was used. Results relating to potable water decontamination were reported in Ni *et al.* [108].

6.1 Microbial decontamination of potable water

As detailed in the literature review, water decontamination with air plasma is primarily due to the generation of ROS with a high oxidation potentials, such as Ozone. Such species are ideal as they are capable of high levels of microbial and chemical removal with no resulting change in the colour, taste or odour of the water; this is in contrast to techniques such as chlorination.

In SBD systems, ozone is assumed to be the primary decontamination agent, chapter 2 demonstrated that it is generated in high concentrations and it is known to be very effective against bacteria. Results in the literature have shown that 0.1 ppm of chlorine requires 4 hours to achieve a 4 log reduction of *E. coli*, whereas for 0.1 ppm of Ozone requires only 5 seconds to reach the same inactivation rate [113]. While Ozone is clearly effective, it is important to note that the inactivation rate is affected by the type of organism, temperature, pH, etc. In addition to ozone, air plasma produces a variety of other RONS that also contribute to the level of decontamination. The objective of this investigation was to explore different plasma generation conditions on the efficacy of plasma decontamination of potable water.

6.1.1 Water decontamination setup

To assess the decontamination potential of plasma for potable water, two common waterborne bacterial species were used, *E. coli* and *P. fluorescens*. Solution samples with a volume of 25 ml were prepared with autoclaved tap water and with an initial concentration of approximately 10^8 CFU/ml of *E. coli or P. fluorescens*. While many reports in the literature detail plasma based decontamination of liquid, the vast majority consider extremely small liquid volumes (~ 1 ml). This investigation considers 25 ml, while this is still a relatively small volume it is more realistic to the real world situation where a small plasma system could be used to provide clean drinking water in an emergency situation. The experimental setup for the water decontamination tests is the same as that described in Chapter 4.2. Both the continuous mode and pulsed width modulation (PWM) mode were considered, as detailed in chapter 3.1.

To analysis the decontamination results, plasma treated samples were later diluted to 10^{-5} in 96-well plates. Then 10 µL of each diluted sample was spread on TSA plates with three groups of repetitions for each dilution. Same protocols were applied to the control groups except for plasma treatment. Plates were incubated overnight at 37 °C for E. coli and 26 °C for P. fluorescens. The limit of detection was around 5.0 x 10^2 bacteria.

6.1.2 Water decontamination results & discussion

The decontamination efficiency of the optimised SBD system as a function of treatment time is shown in Figure 6.1, both continuous and pulse modulated modes of operation were considered. To provide additional insight the pH of the solution is also included (data discussed in chapter 4.2). Figure 6.1(a) shows the decontamination efficiency in a continuous mode of operation (0.15 W/cm), 6.1(b) shows results from a pulse modulated mode of operation, with an equivalent power dissipation 0.038 W/cm. In the pulse modulated case, samples were treated four time longer compared to the continuous mode, given that the duty cycle was 25 %,

the amount of plasma on time is equivalent in both cases. In all tests, the temperature of the sample after treatment was not found to surpass 25 °C.

From the results of continuous mode in Figure 6.1(a), it can be seen that for the first 120 seconds of plasma treatment, both *E. coli* and *P. fluorescens* show a similar inactivation rate. After 120 seconds, the inactivation rate of *E. coli* accelerates, reaching a significant 8 log reduction, which is total inactivation, within 180 seconds of plasma ignition. *P. fluorescens* shows a similar trend, albeit at a slow rate; a 3 log reduction is reached at 180 seconds and a total inactivation is achieved by 240 seconds. Conversely, in pulse modulated mode, *E. coli* is more responsive to plasma treatment than *P. fluorescens*. The level of inactivation rate reaches over 2.5 log for *E. coli* at 240 seconds, whereas only 0.5 log reduction is observed for *P. fluorescens*. Critically, longer treatment times did not lead to a higher level of inactivation of *E. coli*, even after 960 seconds of treatment, the log reduction remained around 2.5. The inactivation level of *P. fluorescens* increased slowly with treatment time, reaching a 1 log reduction after 720 seconds and a 2 log reduction after 960 seconds. It is worth noting that the variation in decontamination results for P. fluorescens is large, varying between 1 and 3 log reduction, making it difficult to draw a firm conclusion.

To interpret the decontamination results it is necessary to consider the gas phase chemistry produced above the liquid sample by the SBD. As highlighted in chapter 4, Figure 4.7, the ozone concentration during both the continuous and pulse modulated modes of operation both exceed 2100 ppm. However, from the results presented in Figure 6.1, the decontamination efficiency under the two different modes of operation vary considerably. An 8 log reduction of *E. coli* and *P. Fluorescens* is observed within 4 minutes of continuous treatment, yet less than 3 log reduction is observed within 16 minutes of pulse modulated treatment, this is despite the same amount of plasma being generated in both cases. From this result, it is possible to conclude that the microbial decontamination effect is not only attributed to ozone, but other ROS and RNS must play a role.

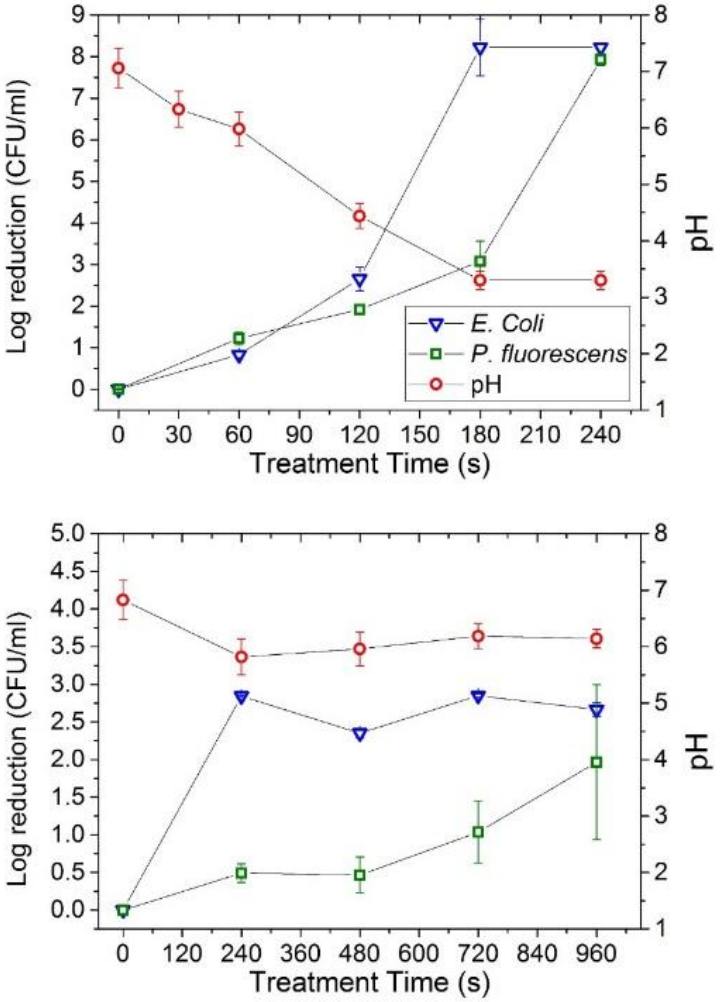

Figure 6.1 Drinking-water treatment results with continuous mode (a) and PWM mode (b).

The pH of the treated solution provides a key insight in to the differing inactivation efficiencies between the two modes. Under pulse modulated operation the pH shows only a minor decrease from 6.8 to around 6; in contrast, the pH drops sharply to 3.5 in the continuous case. According to Small *et al.*, the normal growth pH range for *E. coli* is between 5.0 and 9.0, but it can survive over 2 hours at a pH below 3.0 [114]. In the experiments reported here, samples were immediately recovered after plasma treatment then diluted and spread on to agar. Under these conditions, it is assumed that acidification of the water is not the only factor dictating microbial inactivation.

The level of inactivation of *E. coli* observed in the pulse modulated mode is consistent with that observed during the first 120 seconds of continuous mode treatment. From the temporal evolution of gas phase species shown in Figure 4.7, it is clear that the afterglow chemistry in the pulse modulated mode is very similar to that observed in the first 120 seconds of continuous operation, in which ozone is dominant and the concentration of HNO_3 is at a low level. This suggests that ozone is one of the major inactivation pathways under neutral and weakly acidic conditions; this finding is in agreement with several previous studies, such Pavlovich *et al.*, where aqueous phase ozone was identified as the dominant inactivation mechanism [58].

At lower pH levels, the enhanced level of decontamination is likely a consequence of the synergistic interaction between several ROS and RNS species. This includes the increased production of H_2O_2 and peroxynitrite radicals ($ONOO^-$), both of which are readily able to penetrate cellular membranes and damage bacteria [115].

6.2 Decontamination of Fungi spores using plasma

Moulds produced by fungi on food can be pathogenic to humans and lead to accelerated spoilage. In general, fungi are extremely problematic in agriculture and human health not only because they can cause illness and spoilage, but can produce mycotoxins that are the secondary metabolites and are typically highly carcinogenic [1, 2]. There are 30 species of fungi known to be pathogenic to humans and *Aspergillus flavus* (*A. flavus*) is one of them [116].

A. flavus is found globally as a saprophytic soil fungus and can cause disease on many agriculture crops with the carcinogenic secondary metabolite aflatoxin. The threats from *A. flavus* are either caused by infection, which is called Aspergillosis, or poisoning from aflatoxin, called Aflatoxicosis [117]. Aspergillosis can be developed after exposure to *A. flavus* spores from the air or water, resulting in asthma, extrinsic alveolitis, or allergic bronchopulmonary [118]. Secondary transmission of fungal spores result from infection via wounds and smoking contaminated plant products such as tobacco [119]. According to reports, *A. flavus* attributed to around

65% of childhood aspergillosis in North America [120]. In addition, animals can also be infected by *A. flavus*, domestic animals like rabbits, chickens, turkeys and geese are prone to aspergillosis [117].

Aflatoxicosis is caused by aflatoxins produced by *A. flavus* and results in stunted growth, immune suppression, and cancer development [106][107]. Animal deaths caused by acute Aflatoxicosis are also frequently reported and are usually related to contaminated feeds [117]. In addition, long-term exposure of aflatoxin B1 produced by *A. flavus* can result in higher risk in cancer. B1 is a potent hepatocarcinogen and induces tumours mostly in the liver, but could also happen to kidney, lung or colon to humans and animals [4, 5].

The study of inactivation of fungi spore using atmospheric pressure air plasma is relatively scarce, and no record of treating fungi spore in liquid suspension is found according to review. Thus the experiment in the chapter will explore new area in cold plasma decontamination application.

6.2.1 Fungi decontamination setup

To explore the ability of plasma to inactivate fungi, two non-mycotoxigenic strains of *A. flavus* were used. Mycosomo microbiological bank Ex of Ljubljana, Slovenia, has provided the fungal strains. The fungi were first grown on fresh potato dextrose agar plates for 7 days at approximately 25 °C. After that the agar plates were flooded with peptone broth (half water half peptone, 0.5% Tween 20) and the spores on the surface were gently scraped with a sterile loop and thus the suspension of spores was made. In order to achieve the highest possible homogeneity, the suspensions were stirred evenly by using a vortex mixer. The number of spores in solution was estimated using a Neubauer Brightline haemotcytometer. Following this the suspension was divided into 3 ml test tubes, each with a concentration of 10^6 spores/ml. The samples were divided into two groups, the first group was prepared as 3 ml suspension containing 10^6/ml spore concentrations and then placed in a petri dish for treatment. In the second group,

the suspension was diluted and spread on fresh agar plates, each contained 10^3 spores initially.

During plasma exposure, a magnetic stirrer was used on which samples were placed. The discharge power conditions for the treatment are the same as those stated in chapter 4.2, which were 0.15 W/cm (low power), 0.23 W/cm (medium power) and 0.31 W/cm (high power) with exposure times from 15 seconds to 16 minutes.

For inactivation of *A. flavus* inoculated on agar surface, the samples would be treated directly by the plasma system with the same conditions and exposure time applied in suspension treatment and later incubated for 48 hours under 25 °C. Log reduction was later calculated by counting the number of new grown colonies.

In addition, spores viability was also tested with MTT assay for *A. flavus* inactivation test. 100 µl of each sample was put into new microcentrifuge tubes to which 20 µl of MTT reagent (3-(4, 5-dimethylthiazol-2-yl)-2, 5-diphenyltetrazolium bromide) was added. The tubes were then incubated overnight at 25 °C. After that 1 ml of acidic isopropanol (1 ml of 12 N HCl in 100 ml of isopropyl alcohol) was added to each test tube followed by centrifugation for 20 minutes at 1900 relative centrifugal force. Supernatants were then collected and its UV-visible light absorbance was measured at 560 nm wavelength. Higher absorbance indicated higher number of viable spores.

6.2.2 Fungi decontamination results

Figures 6.2-6.4 show the fungi spore treatment results for different mediums and plasma conditions. For fungi spread on agar surfaces the log reduction of CFU was calculated; for fungi decontamination in liquid suspension, the log reduction of CFU was calculated and metabolic activity of the spores was measured. In all cases, treatment times of 15, 30, 60, 120, 240 and 480 seconds were considered. Only continuous plasma treatments were considered as the production of both ROS and RNS is likely to be advantageous for fungal decontamination.

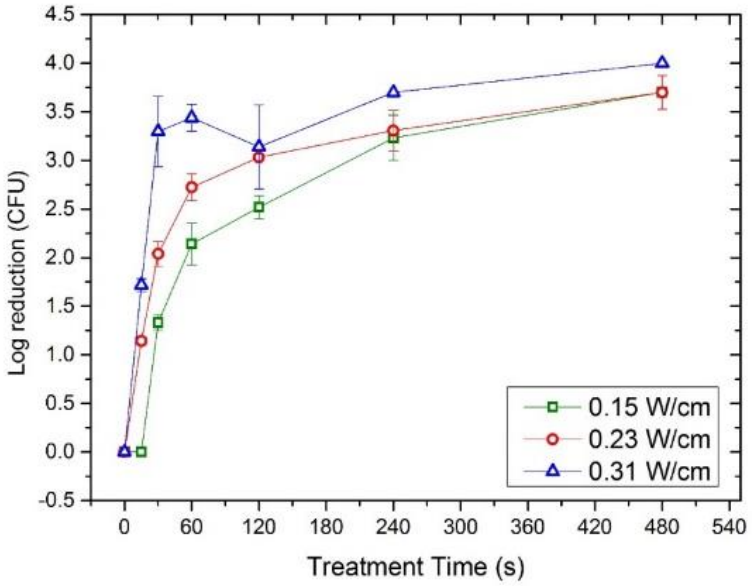

Figure 6.2 Treatment results of spore spread on agar surface.

The decontamination efficiency of fungal spores spread on agar is presented in Figure 6.2. All three plasma power conditions gave at least 3.5 log reduction after 480 seconds of exposure. Differences in inactivation rate at different operating powers can be seen. At 0.31 W/cm, a 1.7 log reduction was observed within 15 seconds of exposure, increasing to 3.3 log reduction after 30 seconds of exposure, the inactivation rate is then observed to reduce and a 4 log reduction after 480 seconds is observed. Under medium power conditions, the inactivation shows a similar trend to that under low power conditions, but with slightly higher reductions.

The decontamination results of fungi spore suspensions are presented in Figure 6.3. Both low and medium power conditions show an almost identical trend, with very little inactivation. Even under the highest power condition, the fungicidal effect is very limited, with a maximum reduction of 0.2 log after 480 seconds of treatment.

Figure 6.4 shows the MTT test results for spores treated in broth solution. The absorbance at 560 nm reflects the level of metabolic activity of spores after treatment, with a lower absorbance indicating reduced metabolic activity. The level of spore activity is directly related to its proteases and aflatoxin productivity of the cell. From the Figure, it can be seen that under high power treatment, the metabolic activity drops with increasing exposure time. Under medium power

conditions, the metabolic activity is seen to increase slightly within the first 30 seconds of treatment time then starts to decrease. For low power treatments, the metabolic activity drops within the first 30 seconds of and then begins to increase slowly.

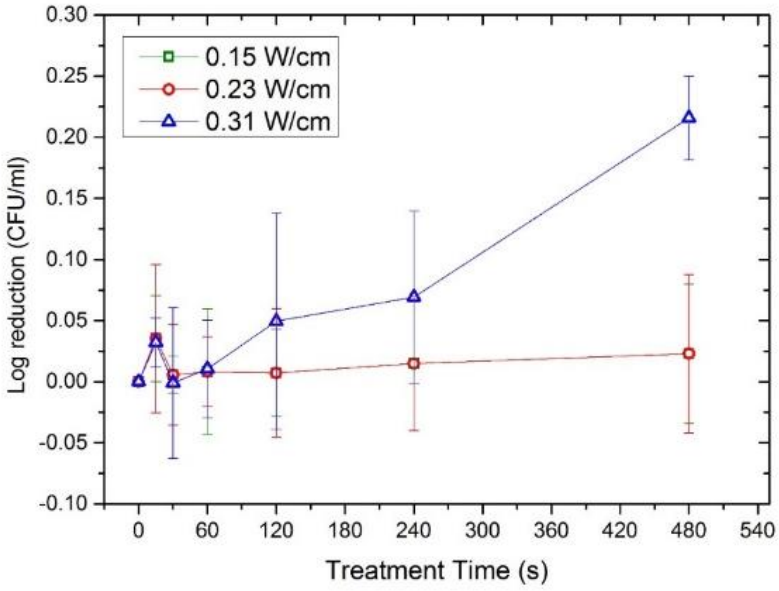

Figure 6.3 Treatment results of spore suspension in peptone broth.

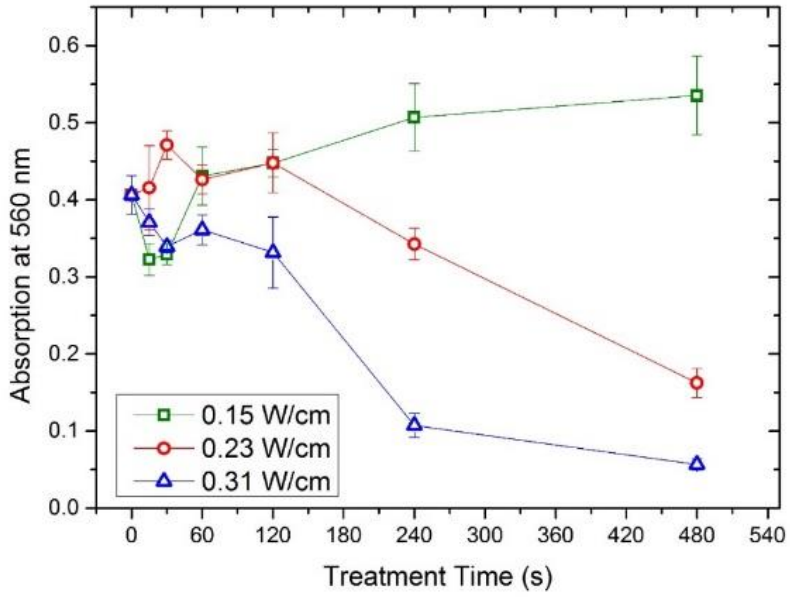

Figure 6.4 MTT assay test results. Metabolic activity level presented by the absorption at 560 nm.

Figure 6.5 shows the temperature change of treated samples as a function of exposure time. In all tests, samples were prepared and left at room temperature for at least 30 minutes to equilibrate prior to plasma treatment. As tests were conducted on different days, the initial temperature of the agar plates was measured at 23 °C and the broth suspension 18 °C. It is clear to see from the graph that the higher the power output the much more the heat dissipated on the samples, and the longer the exposure time the higher the temperature. For treatment on agar the temperature reaches 36, 49 and 56 °C under low, medium and high power exposure respectively. Treatment of broth suspension resulted in a temperature rise to 24, 31 and 34 °C under low, medium and high power conditions respectively.

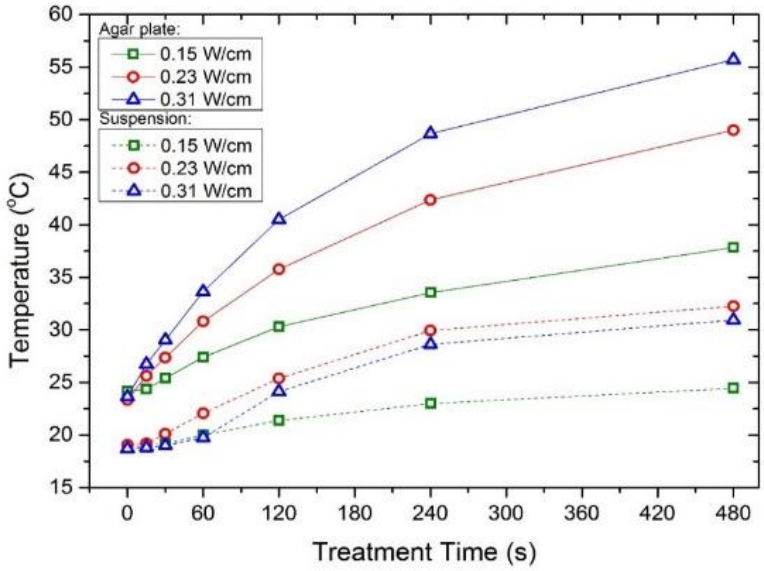

Figure 6.5 Temperature measurement of plasma treated samples. Solid line represents the temperature of the agar plate surface and the dot line represents the temperature of suspension after treatment at different times.

6.2.3 Fungi decontamination discussion

The temperature rise shown in Figure 6.5 is significant; however, according to Agrios *et al.*, *A. flavus* grows well in the 30 – 55 °C temperature range, with the optimum growth occurring at 37 °C; slow growth occurs in the 12 – 15 °C range, and almost ceases at lower temperatures [123]. Based on this evidence, the heat

flux generated by the plasma is unlikely to lead to significant inactivation of *A. flavus*; in fact, the elevated temperature conditions favour their growth in the agar tests. As for the metabolic activity, Oyeleke *et al*. stated that the optimum temperature for proteases produced by *A. flavus* was at 30 °C [124]. In terms of aflatoxin production, the optimal temperature is at 25 °C [125]. Therefore, in agar treatments, the temperatures reached under the highest power treatment conditions may inhibit the toxigenic production of the fungi. While in broth treatment, the temperature after exposure lays in a range which promotes the activity and aflatoxin productivity of *A. flavus* at medium and high power conditions.

The pH is also known to be an important factor that affects both growth and activity of *A. flavus*. At pH 5.5 *A. flavus* has the highest growth rate, with growth inhibited blow pH of 3.0 [126]. As for the protease production, it is known that *A. flavus* produces the most protease at pH 8.0, and the production decreases as pH value decreases [124]. For aflatoxin production, studies suggested that a pH of 5.9 results in the greatest amount of aflatoxin B_1 and the production rate decreases with decreasing pH [125]. Based on these findings, it is suggested that the drop of pH value of the treated broth during plasma exposure would have a significant impact on growth, activity and toxigenic of *A. flavus*. Moreover, the pH measurements for plasma treated broth detailed in Figure 4.8 show significant changes, meaning some change to the behaviour of the fungi is expected, despite the low inactivation rate.

In the tests involving the treatment of fungi in broth, the change in metabolic activity can be explained by considering the evolution of gas and liquid phase species detailed in Chapter 4. During plasma exposure, high concentrations of RONS are transported to the sample. Under high power conditions, the gas phase chemistry is dominated by RNS, including N_2O, HNO_2, HNO_3 and N_2O_5. As described previously, the reaction between these species and the broth solution gives rise to NO_3^- ions, resulting in a pH drop. While RNS dominate the gas phase chemistry, ROS species still occur and the concentration of H_2O_2 was also observed to increase rapidly. In contrast, under low power plasma conditions, ROS dominate the gas phase chemistry, with ozone being the main product. Under these conditions, the concentrations of aqueous species measured are significantly lower than those in high power conditions and the reduction in pH of the broth is reduced.

These trends can explain the changes observed in the spore metabolic activity. H_2O_2 is a well-known disinfectant that has a high oxidation potential, higher concentrations of H_2O_2 increase inactivation of the fungi and a lower overall metabolic activity. When H_2O_2 production is halved in the lower power conditions, spore activity increases. The large amount of NO_2^- produced reacts in the solution to form HNO_2 and HNO_3, leading to a pH drop. Under higher power conditions, the conversation of nitrite to nitrate is accelerated. The high concentrations of both Nitrites and H_2O_2 will lead to increased formation of peroxynitrite ($ONOO^-$) which is a very strong disinfectant, combined with the reduced pH the environment for fungi spores is considerably harsher.

Under low power treatment conditions, the concentration of nitrite is relatively low, shown in Figure 4.10. According to previous characterisation, plasma operates in ROS dominate mode at low power condition and hence higher the level of pH value. Furthermore, a lower concentration of H_2O_2 is produced resulting in less production of $ONOO^-$. Consequently, the concentration of disinfectants is not high enough in the broth and the pH value lays in the range which in favour of fungi's growth and activity, as a result that can be seen from Figure 6.4, the metabolic activity actually raised due to the treatment at low power condition.

When considering the treatment of fungal spores spread directly on agar, the elevated temperatures during plasma treatment promote growth under all power conditions. All power conditions show a good level of decontamination, meaning both ROS and RNS dominant regimes are effective. Under higher power conditions, the inactivation rate is accelerated, reaching a 1.5 log reduction within 15 seconds. Under low power conditions, no decontamination is observed after 15 seconds. All three power treatments achieved a substantial 3 log reduction by the end of the test.

Comparing the results presented in Figure 6.2 for agar and 6.3 for broth show very different levels of *A. flavus* inactivation. This is attributed to the presentation of the spores to the plasma generated species. When treating spores on the surface of an agar plate, plasma generated species directly interact with all spores on the surface. Stacking is assumed to minimal meaning all spores receive an even dosage of RONS. In broth treatments, a very minor reduction is observed in all cases,

although plasma treatment does impact metabolic activity. Comparing the two treatment scenarios, it is clear that spores suspended within broth are considerably more difficult to inactivate. The composition of the broth (half peptone and half water with 0.5% Tween 20) was a wealth of targets for plasma generated RONS to reactive with, meaning the number of species available to inactive the spores is considerably reduced; this is in direct contrast to the direct exposure achieved in the agar test.

6.3 Conclusion

The results reported in this chapter indicate that SBD reactors can be effective for the microbial decontamination of solid surfaces and liquids. For the treatment of potable water, the continuous mode of plasma operation gave better levels of microbial decontamination but a simultaneous drop in pH during treatment would render the water undrinkable. Using pulse modulation to reduce the power dissipated in the plasma was less efficient for microbial decontamination but the pH remained within acceptable range throughout the plasma exposure. Given that ozone is the main product under low power plasma conditions, it is most likely the main agent responsible for microbial decontamination; both UV irradiation and other low-concentration species are likely to play a synergistic role.

For the decontamination of *A. flavus* spores two different conditions were considered, with the spores spread on a nutrient solid rich agar surface and suspended in a nutrient broth. Both conditions mimic typical environments that may be encountered in food security application. The results indicated that plasma decontamination was far more effective for spores spread on the agar surface compared to those in the broth solution. This was not an unexpected result, spores exposed directly to the plasma afterglow on a surface receive a significantly large dose of RONS compared to the scenario where they are surrounded by a nutrient rich fluid. These results indicate plasma could be an effective decontamination technique for fungal spores on a surface, but is unlikely to be useful when spores are suspended within complex liquids unless the parameters of the plasma are significantly different from those investigated here.

In all cases, the trends in decontamination efficiency and metabolic activity can be directly linked to the gas and liquid phase species produced by the plasma. The use of high power discharges tended to yield improved inactivation efficiency at the cost of acidification of liquid samples. From an application perspective, the acidification may or may not be problematic. Overall, the investigations have demonstrated that the effectiveness of plasma for microbial decontamination is highly dependent on the reactive species produced, which are in-turn, strongly influenced by the plasma generation parameters. While this adds to the complexity of the situation, it does provide numerous opportunities to optimise the discharge for enhanced efficiency.

Chapter 7 Plasma decontamination – Real world applications

This chapter considers the use of an SBD to directly decontaminate both beef loins and the packaging materials they are transported in. This investigation was motivated by recent reports indicating the presence of foodborne pathogens on the outside of packed meat that is sold to the consumer. The experiments were carried out in collaboration with Prof. Frans Smulders at the Institute of Meat Hygiene, University of Veterinary Medicine, Vienna. To facilitate this collaboration, a large area SBD was developed in Liverpool and transported to Vienna where the meat testing was conducted, detailed later. As a result, the plasma system employed differed physically from those described in Chapter 3, yet it was design to maintained the key features of those discussed earlier.

7.1 Introduction

The antimicrobial effects of non-thermal atmospheric pressure plasma have in the past years been reported for various food items, particularly carbohydrate-based foods such as soft fruits and salads. Yet, data on its application for muscle foods is relatively scarce, as seen in Chapter 2. This investigation was aimed to explore the impact of plasma treatment on muscle foods, not only in terms of antimicrobial efficacy, but also the physical and chemical changes occurring on the meat surface as a result. In addition, it is well known that the outside of pre-packaged meat hosts a wealth of pathogenic bacteria that has the potential to cause illness in consumers [127]. As a potential solution to reduce the microbial loading on packaged meat, the efficacy of SBD decontamination was assessed and the ability of plasma species to breach the packaging barrier considered.

7.2 Materials and Methods

To assess the efficacy of plasma decontamination of meat, *Staphylococcus aureus* (*S. aureus*), *Listeria monocytogenes* (*L. monocytogenes*) and two *Escherichia coli* (*E. coli*) strains were inoculated on to beef loins. Additionally, to assess the ability of

plasma to decontamination typical packaging materials the same strains were inoculated on to polyamide-polyethylene (PAPE) packaging film. After plasma treatment, the CFU of bacteria remaining on the sample were counted and in the case of meat treatment, several quality parameters, such as surface colour, lipid peroxidation (TBARS), nitrite and nitrate uptake, and myoglobin (Mb) isoform distribution were assessed. All beef samples were vacuum packed for period of 10 days and a subsequent 3 days of aerobic storage, which follows the industrial standards.

7.2.1 Beef and packaging sample preparation

Beef loins were excised from the carcass of three 17 - 18-month-old Fleckvieh bulls, which had been slaughtered, subsequently refrigerated at 2±2 °C, and sectioned to primal cuts, which were vacuum packed and further refrigerated. At 3 days *post mortem,* loin sub-primals were transported to the laboratory in refrigerated containers, and upon arrival portioned in approximately 2 x 5 x 5 cm cross sections to be assigned to plasma treatment or used as control.

The packaging film used was a 90 µm thick polyamide-polyethylene (PAPE) food grade packaging film (Combivac, foil type 20/70), with O_2 permeability of 50 $cm^3/(m^2 \cdot 24\ h \cdot bar)$, CO_2 permeability of 150 $cm^3/(m^2 \cdot 24\ h \cdot bar)$, N_2 permeability of 10 $cm^3/(m^2 \cdot 24\ h \cdot bar)$, and steam permeability of 2.6 $g/(m^2 \cdot 24\ h \cdot bar)$.

7.2.2 Plasma system setup

A new plasma source was constructed to facilitate the experiments, it was similar in design to those detailed previously and consisted of a self-oscillating half-bridge circuit and an SBD electrode panel with a square quartz dielectric sheet, 10 x 10 cm in area. The SBD design mirrored that of the 5 x 5 cm mesh electrode design detailed in Chapter 3. A 50 V DC power supply (Gwinstek programmable DC power supply, model PSP-603) was used to power the system, and the natural resonant frequency of the system was found to be 9 kHz. Photographs of the system under

differing operating conditions were used to calculate the surface coverage of the plasma enabling power densities (W/cm^2) to be calculated, which was different to the previous experiments where power per length (W/cm) was used. Based on FTIR measurements (detailed later), three operating power conditions were established, detailed in table 7.1.

Table 7.1 Plasma operating conditions.

Power conditions	Power input (P_{in}) [W]	Output Voltage (V_{pp}) [kV]	Dissipated Power (P_{out}) [W]	Power Density [W/cm^2]
Low	20.7	8.16	17.87	0.48
Medium	25.4	8.88	21.73	0.56
High	29.9	9.44	25.38	0.67

For all tests, the SBD was suspended 2 cm above the sample, no enclosure was used meaning ambient air was free to move around the sample during treatment. To minimise any heating effects, treatment times were limited to one minute.

7.2.3 Plasma gas phase species characterisation

Key species generated by plasma were characterised using FTIR measurements under different operating power conditions, as described previously in Chapter 3. All characterisation activities on the system were carried out at the University of Liverpool.

7.2.4 Microbiological analysis

The antimicrobial efficacy of the SBD was assessed using four common pathogenic foodborne bacterial strains, namely, *Staphylococcus aureus* DSM 1104 (*S. aureus*), *Listeria monocytogenes* DSM 19094 (*L. monocytogenes*), *Escherichia coli* DSM 1103 (*E. coli*) and an isogenic mutant of *E. coli* O157:H7 EHEC strain EDL 933 (*E. coli*

O157), provided by C. Martin, Unité Microbiologie, INRA Clermont-Ferrand-Theix, France.

Bacteria were kept in 20% glycerol at -80 °C. Before use, strains were separately cultivated in LB broth (10 g/L tryptone, 5 g/L yeast extract, 5g/L NaCl) and incubated overnight at 30 °C to reach the stationary phase. The overnight cultures were diluted in 0.85% saline to 5 log CFU/ml and the bacterial suspension was ready for further tests.

As a first test to ensure the efficacy of the new system, 0.1 ml volumes of bacterial suspension were spread on to agar plates. Once dry, the plates were subjected to SBD treatment. Controls consisted of agar plates inoculated with the original suspensions and decimal dilutions thereof. Plates after treatment were incubated for 48 h at 30 °C and colonies per plate then recorded. In order to exclude growth of contaminant bacteria, the colonies were examined for morphology and the density of colonies was confirmed by testing three colonies per plate with Gram stain and biochemical testing (API 20E, Staph, Listeria schemes, BioMerieux). For plates with no colony growth, a value of 1 CFU/plate was assigned. For each strain and treatment setting, six replicates were processed.

In order to study the efficacy of the SBD treatment of bacteria contaminating a packaging film surface, suspensions (10 µl droplets) of the aforementioned bacteria were placed on a polyamide-polyethylene film and immediately subjected to SBD treatment. To determine the level of microbial reduction, the inoculated film was excised under sterile conditions and then vortexed with sterile glass beads in 10 ml of 0.85% saline, and the suspension processed as indicated above. In addition, for each strain and treatment setting, six replicates were treated.

Finally, to determine the antimicrobial efficacy of the SBD on beef loin, two strains of bacteria were inoculated on to the prepared beef loins (*E. coli* and *S. aureus*). Each beef sample contained approximately 10^5 CFU. Six replicates were done for each strain and power condition.

7.2.5 Beef loin treatment

Three different groups of tests were conducted. A pre-test (test 0) was conducted to examine the antimicrobial efficacy of SBD treatment on beef loins and any 'immediate' effects of plasma treatment on muscle colour. The results from test 0 inspired and motivated two further tests, named test 1 and test 2.

In test 1, the effects of treating beef loins with high and low power plasma conditions were studied over a vacuum storage period of 10 days. Before treatment, samples were stored in refrigerator for 3 days. Furthermore, colourimetry, nitrite/nitrate, myoglobin (Mb) isoforms and lipid peroxidation (TBARS) were measured before and immediately after treatment.

Test 2 included treatment with all 3 power conditions and, besides the 10 days' vacuum storage, aimed at studying 'delayed' effects possibly observed after a subsequent final 3-day period of aerobic storage in a display refrigerator, fitted with a glass door and samples were exposed to day light, at 3±2 °C. Before treatment, samples were stored in refrigerator for 7 days.

Notably, only one side of the beef loin samples were facing the SBD electrode, and all the tests included two control groups. The first control group did not receive any plasma treatment, which reflects the industrial standard currently achieved in commercial practice. The second control group were subjected to plasma treatment whilst being fully sealed in a vacuum pack, this enabled the comparison between directly exposed beef loins with the untreated control group and to examine if plasma species breached the packaging material of the second control group, which would show similar effects to the direct treated samples.

7.2.6 Physical-chemical analysis of beef samples

Temperature and pH measurements were only conducted in test 2. The surface pH and temperature immediately before and after plasma exposure were measured using a pH meter (Testo, model 230) combined with a surface pH electrode

calibrated at pH 4 and pH 7 (Blue Line SI Analytics), and an infrared thermometer (Testo, model 831).

To evaluate changes in the meat surface colour, the L*, a*, b*, Chroma and Hue values were measured using a double beam spectrophotometer (Phyma Codec model 400) with an aperture radius of 8 mm. Results are reported as an average of two scans. Measurements were taken on day 0 (before and immediately after SBD treatment) as well as after a further three and 10 days of vacuum storage at 2±2 °C, this methodology is similar to that reported by Faustman & Phillips [128]. For measurements at seven and 10 days, the samples were unpacked, re-measured and subsequently repacked. The time interval between unpacking and repacking was approximately 1 minute. Colour values after further storage under atmospheric conditions were only measured during test 2 at 13 days after plasma treatment. During all tests, hygienic sample handling was assured by wearing surgical gloves.

After 13 days of storage post-plasma treatment, 5 g of beef loin samples were taken from the treated surface of all vacuum packaged samples to establish sarcoplasmic protein solubility using the method of Hart, described by Swatland *et al*. [129]. The sarcoplasmic protein solubility has been widely used as an indicator of muscle meat quality, and the solubility drops as the meat denaturalise [130]. Although Hart's 1962 test was primarily developed for studying intrinsic denaturation in PSE (pale, soft, exudative) pork, the method has been proven equally useful as an indicator for increased sarcoplasmic protein denaturation in bovine muscle, for example, as resulting from electrical stimulation [131].

In order to measure Nitrite/Nitrate uptake in beef loin samples, 10 g of the homogenised meat samples was mixed with 40 ml distilled water, heated for 15 minutes and filtrated through a folded filter paper (MN 625 ¼, Macherey Nagel, Düren, Germany) as well as a membrane filter (0.2 µm cellulose acetate) according to Schmidt & Schwedt [132]. Nitrate levels were determined using High Performance Liquid Chromatography (HPLC; Waters 600s Controller 626 Pump Bio-Inert, PDA 996). Nitrate was separated on a Spherisorb-NH_2, 5 µm, 250 × 4.6 mm anion-exchange column, equilibrated at 20 °C. The eluent was composed of 95% K_2HPO_4 solution (10 g/1000 ml, adjusted to pH=3 with orthophosphoric acid) and

5% acetonitrile, with a flowrate of 1 ml/min. Total run time was 5 min and the detection was at 205 nm.

To assess the extent of lipid oxidation and its consequent possible effects on colour after plasma treatment [133], the content of Thiobarbituric Acid Reactive Substances (TBARS) was determined according to Witte *et al*. [134].

Furthermore, spectral analysis was conducted on meat surface shavings in order to examine changes in the distribution of Myoglobin (Mb) isoforms following plasma treatment. In the analysis, 10 g of homogenised sample were mixed with either 50 ml distilled water, or (for nitrosomyoglobin analysis) with 50 ml acetone and then cooled for 1 h. After filtration through a folded filter paper (MN 625 1/4; Macherey Nagel, Düren, Germany), the extinction of the filtrate was analysed using spectrophotometer (Hitachi U3000, Japan) at 450-700 nm. Myoglobin (Mb) is the substance that stores oxygen in the muscle and the primarily pigment that is responsible for meat colour. Before binding with oxygen, Mb is in isoform of deoxymyoglobin (DeMb) which is physiologically active and with the colour of purple. After binding with oxygen, oxymyoglobin (MbO) is formed and the colour changes to an attractive cherry-red. Further oxidation may lead to the formation of metmyoglobin (MMb) and the colour changes to an unattractive greyish-brown [135].

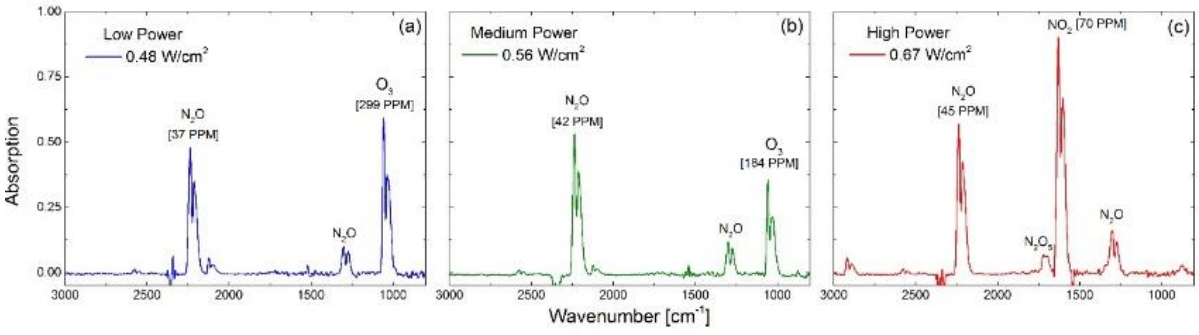

Figure 7.1 Evolution of IR spectrum of key species under different plasma operation conditions.

7.3 Results

7.3.1 Plasma gas phase species

Figure 7.1 shows the steady-state FTIR absorption spectra of the discharge effluent under the low, medium and high power operating conditions highlighted in Table 7.1. Under low power conditions, shown in Figure 7.1 (a), Ozone is the predominate species produced. As the discharge power was increased Ozone production is inhibited due to accelerated thermal degradation and NO_x generation as shown in Figure 7.1 (b) & (c). Under the highest power condition (Figure 7.1 c), NO_2 is the dominant species, resulting from the oxidation of NO in the plasma region. The low power operating point was determined as the minimum dissipated power capable of sustaining plasma over the entire electrode area. The high power operating condition was determined from the FTIR data as the point at which Ozone production was completely inhibited. The medium power operating point was chosen as the mid-point between the high and low power conditions.

7.3.2 Antimicrobial effects

Plasma treated beef loin samples in test 0 did not achieve any significant inactivation of the two tested bacteria under any power conditions used (< 1 log).

Plasma treatment of inoculated agar plates achieved a significant reduction of the four test strains, with low power condition yielding a higher level of reduction than the higher power conditions, as seen in Table 7.2. To demonstrate plasma species do not penetrate food packing material, inoculated agar plates were covered with a sheet of 90 µm polyamide-polyethylene film before treatment, in this scenario no significant reduction in microbial numbers was observed. These results indicate plasma species do not penetrate through the film in significant quantities. A significant reduction of bacteria was also observed when bacteria suspended in 0.85% saline were placed on packaging film and exposed to the SBD, as shown in Table 7.3. This scenario, mimicking a 'fresh' contamination as could occur during packaging, resulted in a >1.5 log reduction at high power condition and a >2 log

reduction at low power condition. Again, the lower power treatment obtained greater bacterial reduction than high power treatment.

Table 7.2 Effect of treatment with atmospheric air plasma (exposure 1 min, 2 cm distance) on bacterial test strains spread onto agar plate. Numbers are expressed as log CFU per plate.

	Untreated control (log cfu/plate)	Treated with low power SBD		Treated with high power SBD	
		Direct	Covered	Direct	Covered
S. aureus DSM 1104	3.8	0.4±0.4	3.6±0.1	0.8±0.4	3.6±0.0
L. monocytogenes DSM 19094	3.4	0.2±0.3	3.5±0.2	0.3±0.3	3.5±0.3
E. coli DSM 1103	3.6	0.1±0.2	3.6±0.0	0.8±0.2	3.7±0.1
E. coli O157	3.4	0.1±0.2	3.5±0.2	0.8±0.2	3.4±0.3

*Table 7.3 Effect of treatment with atmospheric air plasma (exposure 1 min, 2 cm distance) on bacterial test strains inoculated onto a polyamide-polyethylene film. Unless indicated otherwise, numbers are expressed as log CFU/10 µl. * Note that the limit of detection is 2 log CFU/cm^2 when using 0.85% saline suspension.*

	Native film (log cfu/cm^2)	Untreated Control	Treated with low power	Treated with high power
S.aureus DSM 1104	<2*	7.2±0.1	4.2±0.2	5.5±0.2
L. monocytogenes DSM 19094	<2*	8.1±0.1	6.2±0.2	5.9±0.3
E. coli DSM 1103	<2*	7.6±0.2	4.9±0.3	5.9±0.3
E. coli O157	<2*	7.1±0.g	4.7±0.2	5.7±0.2

7.3.3 Physical-chemical effects on beef samples

The pH and temperature measurements revealed that plasma treatment had no significant effect on the surface pH of the treated beef sample, which were essentially constant at 5.8 in all treatment groups. The surface temperature increase was on average between 1.5 to 2 °C under all power conditions.

Colourimetry assessments in test 0 showed that SBD treatment of vacuum-packed beef at high or low power had no significant effect on colour parameters. When freshly cut beef surfaces were directly exposed to the plasma under high power conditions, statistically significant increases of 2.7±0.9 for a*, of 5.3±1.3 for Hue angle and a decrease of 2.2±1.1 for Chroma were observed at day 0; conversely, no significant changes were seen for direct exposure to low power plasma. In order to examine if such differences would persist when the meat was stored in a vacuum-package for up to 10 days, test 1 was designed and conducted.

In test 1, before the plasma treatment, no significant difference was found for the colour parameters of the three sample groups. After 3 and 10 days storage, the exposed and then vacuum packaged group had significantly higher a*, b*, Chroma and Hue angle values than those of the untreated control, or those of vacuum-packed then treated control group, as shown in table 7.4.

Results for test 2 are shown in table 7.5. Comparisons of vacuum-packed beef with plasma treated vacuum-packed beef at three power conditions showed few significant differences.

In terms of Sarcoplasmic protein solubility, no significant difference in transmission values existed between treatment groups, indicating a similar degree of sarcoplasmic protein denaturation (see Table 7.6). The variation in values is similar to that recorded by Den Hertog-Meischke et al. [136], who sampled refrigerated veal loin samples at two days' *post mortem* and (relying on the same method used in this study) also observed mean transmission values to range from roughly 54 to 59 %.

Table 7.4 Test 1: The effects of subjecting (non-packaged/vacuum packaged) beef loin cross sections to plasma treatment on surface colour parameters, as measured after 3 and 10 days storage in vacuum at 2±2 °C; means and standard deviations of 6 replicate measurements.

Test 1: Pre-treatment values at day 0						
	High power treatment			Low power treatment		
	Control	Treat - pack	Pack-treat	Control	Treat - pack	Pack-treat
L*	37.1±2.8	36.1±2.6	37.5±2.3	39.3±2.2	36.9±2.5	38.2±3.3
a*	14.5±1.7	14.0±1.0	14.3±2.3	11.2±1.1	11.3±1.2	10.7±1.0
b*	8.9±1,1	8.6±1.1	9.0±2.2	7.9±1.3	7.4±0.9	7.6±0.8
Chroma	17.0±1.9	16.4±1.6	17.0±3.1	13.7±1.6	13.3±1.6	12.9±1.8
Hue$^{\Delta}$	31.5±1.7	31.4±1.9	32.0±2.1	35.1±2.0	33.1±2.0	33.4±2.6
After 3 days of vacuum storage						
	High power treatment			Low power treatment		
	Control	Treat - pack	Pack-treat	Control	Treat - pack	Pack-treat
L*	34.7±2.4	38.6±2.4	38.6±3.0	36.8±2.6	36.3±2.7	35.6±3.7
a*	13.0±0.4	15.6±0.8	13.5±1.5	9.6±1.1	10.5±1.0	10.2±1.6
b*	8.0±0.6	11.1±1.0	8.0±1.0	5.9±0.9	6.7±1.0	6.2±1.3
Chroma	15.3±2.2	19.1±1.0	15.7±1.7	11.3±2.1	12.4±1.3	11.9±2.0
Hue$^{\Delta}$	31.3±2.0	35.6±1.8	30.6±0.6	31.4±2.1	31.8±2.2	30.6±1.4
After 10 days of vacuum storage						
	High power treatment			Low power treatment		
	Control	Treat - pack	Pack-treat	Control	Treat - pack	Pack-treat
L*	40.0±2.2	41.2±3.8	39.3±2.7	39.5±3.7	39.8±2.1	38.9±3.3
a*	12.2±0.9	14.0±1.3	13.0±0.7	10.8±0.9	10.9±1.1	10.5±1.4
b*	8.1±1.1	11.0±1.4	8.0±0.8	7.6±0.8	7.9±1.0	7.8±1.1
Chroma	14.7±1.2	17.6±1.4	15.6±0.9	13.2±1.1	13.5±1.4	13.1±1.7
Hue$^{\Delta}$	33.4±2.5	37.0±2.9	33.4±1.7	34.9±1.7	35.5±1.3	35.7±0.8

Table 7.5 Test 2: The effects of subjecting vacuum packaged cross sections from beef loins to plasma treatment on surface colour parameters, as measured after 3 and 10 days of further storage in vacuum at 2±2 °C and after a subsequent 3 day aerobic storage in a display refrigerator (3±2 °C); means and standard deviations of 6 replicate measurements.

Test 2: Pre-treatment values at day 0						
	High Power		Medium Power		Low Power	
	Untreated	Pack-treat	Untreated	Pack-treat	Untreated	Pack-treat
L*	35.4±2,4	35.5±3.2	35.4±2,4	37.3±3.3	35.4±2,4	36.1±3.0
a*	13.5±1.3	14.6±1.9	13.5±1.3	13.6±1.6	13.5±1.3	15.3±1.3
b*	8.4±1.5	8.9±1.4	8.4±1.5	7.8±1.5	8.4±1.5	9.8±1.1
Chroma	15.9±1.8	17.1±2.3	15.9±1.8	15.7±2.0	15.9±1.8	18.2±1.4
Hue$^{\Delta}$	31.7±2.4	31.5±0.5	31.7±2.4	29,5±2,6	31.7±2.4	32.7±2.5
After 3 days of further vacuum storage						
	High Power		Medium Power		Low Power	
	Untreated	Pack-treat	Untreated	Pack-treat	Untreated	Pack-treat
L*	36.9±2.1	39.0±2.4	36.9±2.1	37.5±2.2	36.9±2.1	37.2±2.9
a*	11.9±0.8	11.8±1.3	11.9±0.8	11.5±0.9	11.9±0.8	12.3±1.0
b*	7.6±0.8	7.4±1.1	7.6±0.8	6.9±0.7	7.6±0.8	7.4±0.6
Chroma	14.2±1.0	14.0±1.6	14.2±1.0	13.4±1.1	14.2±1.0	14.4±1.1
Hue$^{\Delta}$	32.6±1.4	31.8±1.6	32.6±1.4	31.1±1.7	32.6±1.4	30.9±1.7
After 10 days of further vacuum storage						
	High Power		Medium Power		Low Power	
	Untreated	Pack-treat	Untreated	Pack-treat	Untreated	Pack-treat
L*	38.7±2.3	40.7±1.4	38.7±2.3	40.7±2.5	38.7±2.3	41.4±3.3
a*	11.4±1.2	12.2±0.7	11.4±1.2	11.6±1.1	11.4±1.2	12.0±0.9
b*	7.4±1.1	8.2±0.7	7.4±1.1	7.2±0.9	7.4±1.1	7.4±0.9
Chroma	13.6±1.5	14.7±0.9	13.6±1.5	13.6±1.4	13.6±1.5	14.2±1.0
Hue$^{\Delta}$	32.9±1.2	33.3±1.4	32.9±1.2	31.8±0.8	32.9±1.2	32.0±3.6
After a further 3 days of aerobic storage (13 days after treatment)						
	High Power		Medium Power		Low Power	
	Untreated	Pack-treat	Untreated	Pack-treat	Untreated	Pack-treat
L*	40.6±2.9	42.8±2.5	40.6±2.9	41.9±3.0	40.6±2.9	42.5±2.2
a*	17.5±2.0	19.2±1.2	17.5±2.0	17.1±1.5	17.5±2.0	19.0±1.1
b*	13.9±1.8	15.1±1.6	13.9±1.8	13.7±1.4	13.9±1.8	15.3±1.1
Chroma	22.3±2.6	24.4±1.9	22.3±2.6	21.9±2.0	22.3±2.6	24.4±1.4
Hue$^{\Delta}$	38.4±0.9	38.1±1.5	32.9±1.2	38.6±0.5	38.4±0.9	38.7±1.2

The level of nitrite observed in test 1 was consistently below the limit of quantification (1.4 mg/kg $NaNO_2$), whereas nitrate concentrations, expressed as KNO_3, were in the range of 0.1 to 0.23 mg/kg. The TBARS measurements were below 0.1 mg Malondialdehyde/kg, with the exception of a single sample (0.11 mg/kg). The TBARS values recorded in Test 2 after 3 days of aerobic storage are presented in Table 7.6.

Table 7.6 Lipid peroxidation (TBARS) and sarcoplasmic protein solubility of beef loin samples measured 13 days after treatment with High (HP), Medium (MP) and Low Power (LP) conditions.

	Control	Direct treated			Vacuum packaged then treated		
		HP	MP	LP	HP	MP	LP
TBARS (mg/kg MDA)	0.17± 0.03	0.15±0.03	0.14± 0.02	0.15±0.02	0.14±0.02	0.15±0.03	0.13±0.03
% Transmission	52.6± 7.9	56.9±15.0	-	60.1±18.1	53.9±10.8	-	58.2±12.5

Figure 7.2 shows the results of spectrometric analysis of myoglobin isoforms are presented graphically in tests 1 and 2. The results show the spectrographs of myoglobin isoforms in absorptions as a function of wavelength.

Figure 7.2 (a) and (b) present the spectrograph of sample from four treatment groups in an aquadest homogenous mixture. The spectrum of acetone-mixed homogenates is shown in Figure 4 (c). Numbers indicate the sample groups: (1) vacuum packed, then low power treatment; (2) 'direct' low power treatment, then vacuum packed; (3) vacuum packed, then high power treatment; (4) 'direct' high power treatment, then vacuum packed; (5) untreated control. Note the insert graph in Figure 7.2 subfigure (c), showing a characteristic spectrograph for nitrosomyoglobin in a cured meat product.

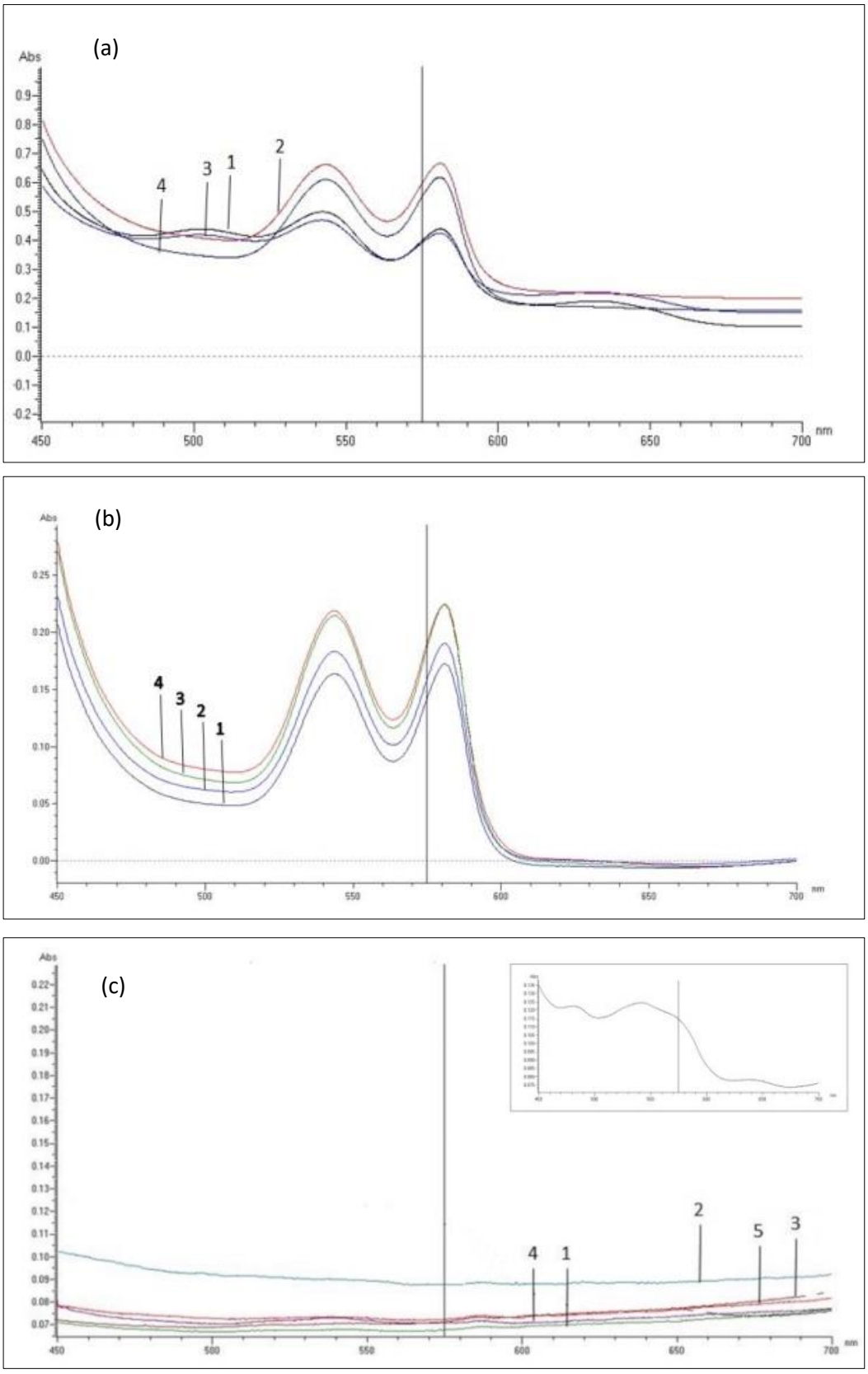

Figure 7.2 Spectrographs of myoglobin isoforms as prevalent in filtrates of aquadest homogenates of plasma treated and control beef loin samples: (a) for Test 1 and (b) for Test 2. Subfigure (c) (Test 1) shows results of nitrosomyglobin analysis (samples homogenised in acetone).

Characteristic extinction peaks for MbO (typically at 544 and 582 nm) can be clearly distinguished, while the characteristic spectral profiles of deoxymyoglobin (peak at 525 nm) and methmyoglobin (peaks at 503 and at 650 nm) cannot be observed [137]. Figure 7.2 (c) provides evidence that nitrosomyoglobin (which is typically observed in cured meats between 500 and 600 nm; see the reference graph insert in Figure 7.2 (c)) is not prevalent in plasma treated samples.

7.4 Discussion

Most studies reported in literature concentrate on the antimicrobial effects on foods directly treated with non-thermal atmospheric pressure plasma, few studies however consider meat, especially fresh beef. However, this study shows no antimicrobial effect of beef samples from the plasma, this is likely due to the in-direct nature of the plasma treatment and the complexity of the sample surface. These tests do indicate the SBD has a marked antimicrobial potential for decontaminating packaging film surfaces. Given that plasma species do not penetrate the packaging film, the use of plasma to clean the outside of meat packages would not be subjected to the same regulatory requirements as the direct exposure of the product. One remaining challenge is that commercial meat processing and packaging lines operate at rather high speeds. Consequently, there are limitations as to the treatment duration. In this study the treatment time was limited to 60 seconds which approaches the maximum time a packaged product may remain on a conveyor belt. Obviously at longer durations, the antimicrobial and physical-chemical effects may be intensified.

Major physical-chemical indications for sensory changes might have changed signs of sarcoplasmic protein denaturation, though which was reflected from observation in the result but possibly leading to higher L* values or oxidation, the latter leading to shifts in the myoglobin isoform distribution pattern, and both would affect meat colour [120, 126, 127].

In test 1, the Hue angles, observed for high power treatment to be consistently higher over time (Table 7.4), would appear to suggest that plasma treatment may

have induced some oxidation. Yet, the results of both TBARS analysis (indicative for lipid oxidation) and Mb isoform analysis (indicative for oxidation of Mb to MMb) failed to substantiate such. Surprisingly, under low power treatment conditions which are dominated by ozone and is known to initiate oxidation reactions, did not result in colour changes in any of the tests.

Under high power conditions plasma treatment it is essential to determine if the samples take up nitrates, as they are toxic and even low quantities can lead to a minor superficial curing effect. As nitrite-uptake of the treated surface tissue was shown not to occur and thus nitrosomyoglobin formation was not observed. If curing had occurred due to plasma treatment, then the product would no longer classify as 'fresh' meat according to international standards (European Union, 2004) [140].

As plasma generated RONS are free to interact with the surface tissue containing intramuscular fat, the potential for lipid oxidation during plasma treatment is high. Reactive oxygen species are able to interact with the unsaturated fatty acid fraction which may lead to lipid peroxidation. Secondary oxidation products, such as aldehydes, may initiate conformational changes in myoglobin causing increased hemeoxidation (hemoglobin) and brown off-colours, and then lead to off-odours and, finally, result in rancid off-flavours [141]. The latter occurs at TBARS threshold values of 0.5-2.0 mg MDA/kg [142]. Results show that the TBARS values measured after 3 and 10 days of vacuum storage were all below the limit of detection of 0.11 mg MDA/kg**.**

This was not an unexpected finding as, firstly, the amount of intramuscular fat in beef is low (around 2%), this predominantly contains saturated and mono unsaturated fatty acids, but relatively little polyunsaturated fatty acids (PUFA) which are known to be particularly vulnerable to oxidative changes [143]. TBARS values are primarily expected to increase in a packaging environment with a high oxygen content and at extended storage times as discussed by Ulbin-Figlewicz & Jarmoluk [144].

In test 2, samples had been continually stored in vacuum until exposed to atmospheric oxygen and daylight at day 10 for a final 3 days. Observation indicates

that TBARS values increased to around 0.15±0.03 mg MDA/kg, which is below the threshold values for off-odours and off-flavours, and values were not different for plasma-treated and untreated samples. These findings correspond to those of Jayasena *et al.*, who report an increase in TBARS values only when beef loin was subjected to 'direct plasma treatment for 10 minutes, as opposed to treatment durations of 2.5, 5 and 7.5 minutes [80].

During the ~70 minute sample preparation time (homogenisation and filtration) preceding myoglobin analysis, the sample is exposed to oxygen. At ambient pressure deoxymyoglobin (DeMb) will have been oxygenated to oxymyoglobin (MbO), and there should only be traces of methmyoglobin (MMb) and deoxymyoglobin (DeMb) [135, 145]. This explains the findings shown in Figure 7.3. Hence, the data suggests that in all samples, treated and untreated alike, Methmyoglobin Reducing Activity (MRA) is still largely intact [146]. Consequently, in this study the 'display life' does not seem to be adversely affected by the plasma treatment. This finding is further supported by comparing the colorimetric data with the 'colour acceptability standards' suggested by Farouk *et al.*, who conducted consumer panel studies involving over 500 panellists evaluating the appearance of beef loin steaks displayed under atmospheric conditions [147]. These authors determined the 'cut off' colour values above or below which a consumer is no longer willing to buy the product and consequently 'display life' has ended. Considering the colour measurement equipment used, desirable values would be: $a^* \geq 14$ and $33 \leq Hue \leq 41$. Tables 7.6 through 7.8 indeed show that samples aerobically stored for the final 3 days still qualify for being displayed, regardless of the plasma power condition applied.

The physical-chemical analysis conducted in this investigation primarily focused on the plasma treatment effects on meat colour. It could be argued that other major sensory attributes may also be subject to changes resulting from such treatment. For instance, plasma induced protein denaturation would affect water-holding ability [135]. Oxidative environments resulting from plasma treatment could conceivably decrease tenderization through inactivation of μ-calpain, or affect the degree of oxidation [135, 138, 148–151].

However, it needs to be mentioned that these biochemical effects would be restricted to a very thin surface layer. Although this needs to be confirmed in further studies, it is questionable if such strictly localised effects would afford significant changes in waterholding/tenderness/flavour traits of the overall product. In contrast to treatment of meat with irradiation which depending on the wavelengths achieving a penetration depth of 3-6 cm with Beta rays and up to 1-2 m with Gamma-rays, non-thermal plasma is a technology that restricts its action to the immediate surface only. Even in set-ups that achieve the highest penetration, such as plasma jet devices, plasma generated species only penetrates the tissue in the micrometers range. For instance, an effective tissue penetration depth of maximally 60 µm has been recorded for high rate flow plasma jet treatment [152]. Consequently, it is likely that the direct treatment of meat with plasmas potentially affects only those quality traits that are principally related to surface-associated phenomena.

7.5 Conclusion

This investigation is one of the first to consider the use of an SBD for the treatment of beef loins. While the decontamination results are far from impressive it is likely that there is considerable room for improvement given the short treatment times and rather large separation between the SBD and the meat surface. Notably, tests showed that plasma treatment did not adversely affect the major physical-chemical quality characteristics of the beef.

Beyond the direct exposure of meat surfaces to plasma species, it was shown that standard food grade packaging films are able to act as a barrier to plasma generated RONS. This is especially important for applications where plasma may be used to decontaminate the outer surfaces of packaging materials. In the context of package decontamination, plasma was shown to be particularly effective at inactivating a wide range of foodborne pathogens on typical food packaging films.

Overall, it is concluded that the SBD treatment of meat for the purpose of microbial decontamination is extremely challenging. Difficulties are assumed to arise due to

the complex nature of the sample surface (fibrous tissue with an abundance of proteinaceous and fatty matter). Plasma treatment was shown to cause relatively few changes to key quality attributes of the exposed meat. SBD treatment of packing material was highly effective and this promising application area should be further investigated to reduce the necessary treatment times.

Chapter 8 Conclusion

8.1 summary

Overall, this PhD thesis demonstrates that non-thermal air plasma is an effective tool for use in microbial decontamination applications. It is a low-cost, environmentally friendly approach that can be applied directly at the point of need. While the recent literature considered a vast array of discharge configurations, the emphasis of this project was on the Surface Barrier Discharge due to its ability to operate in a stable fashion in ambient air for long durations and its ease of scalability. A distinct disadvantage of the SBD configuration is the spatial separation between the plasma region and the sample, which typically ranges from 1 mm to 100 mm. Many applications rely upon the highly reactive RONS produced in the plasma; yet, the spatial separation between the plasma and the sample acts as a filter, meaning only longer-lived species are able to play a role.

In order to reduce the impact of the spatial separation between the discharge and sample and thereby improve application efficiency, this work has systematically explored the influence of the discharge parameters on both species production and transport of reactive species. Using FTIR analysis, two modes of operation were identified. Under low power conditions the gas phase chemistry was observed to be dominated by ozone, increasing the dissipated power led to an abrupt transition to a RNS dominated regime. In humid air, which is typical in many application, HNO_3 was the dominant species produced under high power conditions; in dry conditions, N_2O_5 was the main product. The reasons behind the abrupt transition between the ROS and RNS dominated modes were discussed and attributed to the accelerated production of NO and subsequent quenching of ozone

While the plasma generated RONS impinge on the surface of a liquid, they react to produce a range of other long-lived RONS including H_2O_2, HNO_2 and HNO_3. Furthermore, ozone is soluble in water hence aqueous phase ozone increase with plasma exposure. HNO_2 is less stable and can be oxidised to HNO_3 during the plasma treatment. Under higher power conditions the high concentration of gas

phase species resulted in acidification of the liquid. Given that the pH level can be critical in certain applications, such as the treatment of potable water, such changes are undesirable. To overcome this challenge, a pulsed width modulation (PWM) mode was introduced to reduce power dissipated by the plasma without compromising the area of plasma generation. Measurements showed that no significant pH drop was observed when using PWM.

Beyond the afterglow chemistry, the mass transport of key reactive species and a means to enhance it was also investigated. The body force generated by the SBD plasma system was systematically studied using the particle image velocimetry (PIV) techniques. The aim of these investigations was to increase the velocity of flowing gas in the direction of the sample, thus reducing the transit time of species to the sample. It was observed that both the input power and electrode geometry were key factors in dictating the flow velocity from the electrode unit. It was determined that the optimal electrode configuration consisted of parallel facing strips, with a 1.5 cm separation. It was deemed necessary to strike a compromise between electrode gap spacing and the volume of plasma generated, hence a 1 cm gap separation was chosen for the final SBD device.

After optimisation of the SBD system, various bacterial decontamination scenarios were considered. This included bacteria incubated on agar surfaces, suspended in liquid solutions and inoculated on to muscle meat samples. Results indicated that both solid surfaces and liquid volumes can be effectively and efficiently decontaminated by the plasma, whereas no obvious decontamination was observed for meat samples. This highlights an important point regarding the nature of plasma treatments and the complexity introduced with real-world samples. Many reports in the literature focus on model-system (*e.g.* agar) and show excellent results, this work demonstrates that moving to realistic samples is far from a trivial matter.

Particularly encouraging results were obtained on the treatment of fungal spores (*A. flavus*) where it was observed that plasma decontamination was highly effective. Fungus places a major burden on the food supply chain, if plasma system could be realised that achieves similar levels of reduction on a commercial scale the impact would be significant.

In conclusion, this project has demonstrated that SBD systems are valuable tools in the fight against microbial contamination. They are convenient, easily scaled and require no consumables, hence are extremely attractive for industry. The work has uncovered several novel routes to optimise SBD reactors for microbial decontamination applications and the published outcomes will undoubtedly contribute to the ongoing international effort to realise an industrial scale plasma decontamination system.

8.2 Future research directions

This work has uncovered that the plasma chemistry arriving at the sample is the dominating factor in dictating the efficiency of decontamination. Much work is still to be done on understanding the complex reaction pathways and how these link to the underlying physical properties of the discharge. In the future, modelling and advanced diagnostic techniques should be employed to gain a better insight in to the underpinning processes in the plasma region.

Once a comprehensive understanding of the plasma chemistry has been achieved, further efforts should be devoted to enhancing the mass transport of species. Recent reports in the literature associated with plasma-aerodynamics have demonstrated that flow rates >10 m/s can be generated, this is an order of magnitude higher than what has been achieved in this work. Further efforts should be devoted in to improving this as an order of magnitude increase in flow velocity is likely to result in the transport of species which are typically considered to be confined to the visible discharge region (e.g. OH). Such species are key from microbial decontamination applications and increase the flux of these to the sample would be highly advantageous.

Finally, treatment on beef samples showed comparatively poor levels of decontamination compared to model systems. In the future, the influence of the surface composition and morphology of the sample should be investigated further to identify situations where plasma treatment is highly unlikely to be effective (e.g. fibrous media where bacteria are shielded).

Reference

[1] A. Fridman, *Plasma chemistry*. New York: Cambridge University Press, 2008.

[2] A. Piel, *Plasma Physics: An Introduction to Laboratory, Space, and Fusion Plasmas*. Springer-Verlag Berlin Heidelberg, 2010.

[3] Y.P.Raizer, *Gas Discharge Physics*. Springer-Verlag Berlin Heidelberg, 1991.

[4] U. Kogelschatz, "Dielectric-barrier discharges: Their History, Discharge Physics, and Industrial Applications," *Plasma Chem. Plasma Process.*, vol. 23, no. 1, pp. 1–46, 2003.

[5] G. Artana, J. D'Adamo, L. Leger, E. Moreau, and G. Touchard, "Flow control with electrohydrodynamic actuators," *AIAA J.*, vol. 40, no. 9, pp. 1773–1779, 2002.

[6] National Research Council (U.S.), *Plasma Science: Advancing Knowledge in the National Interest*. Washington, D.C.: The National Academies Press, 2010.

[7] J. Ráheľ, H. Polášková, E. Jonášová, M. Hudcová, M. Zahoran, and P. Nasadil, *Plasma for Bio-Decontamination, Medicine and Food Security*. Dordrecht: Springer Science Business Media, Inc., 2012.

[8] J. Jiang *et al.*, "Effect of Cold Plasma Treatment on Seed Germination and Growth of Wheat," *Plasma Sci. Technol.*, vol. 16, no. 1, pp. 54–58, 2014.

[9] R. Thirumdas, C. Sarangapani, and U. S. Annapure, "Cold Plasma: A novel Non-Thermal Technology for Food Processing," *Food Biophys.*, vol. 10, no. 1, pp. 1–11, 2014.

[10] H. G. Gorchev and G. Ozolins, "WHO guidelines for drinking-water quality.," *WHO Chron.*, vol. 38, pp. 104–108, 2011.

[11] Who and Unicef, "Progress on sanitation and drinking-water - 2014 update," *… Monit. Program. water supply Sanit. …*, pp. 1–78, 2014.

[12] H. Bridle, "Waterborne Pathogens: Introduction," in *Waterborne Pathogens: Detection Methods and Applications*, Elsevier B.V., pp. 1–5, 2014.

[13] M. F. Craun, Gunther F. Craun, R. L. Calderon, and M. J. Beach, "Waterborne outbreaks reported in the United States Michael," *J. Water Health*, vol. 4, no. 2, pp. 277–288, 2006.

[14] European Centre for Disease Prevention and Control, "Surveillance of six priority food- and waterborne diseases in the EU/EEA 2006-2009," Stockholm, 2013.

[15] WHO, *WHO estimates of the global burden of foodborne diseases: Foodborne Disease Burden Epidemiology Reference Group 2007-2015*. World Health Organization, 2015.

[16] S. D. Caroline and R. Nadine, "Food Safety Around the World," *Glob. Local*, no. June, p. 95, 2005.

[17] L. H. Gould *et al.*, "Surveillance for foodborne disease outbreaks - United States, 1998-2008.," *MMWR. Surveill. Summ.*, vol. 62, no. 2, pp. 1–34, 2013.

[18] G. K. Adak, S. M. Long, and S. J. O'Brien, "Trends in indigenous foodborne disease and deaths, England and Wales: 1992 to 2000.," *Gut*, vol. 51, no. 6, pp. 832–41, Dec. 2002.

[19] O. A. Oyarzabal and S. Backert, *Microbial Food Safety: An Introduction*. Springer Science Business Media, LLC, 2012.

[20] B. Ray, *Fundamental Food Microbiology*, Third Edit. CRC Press LLC, 2004.

[21] N. G. Marriott and R. B. Gravani, *Principles of Food Sanitation*, vol. 53, no. 9. Springer Science Business Media, Inc., 2006.

[22] M. Laroussi, "Nonthermal decontamination of biological media by atmospheric-pressure plasmas: Review, analysis, and prospects," *IEEE Trans. Plasma Sci.*, vol. 30, no. 4 I, pp. 1409–1415, 2002.

[23] A. Shaw, G. Shama, and F. Iza, "Emerging applications of low temperature gas plasmas in the food industry," *Biointerphases*, vol. 10, no. 2, p. 29402, 2015.

[24] M. Laroussi, "Sterilization of contaminated matter with an atmospheric pressure plasma," *IEEE Trans. Plasma Sci.*, vol. 24, no. 3, pp. 1188–1191, 1996.

[25] M. Laroussi, J. P. Richardson, and F. C. Dobbs, "Biochemical pathways in the interaction of nonequilibrium plasmas with bacteria," *Proc. Electromed 2001 (Portsmouth, VA, 2001)*, vol. 33, 2001.

[26] R. Ben Gadri *et al.*, "Sterilization and plasma processing of room temperature surfaces with a one atmosphere uniform glow discharge plasma (OAUGDP)," *Surf. Coatings Technol.*, vol. 131, no. 1–3, pp. 528–541, 2000.

[27] J. Ehlbeck *et al.*, "Low temperature atmospheric pressure plasma sources for microbial decontamination," *J. Phys. D. Appl. Phys.*, vol. 44, no. 1, pp. 453–459, 2011.

[28] K. Kelly-Wintenberg *et al.*, "Use of a one atmosphere uniform glow discharge plasma to kill a broad spectrum of microorganisms," *J. Vac. Sci. Technol. A*, vol. 17, no. 4, pp. 1539–1544, 1999.

[29] F. J. Critzer, K. Kelly-Wintenberg, S. L. South, and D. A. Golden, "Atmospheric plasma inactivation of foodborne pathogens on fresh produce surfaces," *J. Food Prot.*, vol.

70, no. 10, pp. 2290–2296, Oct. 2007.

[30] K. Kelly-Wintenberg *et al.*, “Air filter sterilization using a one atmosphere uniform glow discharge plasma (the volfilter),” *IEEE Trans. Plasma Sci.*, vol. 28, no. 1, pp. 64–71, 2000.

[31] K. D. Weltmann, E. Kinde, T. Von Woedtke, M. Hähnel, M. Stieber, and R. Brandenburg, “Atmospheric-pressure plasma sources: Prospective tools for plasma medicine,” *Pure Appl. Chem.*, vol. 82, no. 6, pp. 1223–1237, 2010.

[32] K. Oehmigen, M. Hähnel, R. Brandenburg, C. Wilke, K. D. Weltmann, and T. Von Woedtke, “The role of acidification for antimicrobial activity of atmospheric pressure plasma in liquids,” *Plasma Process. Polym.*, vol. 7, no. 3–4, pp. 250–257, 2010.

[33] H. Eto, Y. Ono, A. Ogino, and M. Nagatsu, “Low-temperature sterilization of wrapped materials using flexible sheet-type dielectric barrier discharge,” *Appl. Phys. Lett.*, vol. 93, no. 22, pp. 5–8, 2008.

[34] A. Schwabedissen, P. ŁAcińSki, X. Chen, and J. Engemann, “PlasmaLabel - A new method to disinfect goods inside a closed package using dielectric barrier discharges,” in *Contributions to Plasma Physics*, vol. 47, no. 7, pp. 551–558, 2007.

[35] H. W. Lee, S. H. Nam, A. A. H. Mohamed, G. C. Kim, and J. K. Lee, “Atmospheric pressure plasma jet composed of three electrodes: Application to tooth bleaching,” *Plasma Process. Polym.*, vol. 7, no. 3–4, pp. 274–280, 2010.

[36] G. Daeschlein, T. Von Woedtke, E. Kindel, R. Brandenburg, K. D. Weltmann, and M. Jünger, “Antibacterial activity of an atmospheric pressure plasma jet against relevant wound pathogens in vitro on a simulated wound environment,” *Plasma Process. Polym.*, vol. 7, no. 3–4, pp. 224–230, 2010.

[37] H. W. Herrmann, I. Henins, J. Park, and G. S. Selwyn, “Decontamination of chemical and biological warfare (CBW) agents using an atmospheric pressure plasma jet (APPJ),” *Phys. Plasmas*, vol. 6, no. 5, pp. 2284–2289, 1999.

[38] R. E. J. Sladek and E. Stoffels, “Deactivation of Escherichia coli by the plasma needle,” *J. Phys. D. Appl. Phys.*, vol. 38, pp. 1716–1721, 2005.

[39] M. Laroussi, C. Tendero, X. Lu, S. Alla, and W. L. Hynes, “Inactivation of bacteria by the plasma pencil,” *Plasma Process. Polym.*, vol. 3, no. 6–7, pp. 470–473, 2006.

[40] H. S. Uhm, J. P. Lim, and S. Z. Li, “Sterilization of bacterial endospores by an atmospheric-pressure argon plasma jet,” *Appl. Phys. Lett.*, vol. 90, no. 26, pp. 2–5, 2007.

[41] J. Ehlbeck, R. Brandenburg, T. von Woedtke, U. Krohmann, M. Stieber, and K.-D. K.-D. Weltmann, “PLASMOSE - antimicrobial effects of modular atmospheric plasma sources,” *GMS Krankenhhyg. Interdiszip.*, vol. 3, no. 1, p. Doc14, 2008.

[42] S. Perni, D. W. Liu, G. Shama, and M. G. Kong, “Cold atmospheric plasma decontamination of the pericarps of fruit,” *J. Food Prot.*, vol. 71, no. 2, pp. 302–308, Feb. 2008.

[43] D. Y. Kim, C. S. Park, J. Y. Leem, and S. O. Kim, “Raw food sterilization of flexible dielectric barrier discharge device using biocompatible tubing,” *IEEE Trans. Plasma Sci.*, vol. 42, no. 10, pp. 2758–2759, 2014.

[44] C. Mok, T. Lee, and P. Puligundla, “Afterglow corona discharge air plasma (ACDAP) for inactivation of common food-borne pathogens,” *Food Res. Int.*, vol. 69, no. 2, pp. 418–423, 2015.

[45] L. F. Gaunt, C. B. Beggs, and G. E. Georghiou, “Bactericidal action of the reactive species produced by gas-discharge nonthermal plasma at atmospheric pressure: A review,” *IEEE Trans. Plasma Sci.*, vol. 34, no. 4 II, pp. 1257–1269, 2006.

[46] X. Deng, J. Shi, and M. G. Kong, “Physical mechanisms of inactivation of Bacillus subtilis spores using cold atmospheric plasmas,” *IEEE Trans. Plasma Sci.*, vol. 34, no. 4 II, pp. 1310–1316, 2006.

[47] M. Yamamoto, M. Nishioka, and M. Sadakata, “Sterilization by H2O2 droplets under corona discharge,” *J. Electrostat.*, vol. 55, no. 2, pp. 173–187, 2002.

[48] M. J. Gallagher *et al.*, “Rapid inactivation of airborne bacteria using atmospheric pressure dielectric barrier grating discharge,” *IEEE Trans. Plasma Sci.*, vol. 35, no. 5 II, pp. 1501–1510, Oct. 2007.

[49] K. Y. Lee *et al.*, “Sterilization of Escherichia coli and MRSA using microwave-induced argon plasma at atmospheric pressure,” *Surf. Coatings Technol.*, vol. 193, no. 1–3 SPEC. ISS., pp. 35–38, Apr. 2005.

[50] J. H. Choi *et al.*, “Analysis of sterilization effect by pulsed dielectric barrier discharge,” *J. Electrostat.*, vol. 64, no. 1, pp. 17–22, Jan. 2006.

[51] B. J. Park *et al.*, “Sterilization using a microwave-induced argon plasma system at atmospheric pressure,” *Phys. Plasmas*, vol. 10, no. 11, p. 4539, 2003.

[52] X. Lu, M. Laroussi, and V. Puech, “On atmospheric-pressure non-equilibrium plasma jets and plasma bullets,” *Plasma Sources Sci. Technol.*, vol. 21, p. 34005, 2012.

[53] X. Lu *et al.*, “The roles of the various plasma agents in the inactivation of bacteria,” *J. Appl. Phys.*, vol. 104, no. 5, 2008.

[54] Z. Xiong, X. P. Lu, A. Feng, Y. Pan, and K. Ostrikov, “Highly effective fungal inactivation in He+ O2 atmospheric-pressure nonequilibrium plasmas,” *Phys. Plasmas*, vol. 17, no. 12, Dec. 2010.

[55] Y. Cao *et al.*, “Efficacy of atmospheric pressure plasma as an antibacterial agent against enterococcus faecalis in vitro,” *Plasma Sci. Technol.*, vol. 13, no. 1, pp. 93–98, Feb. 2011.

[56] D. B. Graves, “The emerging role of reactive oxygen and nitrogen species in redox biology and some implications for plasma applications to medicine and biology,” *J. Phys. D. Appl. Phys.*, vol. 45, no. 26, p. 42, 2012.

[57] Y. Sakiyama, D. B. Graves, H.-W. Chang, T. Shimizu, and G. E. Morfill, “Plasma chemistry model of surface microdischarge in humid air and dynamics of reactive neutral species,” *J. Phys. D. Appl. Phys.*, vol. 45, no. 42, p. 425201, Oct. 2012.

[58] M. J. Pavlovich, H.-W. Chang, Y. Sakiyama, D. S. Clark, and D. B. Graves, “Ozone correlates with antibacterial effects from indirect air dielectric barrier discharge treatment of water,” *J. Phys. D. Appl. Phys.*, vol. 46, no. 14, p. 145202, 2013.

[59] D. X. Liu *et al.*, “Aqueous reactive species induced by a surface air discharge: Heterogeneous mass transfer and liquid chemistry pathways,” *Sci. Rep.*, vol. 6, no. April, p. 23737, 2016.

[60] M. Laroussi and F. Leipold, “Evaluation of the roles of reactive species, heat, and UV radiation in the inactivation of bacterial cells by air plasmas at atmospheric pressure,” *Int. J. Mass Spectrom.*, vol. 233, pp. 81–86, 2004.

[61] F. C. Fang, “Antimicrobial reactive oxygen and nitrogen species: concepts and controversies.,” *Nat. Rev. Microbiol.*, vol. 2, no. October, pp. 820–832, 2004.

[62] M. L. Jones, J. G. Ganopolsky, A. Labbé, C. Wahl, and S. Prakash, “Antimicrobial properties of nitric oxide and its application in antimicrobial formulations and medical devices,” *Appl. Microbiol. Biotechnol.*, vol. 88, no. 2, pp. 401–407, 2010.

[63] F. C. Fang, “Perspectives series: host/pathogen interactions. Mechanisms of nitric oxide-related antimicrobial activity.,” *J. Clin. Invest.*, vol. 99, no. 12, pp. 2818–25, Jun. 1997.

[64] R. X. Wang *et al.*, “Atmospheric-pressure cold plasma treatment of contaminated fresh fruit and vegetable slices: inactivation and physiochemical properties evaluation,” *Eur. Phys. J. D*, vol. 66, no. 10, p. 276, Oct. 2012.

[65] M. Baier, M. Görgen, J. Ehlbeck, D. Knorr, W. B. Herppich, and O. Schlüter, “Non-thermal atmospheric pressure plasma: Screening for gentle process conditions and antibacterial efficiency on perishable fresh produce,” *Innov. Food Sci. Emerg. Technol.*, vol. 22, pp. 147–157, 2014.

[66] S. Deng, R. Ruan, C. K. Mok, G. Huang, X. Lin, and P. Chen, “Inactivation of Escherichia coli on almonds using nonthermal plasma,” vol. 72, no. 2, Mar. 2007.

[67] B. a. Niemira, “Cold Plasma Reduction of Salmonella and Escherichia coli O157: H7 on Almonds Using Ambient Pressure Gases,” *J. Food Sci.*, vol. 77, no. 3, pp. 171–175, 2012.

[68] B. A. Niemira and J. Sites, “Cold plasma inactivates Salmonella Stanley and Escherichia coli O157:H7 inoculated on golden delicious apples,” *J. Food Prot.*, vol. 71, no. 7, pp. 1357–1365, Jul. 2008.

[69] Y. Bai, J. Chen, Y. Yang, L. Guo, and C. Zhang, “Degradation of organophosphorus pesticide induced by oxygen plasma: Effects of operating parameters and reaction mechanisms,” *Chemosphere*, vol. 81, no. 3, pp. 408–414, 2010.

[70] A. Fernández, E. Noriega, and A. Thompson, “Inactivation of Salmonella enterica serovar Typhimurium on fresh produce by cold atmospheric gas plasma technology,” *Food Microbiol.*, vol. 33, no. 1, pp. 24–29, 2013.

[71] D. Bermúdez-Aguirre, E. Wemlinger, P. Pedrow, G. Barbosa-Cánovas, and M. Garcia-Perez, “Effect of atmospheric pressure cold plasma (APCP) on the inactivation of Escherichia coli in fresh produce,” *Food Control*, vol. 34, no. 1, pp. 149–157, 2013.

[72] M. Baier *et al.*, “Direct non-thermal plasma treatment for the sanitation of fresh corn salad leaves: Evaluation of physical and physiological effects and antimicrobial efficacy,” *Postharvest Biol. Technol.*, vol. 84, pp. 81–87, 2013.

[73] D. Ziuzina, S. Patil, P. J. J. Cullen, K. M. M. Keener, and P. Bourke, “Atmospheric cold plasma inactivation of Escherichia coli, Salmonella enterica serovar Typhimurium and Listeria monocytogenes inoculated on fresh produce,” *Food Microbiol.*, vol. 42, pp. 109–116, 2014.

[74] S. Preechayan, K. Tonmitr, A. Suksri, and P. Siriputthaiwan, “Decontamination of aflatoxin producing fungi on agriculture product by atmospheric glow discharge plasma,” *Asia-Pacific J. Sci. Technol.*, vol. 15, no. 3, pp. 202–213, 2010.

[75] P. Basaran, N. Basaran-Akgul, and L. Oksuz, “Elimination of Aspergillus parasiticus from nut surface with low pressure cold plasma (LPCP) treatment,” *Food Microbiol.*, vol. 25, no. 4, pp. 626–632, 2008.

[76] H. Kim *et al.*, “Effects of dielectric barrier discharge plasma on pathogen inactivation and the physicochemical and sensory characteristics of pork loin,” *Curr. Appl. Phys.*, vol. 13, no. 7, pp. 1420–1425, 2013.

[77] A. Fröhling, J. Durek, U. Schnabel, J. Ehlbeck, J. Bolling, and O. Schlüter, “Indirect plasma treatment of fresh pork: Decontamination efficiency and effects on quality attributes,” *Innov. Food Sci. Emerg. Technol.*, vol. 16, pp. 381–390, 2012.

[78] S. Choi *et al.*, “Corona discharge plasma jet for inactivation of Escherichia coli O157:H7 and Listeria monocytogenes on inoculated pork and its impact on meat quality attributes,” *Ann. Microbiol.*, 2015.

[79] B. Kim *et al.*, “Effect of atmospheric pressure plasma on inactivation of pathogens inoculated onto bacon using two different gas compositions,” *Food Microbiol.*, vol. 28, no. 1, pp. 9–13, Feb. 2011.

[80] D. D. Jayasena *et al.*, “Flexible thin-layer dielectric barrier discharge plasma treatment of pork butt and beef loin: Effects on pathogen inactivation and meat-quality attributes,” *Food Microbiol.*, vol. 46, pp. 51–57, 2015.

[81] S. Rød, F. Hansen, F. Leipold, and S. Knøchel, “Cold atmospheric pressure plasma

treatment of ready-to-eat meat: Inactivation of Listeria innocua and changes in product quality," *Food Microbiol.*, vol. 30, no. 1, pp. 233–8, May 2012.

[82] H. P. Song *et al.*, "Evaluation of atmospheric pressure plasma to improve the safety of sliced cheese and ham inoculated by 3-strain cocktail Listeria monocytogenes," *Food Microbiol.*, vol. 26, no. 4, pp. 432–436, 2009.

[83] E. E. Noriega *et al.*, "Cold atmospheric gas plasma disinfection of chicken meat and chicken skin contaminated with Listeria innocua," *Food Microbiol.*, vol. 28, no. 7, pp. 1293–1300, 2011.

[84] H. J. Lee, H. Jung, W. Choe, J. S. Ham, J. H. Lee, and C. Jo, "Inactivation of Listeria monocytogenes on agar and processed meat surfaces by atmospheric pressure plasma jets," *Food Microbiol.*, vol. 28, no. 8, pp. 1468–1471, 2011.

[85] L. Ragni *et al.*, "Non-thermal atmospheric gas plasma device for surface decontamination of shell eggs," *J. Food Eng.*, vol. 100, no. 1, pp. 125–132, 2010.

[86] S. Y. Moon *et al.*, "Feasibility study of the sterilization of pork and human skin surfaces by atmospheric pressure plasmas," *Thin Solid Films*, vol. 517, no. 14, pp. 4272–4275, 2009.

[87] M. Heise, W. Neff, O. Franken, P. Muranyi, and J. Wunderlich, "Sterilization of polymer foils with dielectric barrier discharges at atmospheric pressure," *Plasmas Polym.*, vol. 9, no. 1, pp. 23–33, 2004.

[88] H. Yun *et al.*, "Inactivation of Listeria monocytogenes inoculated on disposable plastic tray, aluminum foil, and paper cup by atmospheric pressure plasma," *Food Control*, vol. 21, no. 8, pp. 1182–1186, 2010.

[89] F. Leipold, Y. Kusano, F. Hansen, and T. Jacobsen, "Decontamination of a rotating cutting tool during operation by means of atmospheric pressure plasmas," *Food Control*, vol. 21, no. 8, pp. 1194–1198, 2010.

[90] J.-J. Wang, K.-S. Choi, L.-H. Feng, T. N. Jukes, and R. D. Whalley, "Recent developments in DBD plasma flow control," *Prog. Aerosp. Sci.*, vol. 62, pp. 52–78, Oct. 2013.

[91] L. E. Amand and C. J. Tullin, "The Theory Behind FTIR analysis," Boras, 1999.

[92] F. a Miller and C. H. Wilkins, "Infrared Spectra and Characteristic Frequencies of Inorganic Ions," *Anal. Chem.*, vol. 24, pp. 1253–1294, 1952.

[93] G. Laroche *et al.*, "Fourier transform infrared absorption spectroscopy characterization of gaseous atmospheric pressure plasmas with 2 mm spatial resolution.," *Rev. Sci. Instrum.*, vol. 83, no. 10, p. 103508, Oct. 2012.

[94] Z. Abd Allah, "NON - THERMAL ATMOSPHERIC PRESSURE PLASMA FOR REMEDIATION OF VOLATILE ORGANIC COMPOUNDS," The University of Manchester, 2012.

[95] M. Kihlman, “Application of solar FTIR spectroscopy for quantifying gas emissions,” Chalmers University of Technology, 2005.

[96] J. Westerweel, “Fundamentals of digital particle image velocimetry,” *Meas. Sci. Technol.*, vol. 8, pp. 1379–1392, 1997.

[97] J. P. Boeuf, Y. Lagmich, T. Unfer, T. Callegari, and L. C. Pitchford, “Electrohydrodynamic force in dielectric barrier discharge plasma actuators,” *J. Phys. D. Appl. Phys.*, vol. 40, no. 3, pp. 652–662, 2007.

[98] R. D. Whalley and J. L. Walsh, “Turbulent jet flow generated downstream of a low temperature dielectric barrier atmospheric pressure plasma device,” *Nat. Publ. Gr.*, no. August, pp. 1–7, 2016.

[99] E. Moreau *et al.*, “Surface Dielectric Barrier Discharge Plasma Actuators,” *ERCOFTAC Bull.*, vol. 94, pp. 5–10, 2013.

[100] A. Santhanakrishnan and J. D. Jacob, “Flow Control Using Plasma Actuators and Linear/Annular Plasma Synthetic Jet Actuators,” in *3rd AIAA Flow Control Conference*, pp. 1–30, 2006.

[101] R. D. Whalley and K.-S. Choi, “The starting vortex in quiescent air induced by dielectric-barrier-discharge plasma,” *J. Fluid Mech.*, vol. 703, pp. 192–203, Jun. 2012.

[102] M. J. Pavlovich, D. S. Clark, and D. B. Graves, “Quantification of Air Surface Micro-Discharge Chemistry for Surface Disinfection,” *Plasma Sources Sci. Technol.*, vol. 65036, 2014.

[103] U. Kogelschatz, B. Eliasson, and M. Hirth, “Ozone Generation from Oxygen and Air: Discharge Physics and Reaction Mechanisms,” *Ozone Sci. Eng.*, vol. 10, no. 4, pp. 367–377, 1988.

[104] U. Kogelschatz, B. Eliasson, W. Egli, U. Kogelschatz, B. Eliasson, and W. E. D. D. Principle, “Dielectric-Barrier Discharges . Principle and Applications,” *J. Phys. IV*, vol. 7, no. C4, pp. 47–66, 1997.

[105] T. Shimizu, Y. Sakiyama, D. B. Graves, J. L. Zimmermann, and G. E. Morfill, “The dynamics of ozone generation and mode transition in air surface micro-discharge plasma at atmospheric pressure,” *New J. Phys.*, vol. 14, no. 10, p. 103028, Oct. 2012.

[106] Y. Sakiyama and D. B. Graves, “Efficient modeling of atmospheric pressure surface micro-discharge plasma chemistry,” *Plasma Sources Sci. Technol.*, vol. 22, no. 1, p. 12003, Feb. 2013.

[107] B. R. Locke and K.-Y. Shih, “Review of the methods to form hydrogen peroxide in electrical discharge plasma with liquid water,” *Plasma Sources Sci. Technol.*, vol. 20, no. 3, p. 34006, Jun. 2011.

[108] Y. Ni, M. J. Lynch, M. Modic, R. D. Whalley, and J. L. Walsh, “A solar powered

handheld plasma source for microbial decontamination applications," *J. Phys. D. Appl. Phys.*, vol. 49, no. 35, p. 355203, 2016.

[109] P. Olszewski, J. F. F. Li, D. X. X. Liu, and J. L. L. Walsh, "Optimizing the electrical excitation of an atmospheric pressure plasma advanced oxidation process.," *J. Hazard. Mater.*, vol. 279, pp. 60–66, Aug. 2014.

[110] Z. Machala, B. Tarabova, K. Hensel, E. Spetlikova, L. Sikurova, and P. Lukes, "Formation of ROS and RNS in water electro-sprayed through transient spark discharge in air and their bactericidal effects," *Plasma Process. Polym.*, vol. 10, no. 7, pp. 649–659, 2013.

[111] J. P. Boeuf and L. C. Pitchford, "Electrohydrodynamic force and aerodynamic flow acceleration in surface dielectric barrier discharge," *J. Appl. Phys.*, vol. 97, no. 10, 2005.

[112] J. Kriegseis, S. Grundmann, and C. Tropea, "Power consumption, discharge capacitance and light emission as measures for thrust production of dielectric barrier discharge plasma actuators," *J. Appl. Phys.*, vol. 110, no. 1, 2011.

[113] Z. Buntat, "Ozone generation using electrical discharges : a comparative study between pulsed streamer discharge and atmospheric pressure glow discharge," Loughborough Unicersity, 2005.

[114] P. Small, D. Blankenhorn, D. Welty, E. Zinser, and J. L. Slonczewski, "Acid and base resistance in Escherichia coli and Shigella flexneri: Role of rpoS and growth pH," *J. Bacteriol.*, vol. 176, no. 6, pp. 1729–1737, 1994.

[115] Z. C. Liu *et al.*, "Physicochemical processes in the indirect interaction between surface air plasma and deionized water," *J. Phys. D. Appl. Phys.*, vol. 48, no. 49, p. 495201, 2015.

[116] L. H. Taylor, S. M. Latham, and M. E. J. Woolhouse, "Risk factors for human disease emergence," *Philos. Trans. R. Soc. London Ser. B-Biological Sci.*, vol. 356, no. 1411, pp. 983–989, 2001.

[117] S. Amaike and N. P. Keller, "Aspergillus flavus," *Annu. Rev. Phytopathol.*, vol. 49, no. 1, pp. 107–133, 2011.

[118] M. T. Hedayati, A. C. Pasqualotto, P. A. Warn, P. Bowyer, and D. W. Denning, "Aspergillus flavus: Human pathogen, allergen and mycotoxin producer," *Microbiology*, vol. 153, no. 6, pp. 1677–1692, 2007.

[119] V. PE, K. JJ, V. AA, and M. JF., "Fungal contamination of tobacco and marijuana," *J. Am. Med. Assoc.*, vol. 284, no. 22, pp. 2869–2875, 2000.

[120] C. Hedberg, "Food-related illness and death in the United States.," *Emerg. Infect. Dis.*, vol. 5, no. 6, pp. 840–2, 1999.

[121] K. F. Cardwell and S. H. Henry, "Risk of Exposure to and Mitigation of Effect of

Aflatoxin on Human Health: A West African Example," *Toxin Rev.*, vol. 23, no. 2–3, pp. 217–247, 2004.

[122] E. O. Farombi, "Aflatoxin contamination in foods in developing countries: implications for hepatocellular carcinoma and chemopreventive strategies," *African J. Biotechnol.*, vol. 5, no. January, pp. 1–14, 2006.

[123] G. Agrios, "Plant pathology," *Mol. Plant Pathol.*, vol. 15, no. 4, pp. 315–8, 2004.

[124] S. B. Oyeleke, E. C. Egwim, and S. H. Auta, "Screening of Aspergillus flavus and Aspergillus fumigatus strains for extracellular protease enzyme production," *J. Microbiol. Antimicrob.*, vol. 2, no. 7, pp. 83–87, 2010.

[125] A. C. Ritter, M. Hoeltz, and I. B. Noll, "Toxigenic potential of Aspergillus flavus tested in different culture conditions," *Ciência e Tecnol. Aliment.*, vol. 31, no. 3, pp. 623–628, 2011.

[126] A. López-Malo, S. M. Alzamora, and E. Palou, "Aspergillus flavus growth in the presence of chemical preservatives and naturally occurring antimicrobial compounds," *Int. J. Food Microbiol.*, vol. 99, no. 2, pp. 119–128, 2005.

[127] W. A. Harrison, C. J. Griffith, D. Tennant, and A. C. Peters, "Incidence of Campylobacter and Salmonella isolated from retail chicken and associated packaging in South Wales," *Lett. Appl. Microbiol.*, vol. 33, no. 6, pp. 450–454, Dec. 2001.

[128] C. Faustman and A. Phillips, "Measurement of Discoloration In Fresh Meat," in *Handbook of Food Analytical Chemistry: Water, Proteins, Enzymes, Lipids, and Carbohydrates*, R. E. Wrolstad, T. E. Acree, E. A. Decker, M. H. Penner, D. S. Reid, S. J. Schwartz, C. F. Shoemaker, D. Smith, and P. Sporns, Eds. Hoboken: John Wiley & Sons, Inc, pp. 139–152, 2005.

[129] H. J. Swatland, *On-line evaluation of meat*. Technomic Publishing Company, Inc., 1995.

[130] C. Lopez-Bote, P. D. Warriss, and S. N. Brown, "The Use of Muscle Protein Solubility Measurements to Assess Pig Lean Meat Quality," *Meat Sci.*, vol. 26, pp. 167–175, 1989.

[131] G. Eikelenboom and F. J. M. Smulders, "Effect of electrical stimulation on veal quality," *Meat Sci.*, vol. 16, no. 2, 1986.

[132] B. Schmidt and G. Schuedt, "HPLC-Verfahren zur Nitratbestimmung in pflanzlichen Lebensmitteln im Vergleich zur photo-und potentiometrischen Analyse," *Dtsch. Leb. Rundsch*, vol. 80, pp. 137–140, 1984.

[133] C. Faustman, Q. Sun, R. Mancini, and S. P. Suman, "Myoglobin and lipid oxidation interactions: Mechanistic bases and control," *Meat Sci.*, vol. 86, no. 1, 2010.

[134] V. C. WITTE, G. F. KRAUSE, and M. E. BAILEY, "A NEW EXTRACTION METHOD FOR

DETERMINING 2-THIOBARBITURIC ACID VALUES OF PORK AND BEEF DURING STORAGE," *J. Food Sci.*, vol. 35, no. 5, pp. 582–585, Sep. 1970.

[135] F. Smulders, P. Hofbauer, and G. H. Geesink, "The Conversion of Muscle to Meat," *Meat Insp. Control Slaughterh.*, pp. 399–421, 2014.

[136] M. J. A. den Hertog-Meischke, R. E. Klont, F. J. M. Smulders, and J. G. van Logtestijn, "Variation in post-mortem rate of glycolyis does not necessarily affect drip loss of non-stimulated veal," *Meat Sci.*, vol. 47, no. 3, pp. 323–329, 1997.

[137] Association American Meat Science, *AMSA Meat Color Measurement Guidelines*. American Meat Science Association, 2012.

[138] S. . Joo, R. . Kauffman, B. . Kim, and G. . Park, "The relationship of sarcoplasmic and myofibrillar protein solubility to colour and water-holding capacity in porcine longissimus muscle," *Meat Sci.*, vol. 52, no. 3, pp. 291–297, 1999.

[139] C. FAUSTMAN and R. G. CASSENS, "THE BIOCHEMICAL BASIS FOR DISCOLORATION IN FRESH MEAT: A REVIEW," *J. Muscle Foods*, vol. 1, no. 3, pp. 217–243, Jul. 1990.

[140] *REGULATION (EC) No 853/2004 OF THE EUROPEAN PARLIAMENT AND OF THE COUNCIL of 29 April 2004 laying down specific hygiene rules for food of animal origin*, no. 853, pp. 69–74, 2007.

[141] F. Shahidi and U. N. Wanasundara, "Methods for measuring oxidative rancidity in fats and oils," in *Food Lipids: Chemistry, Nutrition, and Biotechnology*, 3rd Editon., C. C. Akoh and D. B. Min, Eds. CRC Press, pp. 387–403, 2008.

[142] P. Chang, M. T. Younathan, and B. M. Watts, "Lipid oxidation in pre-cooked beef preserved by refrigeration, freezing, and irradiation.," *Food Technol., 15 168-71.*, 1961.

[143] S. W. Souci, W. Fachmann, and H. Kraut, *Food composition and nutrition tables*, 8th revise. Stuttgart: Medpharm Scientific Publishers, 2016.

[144] N. Ulbin-Figlewicz and A. Jarmoluk, "Effect of low-pressure plasma treatment on the color and oxidative stability of raw pork during refrigerated storage," *Food Sci. Technol. Int.*, vol. 22, no. 4, 2015.

[145] L. H. Skibsted, "Chemical changes in meat and meat products during storage, transportation and retail display: theoretical considerations," in *Meat quality and meat packaging*, S. S. A. Taylor, Ed. 1996, pp. 169–181.

[146] A. E. D. Bekhit and C. Faustman, "Metmyoglobin reducing activity," *Meat Sci.*, vol. 71, pp. 407–439, 2005.

[147] M. Farouk, A. Bekhit, P. Dobbie, and J. Waller, "Towards benchmarking beef loin steak colour acceptability using Minolta and Hunter Colourimeters," in *In Proceedings of the 53th International Congress of Meat Science & Technology*, pp. 405–406, 2007.

[148] H. Zhang *et al.*, “Effects and mechanism of atmospheric-pressure dielectric barrier discharge cold plasma on lactate dehydrogenase (LDH) enzyme,” *Sci. Rep.*, vol. 5, 2015.

[149] L. J. Rowe, K. R. Maddock, S. M. Lonergan, and E. Huff-Lonergan, “Oxidative environments decrease tenderization of beef steaks through inactivation of μ-calpain,” *J. Anim. Sci.*, vol. 82, no. 11, 2004.

[150] H. I. Yong *et al.*, “Evaluation of pathogen inactivation on sliced cheese induced by encapsulated atmospheric pressure dielectric barrier discharge plasma,” *Food Microbiol.*, vol. 46, 2015.

[151] B. Surowsky, A. Fischer, O. Schlueter, and D. Knorr, “Cold plasma effects on enzyme activity in a model food system,” *Innov. Food Sci. Emerg. Technol.*, vol. 19, 2013.

[152] C. Hoffmann, C. Berganza, and J. Zhang, “Cold Atmospheric Plasma: Methods of production and application in dentistry and oncology,” *Med. Gas Res.*, vol. 3, no. 1, 2013.